学位論文

Study of the Biogenesis of the Golgi Apparatus in Plant Cells

（植物細胞におけるゴルジ体形成機構の研究）

平成 25 年　12 月　博士（理学）申請

東京大学大学院理学系研究科

生物科学専攻

伊藤　容子

Abstract

The Golgi apparatus forms stacks of cisternae in many eukaryotic cells. However, little is known about how such a stacked structure is formed and maintained. To address this question, plant cells provide a system suitable for live imaging approaches because individual Golgi stacks are well separated in the cytoplasm. I established tobacco BY-2 cell lines expressing multiple Golgi markers tagged by different fluorescent proteins and observed their responses to brefeldin A (BFA) treatment and BFA removal. BFA treatment disrupted *cis,* medial and *trans* cisternae but caused distinct relocalization patterns depending on the proteins examined. Medial- and *trans*-Golgi proteins, as well as one *cis*-Golgi protein, were absorbed into the endoplasmic reticulum (ER), but two other *cis*-Golgi proteins formed small punctate structures. One of the latter was revealed to localize to the *cis*-most cisternae of the Golgi stacks. After BFA removal, these puncta coalesced first and then the Golgi stacks regenerated from them in the *cis*-to-*trans* order. I suggest that these structures function as the scaffold of Golgi regeneration. Furthermore, I propose that the *cis*-most cisternae have a special property similar to the ER-Golgi intermediate compartment. In addition, to reveal the relationship between the Golgi and the TGN, I visualized them and observed their dynamic behaviors similarly. The TGN behaved differently from the Golgi stacks upon BFA treatment with a low concentration; the TGN proteins relocalized to numerous vesicle-like structures dispersed

throughout the cytoplasm. The TGN started to regenerate earlier than the Golgi stacks completed their regeneration after BFA removal, and the two organelles were independent from each other at the early stage of regeneration. However, the TGN and the Golgi associated later during regeneration. I suggest that the TGN does not fully depend on the Golgi, but the association between the two organelles is indispensable for their functions.

Table of Contents

Acknowledgments

First of all, I would like to express my deepest appreciation to my supervisor, Professor Akihiko Nakano, for giving me the opportunity to do my dissertation work in his laboratory, and for his valuable guidance and encouragement throughout this work. I am also deeply grateful to Associate Professor Takashi Ueda for giving me illuminating advice and suggestions. I would also like to express my gratitude to Assistant Professor Tomohiro Uemura for not only sharing experimental materials but also helpful advice and encouragement throughout this study.

I would like to thank Dr. Gerd Jürgens (Universität Tübingen), Dr. Tsuyoshi Nakagawa (Shimane University), and Ms. Keiko Shoda (RIKEN BSI) for sharing materials. I also want to thank Dr. Kiminori Toyooka (RIKEN CSRS) for valuable discussion. I would like to show my appreciation to Dr. Masaru Fujimoto (The University of Tokyo), Dr. Choi Seung-won (RIKEN CSRS), Dr. Rin Asaoka (Tohoku University), Dr. Atsuko Era (National Institute of Genetics), and all the members of Live Cell Molecular Imaging Research Team and the former Molecular Membrane Biology Laboratory (RIKEN) for technical supports, insightful discussion, and sincere encouragement.

At last, I would like to thank all the Lab members, especially Dr. Emi Ito and Dr. Kazuo Ebine, for generous and wide-ranging supports throughout the years.

Abbreviations

BFA	brefeldin A
ER	endoplasmic reticulum
ERES	ER exit site(s)
ERGIC	ER-Golgi intermediate compartment
GEF	guanine nucleotide exchange factor
GFP	green fluorescent protein
LatB	latrunculin B
MVE	multivesicular endosome
mRFP	monomeric red fluorescent protein
SCLIM	super-resolution confocal live imaging microscopy
TIRFM	total internal reflection fluorescence microscopy
YFP	yellow fluorescent protein

Chapter 1

General Introduction

Eukaryotic cells have a variety of intracellular organelles, each of which has a distinct identity and contributes to the efficiency of biochemical reactions. The Golgi apparatus is one of the single-membrane-bounded organelles, and plays essential roles in intracellular trafficking and protein and lipid modification. It was named after Camillo Golgi, who discovered it in the Purkinje cells of the cerebellum using the staining method he had developed (Golgi, 1898). However, because of the absence of sufficient microscopic techniques, the structure was once suspected to be an artefact, and its existence was under a debate for a long time (Beams and Kessel, 1968; Bentivoglio, 1998). After all over the half-century of discussion, the application of electron microscopy finally confirmed its existence (Dalton, 1951), and the fine structure of the Golgi apparatus in vertebrate cells was revealed: concentrically arranged numerous flattened sacs of smooth-surfaced membranes with small vesicles (Dalton and Felix, 1954; Sjöstrand and Hanzon, 1954). Such characteristic structure was soon found also in non-vertebrate organisms including various kind of plants, therefore the Golgi apparatus became to be recognized as an intracellular structure, which is conserved among most eukaryotes (Beams *et al.*, 1956; Beams and Kessel, 1968). Since then, the unique stacked structure of the Golgi apparatus is regarded as one of the biggest features of the organelle.

In each Golgi stack, the cisternae are polarized between the *cis* side, receiving cargo from the endoplasmic reticulum (ER), and the *trans* side, sending cargo forward to post-Golgi organelles (Mellman and Warren, 2000). Along this axis, many glycosylation enzymes for sugar chain

modification on glycoproteins and glycolipids are arranged in specific order. This sequential distribution is thought to mirror the order of glycosylation steps, so that the cargoes are modified sequentially by passing across the Golgi from *cis* to *trans* (Dunphy and Rothman, 1985; Moore *et al.*, 1991). In addition to the glycosylation enzymes, many proteins involved in membrane trafficking such as tethering factors and SNAREs localize to the specific cisternae of the Golgi apparatus (Uemura *et al.*, 2004; Latijnhouwers *et al.*, 2007; Sztul and Lupashin, 2009).

Although most eukaryotes possess stacked Golgi, there are some exceptions. In the budding yeast *Saccharomyces cerevisiae*, the Golgi membranes rarely form stacks and scatter in the cytoplasm as individual cisternae, each of which can be defined as *cis*, medial, and *trans* by the localization of the marker proteins (Preuss *et al.*, 1992; Matsuura-Tokita *et al.*, 2006; Figure 1A). Moreover, in certain parasitic protists, the stacked Golgi structure was never found and thus these species were considered as “Golgi-lacking” organisms (Jékely, 2008; Mowbrey and Dacks, 2009). Because many of such organisms also lack identifiable mitochondria and peroxisomes, they were thought to have evolved very early before the innovation of the Golgi in the early studies (Cavalier-Smith, 1987). However, improved phylogenetic analyses revealed later that they are spread throughout the eukaryotic tree, and each of them is located in the clade of organisms with the stacked Golgi (Mowbrey and Dacks, 2009; Klute *et al.*, 2011). Therefore, the ancestral eukaryote must have had stacked Golgi and the structure has been inherited to most descendants during

evolution, whereas some species such as *S. cerevisiae* have lost the structure secondarily. This indicates that the stacked structure is important for the Golgi function and therefore for better survival of most eukaryotes.

Among the organisms with stacked Golgi, in spite of the conservation of their fine stacked structure at the electron microscopic level, the organization and dynamics of the whole Golgi apparatus are quite different among species. In vertebrate cells, as Camillo Golgi described as “internal reticular apparatus,” the Golgi apparatus typically exhibits a twisted network, which is called the “Golgi ribbon” after its appearance under the light microscope (Golgi, 1898; Wei and Seemann, 2010; Lowe, 2011; Figure 1B). It is closely associated with the centrosome (or microtubule-organizing center; MTOC), which is usually located near the nucleus in non-polarized mammalian cells. The Golgi ribbon consists of many pieces with typical stacked structure (the ministacks), which are centralized by dynein motors along the radial patterned microtubules to be laterally interconnected (Rios and Bornens, 2003). On the other hand in plant cells, the Golgi apparatus consists of numerous, sometimes hundreds of individual stacks of disk-like cisternae, and they are usually dispersed throughout the cytoplasm (Figure 1C). Each unit has a clearly stacked structure and *cis-trans* polarity, which can be confirmed either by the fine architecture under the electron microscope or by the localization of the marker proteins such as glycosylation enzymes and proteins involved in the trafficking machinery (Dupree and Sherrier, 1998; Staehelin and Kang,

2008; Schoberer and Strasser, 2011). The movement of plant Golgi stacks is actomyosin dependent, and exhibits stop-and-go pattern; the Golgi stacks alternate between pause for seconds to minutes and rapid directed movement, for example, up to 7 μm/s in highly vacuolated Arabidopsis root cells (Boevink *et al.*, 1998; Nebenführ *et al.*, 1999; Akkerman *et al.*, 2011; Sparkes, 2011).

The unique stacked structure of the Golgi apparatus attracts many biologists, and its biogenesis process has been studied for a variety of cells. Especially some parasitic protozoa have only one Golgi stack per cell, which makes it easy to track the behaviors of the single Golgi. For example, in *Trichomonas*, the Golgi stack elongates laterally and undergoes medial fission before mitosis, and the fission appears to occur from *trans* to *cis* direction in electron microscopy (Benchimol *et al.*, 2001). In *Toxoplasma gondii*, similar lateral growth and fission are followed by an additional fission, and the resulting four stacks are partitioned to the daughter cells in pairs. They subsequently coalesce into a single Golgi in each daughter cell (Pelletier *et al.*, 2002). In contrast to these species, the new Golgi stack is formed *de novo* near the old Golgi in *Trypanosoma brucei*. The new stack is supplied with materials not only by the ER but also by the old Golgi (He *et al.*, 2004).

Among the multicellular organisms, mammalian Golgi apparatus disassembles upon mitosis, and reassembles in the daughter cells at telophase. What occurs during Golgi disassembly is still under debate; whether the Golgi cisternae fragment into small vesicles, or the Golgi components

are absorbed into the ER (Zaal *et al.*, 1999; Axelsson and Warren, 2004; Persico *et al.*, 2009). In contrast, the Golgi stacks remain intact all through the cell cycle in plant cells (Dupree and Sherrier, 1998; Nebenführ *et al.*, 2000). Unlike the mammalian cells in which the ER export is arrested during mitosis (Hammond and Glick, 2000), plant cells require active secretion in order to form the cell plate for cytokinesis. Therefore, the Golgi apparatus keeps working to supply new membranes and wall materials (Dupree and Sherrier, 1998). Because the plant Golgi stacks do not disassemble at any stages, they must somehow increase in number during cell cycle. Actually, some reports suggest that the plant Golgi stacks doubles in number prior to cytokinesis (Garcia-Herdugo *et al.*, 1988; Seguí-Simarro and Staehelin, 2006).

In spite of these studies, detailed observation of time-dependent biogenesis process of the Golgi apparatus in living cells is still missing, and the behaviors of each cisterna during stack formation is unclear. Moreover, the molecular mechanisms that govern the formation of the stacked structure are mostly unknown.

In order to study the dynamic behaviors of the Golgi stacked structure, it is necessary to visualize the structure in living cells by light microscopy. *S. cerevisiae* greatly contributed to resolve the molecular mechanisms of intracellular trafficking as a model organism (Schekman, 1992), however, it is impossible to investigate the stacked structure by using it. Although major progress in the Golgi research has been made by using mammalian cells, the complexity of the Golgi ribbon

makes it difficult to observe the stacked structure by light microscopy. By contrast, thanks to the simple and elegant structure, the Golgi stacking can be easily studied by light microscopy in plant cells. The morphological features of the plant Golgi provide a great advantage for detailed analysis of the stacked structure by live imaging (Ito *et al.*, in press).

To discuss the formation of the Golgi structure, the long-lasting debate about intra-Golgi trafficking cannot be skipped (Glick and Nakano, 2009; Nakano and Luini, 2010; Glick and Luini, 2011). It is about how cargo molecules are transported through the Golgi stack. Among many models proposed, two major models were the issue of dispute; one is the vesicular transport (stable compartments) model, and the other is the cisternal maturation model. In the vesicular transport model, the Golgi stack is viewed as a series of distinct suborganelles, each of which has a characteristic set of resident proteins. Cargo molecules travel from one cisterna to the next by anterograde COPI vesicles, and the Golgi resident proteins remain in the cisterna by exclusion from the vesicles (Figure 2A). On the other hand, in the cisternal maturation model, the Golgi cisternae themselves are thought as the cargo carriers, which are transient and continuously turn over. Homotypic fusion of ER-derived COPII vesicles nucleates the new *cis*-cisternae, which progress forward along the secretory pathway. The Golgi resident proteins are recycled from later to earlier cisternae by retrograde COPI vesicles, and the nature of the cisternae gradually changes into that of

the later cisternae (maturation; Figure 2B).

Recent data from *S. cerevisiae* by high-resolution confocal microscopy have revealed that the protein components in a single cisterna change from *cis*-Golgi proteins to *trans*-Golgi proteins over time, giving a strong support for cisternal maturation (Losev *et al.*, 2006; Matsuura-Tokita *et al.*, 2006). Detailed morphological studies by electron tomography of many kinds of cells with stacked Golgi also support the cisternal maturation model (Mogelsvang *et al.*, 2003; Storrie *et al.*, 2012; Donohoe *et al.*, 2013). Therefore, the basic concept of the cisternal maturation model appears to be more widely accepted now. However, there are also some conflicting data to the model (Orci *et al.*, 2000; Cosson *et al.*, 2002; Kweon *et al.*, 2004; Patterson *et al.*, 2008). Recently, two studies using similar procedures reported completely opposite results; one supported the cisternal maturation, and the other did not (Lavieu *et al.*, 2013; Rizzo *et al.*, 2013). The debate is still going on, and further investigations are needed.

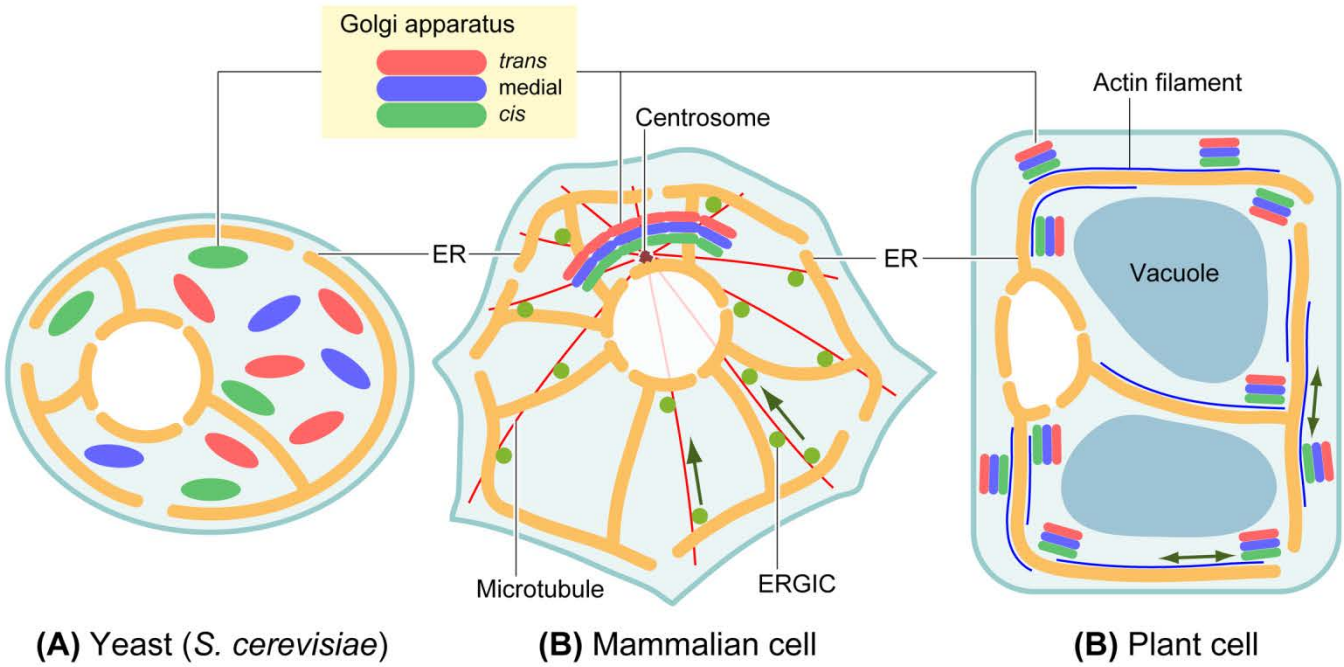

Figure 1. Comparison of the Golgi organization among eukaryotes.

(A) In *S. cerevisiae*, the Golgi apparatus rarely forms stacks, and individual *cis*, medial, and *trans* cisternae scatter in the cytoplasm.

(B) In mammalian cells, microtubules are organized in a radial pattern around the centrosome. The Golgi stacks are centralized by dynein motors on the microtubules and interconnected to form the Golgi ribbon. ERGIC is formed near the ER, and ERGIC itself or transport vesicles from it travel to the Golgi ribbon along the microtubules.

(C) In plant cells, individual Golgi stacks with clearly stacked structure are spread in the cytoplasm. Actin filaments are often arranged along the ER, and the Golgi stacks move on them by myosin motors.

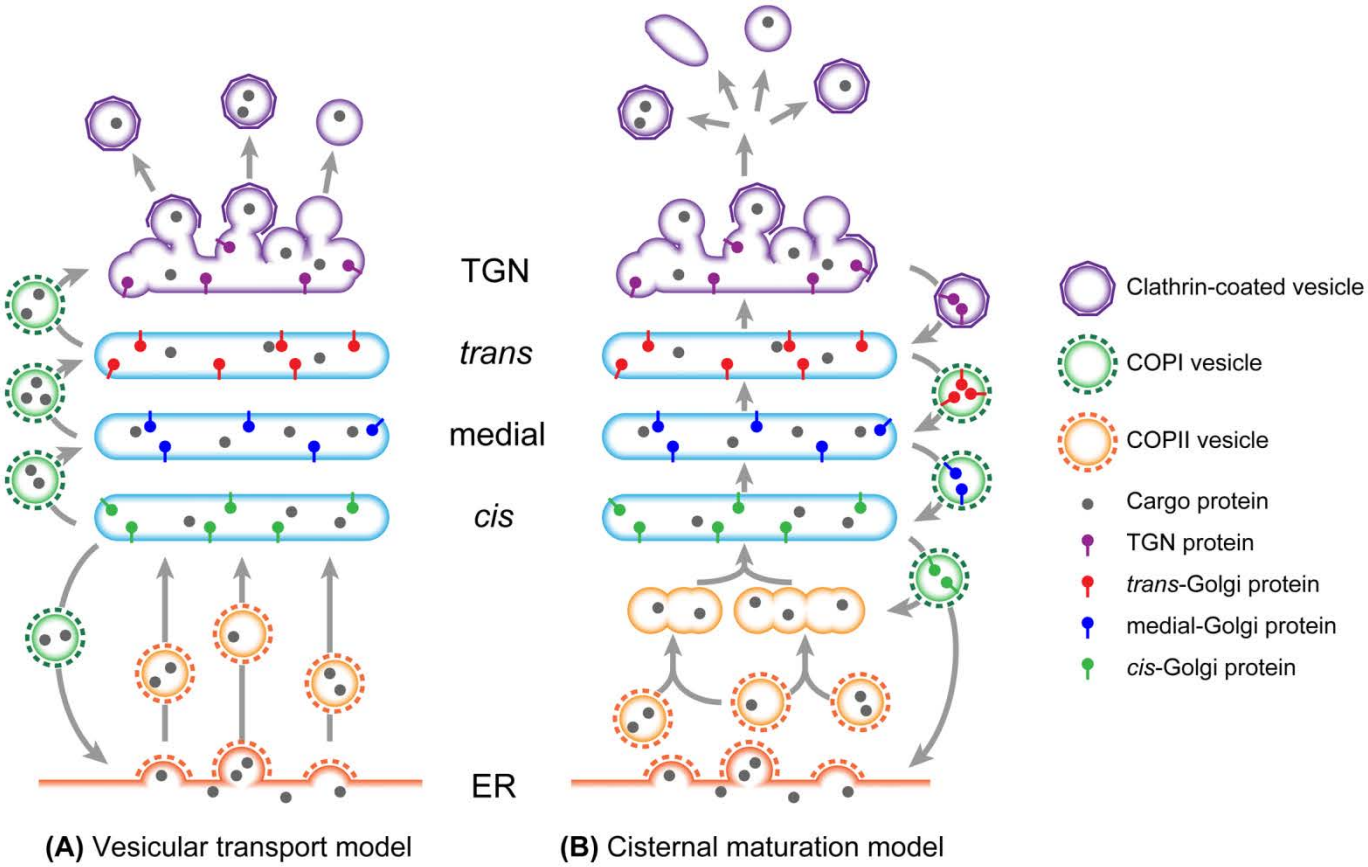

Figure 2. Two major models for intra-Golgi trafficking.

(A) The vesicular transport (stable compartments) model. In this model, the Golgi cisternae are stable and distinct suborganelles with different resident proteins. Cargo proteins are transported from one cisterna to the next by anterograde COPI vesicles, whereas the Golgi proteins are excluded from them and remain in the cisternae. Cargo proteins reach the TGN and exit by clathrin-coated vesicles or other carriers.

(B) The cisternal maturation model. In this model, the Golgi cisternae themselves function as the cargo carriers. They are transient compartments that are newly formed by homotypic fusion of COPII vesicles, progress from *cis* to *trans*, and break down at the TGN stage. The Golgi proteins recycle back from later to earlier cisternae by retrograde COPI vesicles, and the nature of the cisternae gradually changes as they progress.

Chapter 2

cis-Golgi proteins accumulate near the ER exit sites and act as the scaffold for Golgi regeneration after brefeldin A treatment in plant cells

Introduction

The transport between the ER and the Golgi apparatus is thought to be achieved mainly by COPI and COPII vesicles. COPI vesicles act in Golgi-to-ER retrograde trafficking, and COPII vesicles act in the opposite ER-to-Golgi anterograde rout (Mellman and Warren, 2000; Brandizzi and Barlowe, 2013). COPI vesicles are also believed to function in intra-Golgi transport between cisternae, whereas the transport direction is still controversial between the two intra-Golgi transport models (Glick and Nakano, 2009; Nakano and Luini, 2010; Glick and Luini, 2011; Figure 2). Formation of COPI and COPII vesicles is regulated by small GTPases ARF1 and SAR1, respectively. The two GTPases cycle between GDP-bound inactive cytosolic state and GTP-bound active membrane-anchored state, and their activation is necessary for recruitment of coat proteins on the membranes. This activation step is catalyzed by specific guanine nucleotide exchange factors (GEFs) (Sato and Nakano, 2007; Popoff *et al.*, 2011).

Brefeldin A (BFA), an antibiotic compound produced by fungi, is known as a potent inhibitor of GEFs for ARF1 (Donaldson *et al.*, 1992; Helms and Rothman, 1992). ARF GEFs are characterized by a conserved Sec7 catalytic domain, and BFA is hypothesized to bind between ARF1-GDP and the Sec7 domain to stabilize abortive ARF1-GDP:BFA:Sec7 domain complex (Chardin and McCormick, 1999; Jackson and Casanova, 2000). In mammalian cells, BFA treatment

has been shown to cause the release of ARF1 and COPI coats from the Golgi membranes, and subsequent disassembly of the Golgi apparatus with Golgi resident enzymes being absorbed into the ER (Fujiwara *et al.*, 1988; Lippincott-Schwartz *et al.*, 1989; Donaldson *et al.*, 1990; Robinson and Kreis, 1992; Scheel *et al.*, 1997). Such effects by BFA treatment are reversible; the Golgi apparatus regenerates and recovers its functions after removal of the compound (Lippincott-Schwartz *et al.*, 1989; Alcalde *et al.*, 1992).

Similar effects of BFA have also been reported for tobacco and Arabidopsis cultured cells (Takeuchi *et al.*, 2000; Ritzenthaler *et al.*, 2002; Takeuchi *et al.*, 2002). In tobacco BY-2 cells, hybrid structures of the ER and the Golgi stacks have been observed upon BFA treatment by electron microscopy, which indicates direct fusion of the two organelles (Ritzenthaler *et al.*, 2002). The absorption of the Golgi proteins to the ER is proposed to be caused by this fusion. This phenomenon is hypothesized to be due to Golgi accumulation of the SNARE proteins responsible for fusion of Golgi derived COPI vesicles to the ER, whereas there is no experimental support.

In this study, in order to get insights into the mechanisms of Golgi biogenesis in plant cells, I investigated the dynamic behaviors of each cisterna of the Golgi stacks upon BFA treatment and its removal. I have shown that particular membrane proteins located at the *cis*-Golgi cisternae accumulate in small punctate structures upon BFA treatment. After BFA removal, coalescence of these punctate structures initiates the Golgi regeneration, therefore, I propose that the punctate

structures act as the scaffold for Golgi regeneration. Moreover, because the *cis*-Golgi protein which localizes to the punctate structures upon BFA treatment has been shown to localize at the cisternae nearer to the *cis*-end of the stacks in untreated cells, I suggest that the *cis* most cisternae have special features compared to the later cisternae.

Results

Visualization of the Golgi stacks

To observe the dynamics of each cisterna of the Golgi apparatus in living cells, I established a tobacco BY-2 cell line expressing the *cis*-Golgi marker SYP31 (Qa-SNARE; Uemura *et al.*, 2004) tagged with green fluorescent protein (GFP-SYP31) and the *trans*-Golgi marker ST (the cytoplasmic, transmembrane, and stem regions of rat sialyltransferase; Boevink *et al.*, 1998) tagged with monomeric red fluorescent protein (ST-mRFP). By confocal laser scanning microscopy, many dual-colored punctate structures were observed (Figure 3A), and they were moving actively in the cytoplasm. The fluorescence of GFP and mRFP were located side by side with partial overlap, which was apparent from the fluorescence profile across the structure (Figure 3B). These dual-colored punctate structures are typical images of the Golgi stacks. Because overexpression of a similar construct was reported to perturb the endomembrane system (Bubeck *et al.*, 2008), the effects of overexpression of GFP-SYP31 were carefully assessed by looking at localization patterns of the markers of the later compartments of the secretory pathway: ST-mRFP and mRFP-VAM3 (Qa-SNARE of the vacuole; Uemura *et al.*, 2004). In my experimental system, GFP-SYP31 did not affect the normal localization of the marker proteins (Figure 3 and 4).

Behaviors of SYP31 and ST upon BFA treatment

I first observed the dynamics of the Golgi stacks upon BFA treatment in the cells expressing GFP-SYP31 and ST-mRFP. As previously reported (Saint-Jore *et al.*, 2002), ST-mRFP relocalized to the ER membrane after BFA treatment (Figure 5A). This relocation of ST-mRFP was confirmed by observation of BY-2 cells expressing the ER luminal marker SP-GFP-HDEL (Takeuchi *et al.*, 2000) with ST-mRFP (Figure 6). On the other hand, GFP-SYP31 localized to punctate structures, which were smaller in size and larger in number compared with the *cis*-Golgi cisternae in untreated cells (Figure 5A). These punctate structures of GFP-SYP31 were also different in their shape from the untreated *cis*-Golgi cisternae; they were small dot-like structures, whereas GFP-SYP31 resided on the flat, disk-like structures in untreated cells. A similar result was obtained when BFA treatment was performed with cycloheximide, a protein synthesis inhibitor (Figure 7).

In addition to the major relocalization to the punctate structures, GFP-SYP31 signal seemed to increase slightly in the cytoplasm by BFA treatment (Figure 5A). Because SYP31 is a membrane protein, the cytosolic GFP signal may arise from tiny membrane vesicles. To test this possibility, I performed total internal reflection fluorescence microscopy (TIRFM), which enables selective visualization of sample surface regions with high resolution and high signal-to-noise ratio (Fujimoto *et al.*, 2007; Konopka and Bednarek, 2008). TIRFM detected many small punctate GFP signals in BFA-treated cells but only a few in control cells (Figure 5B).

For detailed investigation of the behaviors of the Golgi cisternae upon BFA treatment, I performed time-lapse observation. First (at 10 min after BFA addition), the double-colored Golgi stacks began to congregate and coalesce into several aggregates in the cytoplasm (Figure 8A). Subsequently, the aggregates gradually disassembled; GFP-SYP31 relocated to the small punctate structures, whereas ST-mRFP was absorbed into the ER membrane (Figure 8A). GFP-SYP31 and ST-mRFP in each aggregate seemed to disperse almost simultaneously from 20 to 25 min after BFA addition (Figure 8B). These results indicate that the disassembly of the Golgi apparatus by BFA treatment follows formation of Golgi aggregates, and that *cis*- and *trans*-Golgi components show different behaviors subsequently.

Distinct behaviors of the* cis-*Golgi markers upon BFA treatment

Next, I observed the behaviors of another *cis*-Golgi protein, RER1B. RER1B is a homolog of yeast Rer1, which is responsible for retrieving a subset of ER membrane proteins from the Golgi to the ER by recognizing the transmembrane region (Sato *et al.*, 1995; Sato *et al.*, 2001; Sato *et al.*, 2003). There are three Rer1 homologs in Arabidopsis (RER1A, RER1B, and RER1C), and RER1B can complement yeast *rer1* deletion the best among them (Sato *et al.*, 1999). I established BY-2 cells expressing GFP-RER1B and ST-mRFP and observed them by confocal microscopy. The fluorescence pattern of GFP-RER1B and ST-mRFP was similar to that of GFP-SYP31 and ST-mRFP

in control and BFA-treated cells (Figure 9A). GFP-RER1B was distributed to small punctate structures similarly to GFP-SYP31. To examine whether the punctate structures of GFP-RER1B were identical to those of GFP-SYP31 observed upon BFA treatment, I observed a BY-2 cell line expressing GFP-RER1B and mRFP-SYP31. After BFA treatment, the two *cis*-Golgi markers colocalized almost completely on small punctate structures (Figure 9B). Thus, SYP31 and RER1B appear to share the common sensitivity to BFA.

In contrast, another *cis*-Golgi protein, ERD2 tagged with GFP, responded to BFA in a distinct manner from the former two *cis*-Golgi proteins. ERD2 protein is a Golgi receptor of ER proteins, first identified in yeast, and acts in retrieval of KDEL-harboring proteins from the Golgi apparatus to the ER (Lewis *et al.*, 1990; Semenza *et al.*, 1990). Homologs of ERD2 are widely conserved among eukaryotes, and Arabidopsis ERD2 has been shown to complement the yeast *erd2* deletion mutant and localize to the Golgi apparatus in Arabidopsis and tobacco cells (Lee *et al.*, 1993; Boevink *et al.*, 1998; Takeuchi *et al.*, 2000; Saint-Jore *et al.*, 2002; Takeuchi *et al.*, 2002). In BY-2 cells coexpressing ERD2-GFP and ST-mRFP, ERD2-GFP localized side-by-side with ST-mRFP (Figure 10A). Upon BFA treatment, ERD2-GFP redistributed to the ER, colocalizing with ST-mRFP after formation of aggregates (Figure 10B). This behavior was clearly different from the other *cis*-Golgi markers described earlier (compare Figure 10B with Figures 5A and 9A). Thus there appear to be at least two types of *cis*-Golgi membrane proteins: one relocates to the ER membrane,

and the other localizes to small punctate structures by BFA treatment.

In order to know what makes ERD2 behave differently from SYP31 and RER1B, I performed detailed observation of intra-Golgi localization of ERD2. By triple-color imaging of GFP-SYP31, ST-mRFP, and ERD2-YFP in BY-2 cells, I found that ERD2 showed slightly different localization from SYP31 (Figure 11A). The peak of the fluorescent signal of ERD2-YFP located between those of GFP-SYP31 and ST-mRFP, which indicates that ERD2 mainly localizes to the cisternae nearer to the *trans*-side than SYP31 (Figure 11B).

intra-Golgi localization of AtCASP and behaviors upon BFA treatment

To gain further insight into the behavior of the Golgi stacks, I searched for a Golgi-resident protein with a property different from the aforementioned Golgi markers. The Golgi proteins that are not solubilized by detergent are called “Golgi matrix,” and they are thought to function in membrane tethering and maintenance of the Golgi structure (Slusarewicz *et al.*, 1994; Nakamura *et al.*, 1995; Barr *et al.*, 1998). In plant cells, a zone surrounding the Golgi stack and the TGN, from which ribosomes are excluded, has been reported by electron microscopic observations (Staehelin *et al.*, 1990; Staehelin and Kang, 2008). This “ribosome-exclusion zone” is thought to be occupied by the Golgi matrix. AtCASP, which was identified based on similarity to human AtCASP in transmembrane region, is one of the putative Golgi matrix proteins of Arabidopsis (Renna *et al.*,

2005). It has been shown to localize to the Golgi cisternal rims in tobacco leaf cells (Latijnhouwers *et al.*, 2007). In BY-2 cells, I could observe similar ring-shaped signals by expressing YFP-AtCASP (Figure 12A). When coexpressed with GFP-SYP31 and ST-mRFP, YFP-AtCASP localized mainly at intermediate cisternae between GFP-SYP31 and ST-mRFP with partial overlap (Figure 12B). The peak of YFP fluorescence located between those of GFP and mRFP along the stack (Figure 12C).

BFA treatment resulted in relocalization of most of the YFP-AtCASP fluorescence to the ER, and a very weak signal was observed on the punctate structures of GFP-SYP31 (Figure 13). In time-lapse observation, YFP-AtCASP and ST-mRFP behaved in a similar time course. At 20 min after BFA treatment, YFP-AtCASP and ST-mRFP were absorbed into the ER membrane, whereas GFP-SYP31 relocated to the small punctate structures (Figure 13).

Disassembly of the Golgi stacks by BFA treatment without actin filaments

To examine whether actin filaments play roles in disassembly of the Golgi upon BFA treatment, I observed the effects of BFA under an actin-depolymerizing condition. With the actin-depolymerizing reagent latrunculin B (LatB), actin filaments visualized with Lifeact-Venus disappeared almost completely by 10 min in BY-2 cells (Figure 14A). After incubating the BY-2 cells expressing GFP-SYP31 and ST-mRFP with LatB for 30 min, I added BFA and performed time-lapse observation of the Golgi apparatus. I found no substantial differences in the response of

the Golgi markers to BFA treatment between LatB-treated and control cells (Figure 14B). Thus I concluded that the response of the Golgi stacks to BFA was independent of actin filaments.

Golgi regeneration after BFA removal

To observe the process of Golgi regeneration, I washed out BFA after 2 h of treatment and chased the behaviors of the Golgi markers. In BY-2 cells coexpressing GFP-RER1B and ST-mRFP, ST-mRFP that had been localized to the ER gradually formed punctate structures probably as cisternae, and GFP-RER1B accompanied these regenerated cisternae (Figure 15). At 2 h after BFA removal, most of the mRFP signal in the ER was relocalized to the Golgi cisternae (Figure 15).

Next, I treated the cells expressing GFP-SYP31 and ST-mRFP with LatB to stop the movement of the organelles during Golgi regeneration, so that the detailed processes of the regeneration could be observed. LatB was added to the cell suspension 30 min before BFA removal, and the regeneration of the Golgi stacks was observed in the presence of LatB and cycloheximide to avoid the involvement of newly synthesized Golgi marker proteins. The time-lapse observation revealed that the punctate structures of GFP-SYP31 gathered first, and subsequently ST-mRFP became concentrated at the structures (Figure 16A and C). The numbers of the punctate structures of GFP-SYP31 were compared between short (0 h) and long (3 h) times after BFA removal. It decreased to about half in 3 h (39 dots at 0 h and 18 dots at 3 h). On the other hand, the average of

the longest diameter of each dot increased by 200 nm (750 nm at 0 h and 960 nm at 3 h; Figure 16B).

In the cells expressing GFP-SYP31, ST-mRFP, and YFP-AtCASP, I found that YFP-AtCASP accumulated to the punctate structures of GFP-SYP31 before ST-mRFP did after BFA removal (Figure 17). These results presumably indicate that small punctate structures bearing GFP-SYP31 reassembled after BFA removal to generate the *cis*-Golgi cisternae, and the regeneration proceeded in a *cis*-to-*trans* order.

Relationship between the punctate structures and the ERES

COPII vesicles are known to bud from specialized domains of the ER membrane called transitional ER (tER) or ER exit/export sites (ERES). In mammal and yeast cells, the COPII coat components have been revealed to be enriched in the ERES by immunoelectron microscopy, therefore, the COPII components became convenient markers for the ERES (Orci *et al.*, 1991; Kuge *et al.*, 1994; Paccaud *et al.*, 1996; Rossanese *et al.*, 1999). By immunofluorescence imaging or live imaging using fluorescent-protein-tagged COPII components, the ERES appear as multiple discrete puncta (Rossanese *et al.*, 1999; Hammond and Glick, 2000; Horton and Ehlers, 2003; Okamoto *et al.*, 2012).

I considered it likely that the small puncta with GFP-SYP31 and GFP-RER1B observed

after BFA treatment were the ERES. To test this possibility, I visualized the ERES by one of the COPII coat proteins SEC13 tagged by YFP, the similar construct used successfully to visualize yeast ERES (Rossanese *et al.*, 1999; Okamoto *et al.*, 2012). In BY-2 cells, SEC13-YFP was observed in the cytosol, on the nuclear envelope in medial optical sections, and on many dot-like structures in confocal sections near the plasma membrane (Figure 18A). The distribution on the nuclear envelope is consistent with previous reports because SEC13 is also a member of the nuclear pore complex (Siniossoglou *et al.*, 1996; Alber *et al.*, 2007). Thus focusing at the cell periphery is appropriate to observe only the ERES. I established a cell line coexpressing SEC13-YFP, GFP-SYP31, and ST-mRFP and examined spatial relationship between these markers. The Golgi stacks were closely associated with the SEC13 dotty signals (Figure 18B). The number of the SEC13 spots was larger than that of the Golgi stacks, and there were SEC13 spots that were free from the Golgi stacks (Figure 18B, arrows). GFP-SYP31 and SEC13-YFP puncta were localized closer than in the case between ST-mRFP and SEC13-YFP (Figure 18C). This perhaps reflects the role of the *cis*-Golgi cisternae receiving COPII vesicles from the ER. Short-interval time-lapse observation demonstrated that one ERES signal moved together with a Golgi stack (Figure 19). I saw no dissociation of the Golgi from its partner ERES.

In the cells expressing YFP-SEC13 and mRFP-SYP31, the rapid motion of the punctate signals of SEC13-YFP that were not associated with the Golgi stacks was unaffected by LatB

treatment. In contrast, the puncta of SEC13-YFP accompanied by the Golgi stacks stopped together with their partner Golgi (Figure 20A). This result suggests that the SEC13-YFP spots with associated Golgi stacks are the active ERES that are exporting cargo to the Golgi.

Using the cell line expressing SEC13-YFP, GFP-SYP31, and ST-mRFP, I examined the relationship between the ERES and the BFA-induced, SYP31-positive punctate structures. After BFA treatment, ST-mRFP dispersed into the ER membrane, and GFP-SYP31 localized to the small dot-like structures as described earlier. On the other hand, the fluorescent pattern of SEC13-YFP did not substantially change by BFA treatment. Almost all punctate structures of GFP-SYP31 appeared to associate with the SEC13-YFP spots, but these signals did not completely overlap (Figure 21A). I also occasionally observed SEC13-YFP signals without accompanying GFP-SYP31 signals (Figure 21A, arrows). By additional LatB treatment, only the movement of the SEC13 spots associated with SYP31 was sensitive, as was the case of control cells (Figure 20A). Thus the relationship between the SEC13 spots and the punctate structures of SYP31 remained similar before and after the BFA treatment (Figure 21B).

In the cell line expressing only SEC13-YFP, I observed similar LatB-sensitive and LatB-insensitive motions of SEC13 puncta with or without BFA treatment (Figure 20B). These results suggest that it is unlikely that the association between SYP31 and the ERES is caused by SYP31 overexpression.

The relationships between the SYP31 puncta and the ER or the ERES were also examined by using super-resolution confocal live imaging microscope (SCLIM), which enables multicolor observation with extremely high speed and sensitivity (Matsuura-Tokita *et al.*, 2006; Nakano and Luini, 2010; Okamoto *et al.*, 2012; Kurokawa *et al.*, 2013; Suda *et al.*, 2013). The cells expressing GFP-SYP31 and ST-mRFP were observed by SCLIM with optical slices 0.2 μm apart on the *Z*-axis, and the images were reconstructed into three dimensions with deconvolution to achieve high spatial resolution. After BFA treatment, the GFP-SYP31 puncta located very close to the ER labeled by ST-mRFP, but the GFP signal did not entirely overlap with the mRFP signal (Figure 22A). The punctate structures were frequently clinging to the tips of the protruding regions of the tubular ER (Figure 22A, arrowheads). Next the BY-2 cell line expressing SEC13-YFP and mRFP-SYP31 was observed in the same way. In control cells, mRFP-SYP31 signals were closely associated with those of SEC13-YFP, as observed by two-dimensional confocal images (Figure 22B). Moreover, by SCLIM, I found that the signal of SEC13-YFP surrounded the Golgi stacks at the cisternal rims, making ring-shaped fluorescent patterns (Figure 22B). This may suggest that the Golgi stacks interact with the ERES at their cisternal rims. By 3D time-lapse imaging, I observed the Golgi stacks moving together with the SEC13 ring (Figure 23). After BFA treatment, the punctate structures of mRFP-SYP31 were still in the proximity of SEC13-YFP spots without full overlap (Figure 22B). The ring patterns of SEC13-YFP around the Golgi cisternae, which were often observed in control

cells, rarely appeared in BFA-treated cells (Figure 22B).

These results indicate that the punctate structures depicted by GFP-SYP31 after BFA treatment are not the ERES themselves but unique structures existing in the close vicinity to the ERES, which have not been characterized before.

Behaviors of the Golgi proteins in Arabidopsis cells upon BFA treatment

In *Arabidopsis thaliana* root cells, an ARF GEF GNOM-LIKE 1 (GNL1) regulates ER-Golgi trafficking. GNL1 primarily localizes to the Golgi stacks and regulates COPI coat recruitment there (Richter *et al.*, 2007). GNL1 has been shown to be BFA insensitive, and BFA treatment does not cause Golgi disruption in Arabidopsis root cells unlike in mammalian and tobacco cells (Teh and Moore, 2007). However, BFA sensitivity of GNL1 can be engineered by single amino-acid substitution without affecting protein function. In the *gnl1* knockout Arabidopsis plants complemented by BFA sensitive GNL1 (*gnl1/GNL1*^{sens}), a release of COPI coat into the cytosol and an accumulation of ST in the ER upon BFA treatment were reported (Richter *et al.*, 2007).

To examine whether the responses of the *cis*-Golgi proteins observed in tobacco BY-2 cells upon BFA treatment also occur in Arabidopsis root cells, I transformed *gnl*, *gnl1/GNL1*^{sens}, and wild type (Columbia) plants with *GFP-RER1B*. In all of the backgrounds, GFP-RER1B labeled intracellular disk-shaped punctate structures, the typical images of the Golgi stacks (Figure 24). In

wild type root cells, the Golgi stacks visualized by GFP-RER1B made some aggregates by BFA treatment, but they were largely unaffected (Figure 24). In contrast, GFP-RER1B relocalized to many small punctate structures in *gnl1* or *gnl1/GNL1*^{sens} plants upon BFA treatment, which was very similar to its behavior in tobacco BY-2 cells (Figure 24). I also transformed *gnl1/GNL1*^{sens} plants with GFP-SYP31, and a very similar result was obtained (Figure 24). On the other hand, ERD2-GFP expressed in the *gnl1/GNL1*^{sens} plants almost completely relocated to the ER membrane by BFA treatment (Figure 24). These results indicate that the three *cis*-Golgi proteins visualized in Arabidopsis root cells behaved similarly to how they do in tobacco cells upon BFA treatment under the condition that GNL1 is BFA sensitive.

Discussion

BFA responses

BFA provides a nice way to study Golgi organization because in mammalian cells its treatment causes relocation of the Golgi proteins into the ER, and its washout leads to reformation of the Golgi. Similar effects have been observed in plant cells as well (Takeuchi *et al.*, 2000; Ritzenthaler *et al.*, 2002; Saint-Jore *et al.*, 2002; Takeuchi *et al.*, 2002; daSilva *et al.*, 2004; Yang *et al.*, 2005; Hanton *et al.*, 2009; Schoberer *et al.*, 2010; Madison and Nebenführ, 2011). Reversibility of the effects after BFA removal would give a good opportunity to observe Golgi stack reorganization by live imaging. In previous studies on the effects of BFA in plant cells, Ritzenthaler *et al.* (2002) reported that the Golgi stacks in BY-2 cells lost their cisternae in a *cis*-to-*trans* direction by ultrastructural level using electron microscopy. Schoberer *et al.* (2010) looked at tobacco leaf epidermal cells and showed that Golgi markers redistributed to the ER in the *trans*-to-*cis* order by BFA treatment. Madison and Nebenführ (2011) also examined the effect of BFA on Golgi proteins in BY-2 cells. Both *cis*- and *trans*-cisternae fused with the ER upon BFA treatment, but no significant difference was found for different cisternae.

In this study, I perforemed detailed time-lapse observation by high-resolution confocal laser scanning microscopy with short time intervals (30-60 s) and demonstrated that the Golgi stacks

formed aggregates first, and then breakdown of GFP-SYP31 labeled *cis*-cisternae into small compartments and the dispersion of the *trans*-Golgi marker ST-mRFP into the ER occurred almost at the same time. The reason for the difference from previous studies is unknown, but the resolution in time and space of microscopic observation could be a critical factor. My data clearly indicate that the collapse of *cis*- and *trans*- cisternae by BFA occurs almost at the same time after the aggregation of Golgi apparatus in tobacco BY-2 cells.

Difference among cis-Golgi proteins

In this study, I noticed a difference in the behaviors of the *cis*-Golgi proteins upon BFA treatment. That is, one membrane protein (KDEL receptor ERD2) is almost completely absorbed into the ER, whereas others (Qa-SNARE SYP31/SED5 and retrieval receptor RER1B) shift their localization to novel structures in the vicinity to the ERES. Although they are closely associated with the ERES, their localizations do not completely overlap with the ERES. What do these structures represent?

There are relevant interesting results in the previous work from our laboratory. Takeuchi et al. (2002) examined the effects of the transient expression of dominant mutants of ARF1 on localization of the Golgi proteins (ERD2, RER1B, and SYP31) in tobacco BY-2 and Arabidopsis cultured cells. In summary, the ARF1 constitutive active (GTP fixed) mutant caused ER relocation of

ERD2 and some alteration of Golgi-like punctate structures for RER1B and SYP31. Furthermore, BFA treatment phenocopied the expression of the ARF1 dominant-negative mutant. These results were interpreted as follows. The steady-state localization of the Golgi proteins was shifted to the ER by the blockade of anterograde ER-to-Golgi traffic. The yeast COPI mutants have primary defects in the retrograde Golgi-to-ER traffic, but they are also impaired in the anterograde ER-to-Golgi traffic indirectly (Gaynor and Emr, 1997). This might be true to plant cells, thus the ARF1 mutants relocated ERD2 to the ER. The reason that RER1B and SYP31 were not significantly affected by the ARF1 mutants was explained as due to the difference of timing between the folding of GFP-tagged proteins and invocation of the secondary anterograde block, because a transient expression system was used in this work. ERD2 might be more slowly folded than RER1B and SYP31, so that when the exogenously expressed GFP-ERD2 became fluorescent the secondary ER-to-Golgi blockade was already in effect, whereas earlier-folding RER1B and SYP31 could escape this block. The difference of BFA effect between ERD2 and RER1B/SYP31 was explained similarly.

In revisiting these results, I was surprised to see the reproducibility of the difference between ERD2 and RER1B/SYP31. In the former work, the Golgi structures of RER1B and SYP31 were judged to be slightly or not significantly affected by the ARF1 mutants or by BFA, but the data now seem to indicate that RER1B and SYP31 may be relocated to smaller dotty structures like those I see in the present study. Because I used the cells stably expressing the fluorescent Golgi markers,

the difference is most probably not due to the folding problem. In addition, I could observe the similar difference of the behaviors upon BFA treatment among the *cis*-Golgi proteins in Arabidopsis root cells with BFA sensitive GNL1. These results indicate that these two classes of *cis*-Golgi proteins might have an intrinsic difference in their properties.

By detailed observation in BY-2 cells, I found that the precise intra-Golgi localizations of SYP31 and ERD2 are different; SYP31 localizes at the cisternae nearer to the *cis*-pole than ERD2 does. From this result, I suggest that this difference of intra-Golgi localization might cause the different behaviors of the proteins upon BFA treatment, although I cannot exclude the possibility that some other properties of the proteins affect their behaviors.

Relationship between the Golgi stacks and the ERES

In the cells with discrete Golgi stacks such as *Pichia pastoris*, *Caenorhabiditis elegans*, and *Drosophila melanogaster*, the ERES and the Golgi stacks are almost always associated to form "secretory units" (Rossanese *et al.*, 1999; Kondylis and Rabouille, 2009; Witte *et al.*, 2011). In mammalian cells, although the Golgi stacks are concentrated near the centrosome, microtubule disruption by nocodazole treatment causes fragmentation of the Golgi ribbon into many "ministacks," and the ministacks locate near the ERES like in invertebrate cells (Polishchuk *et al.*, 1999; Hammond and Glick, 2000).

Also in plant cells, many punctate signals can be observed by using COPII coat subunits as markers. However, conflicting results have been reported about the relationship between the ERES and the Golgi stacks. By immunofluorescence observation of COPII coat proteins, the signals have been shown to label many punctate structures greatly outnumbering the Golgi stacks. Some of them were associated with the Golgi stacks, and such signals were often found on the areas of the ER tubules associated with the Golgi stacks. Moreover, by live imaging of tomato SEC13 tagged with GFP in tobacco BY-2 cells, the signal pattern was similar to the immunofluorescence, and the Golgi stacks were associated with the SEC13-GFP signal (Yang *et al.*, 2005). From these data, the "kiss-and-run" model was suggested: the ERES are relatively stable, and the Golgi stacks temporarily associates with them. The ER-to-Golgi transport takes place during their contacting periods (Figure 25A). On the other hand, tobacco SAR1 and Arabidopsis SAR1 and some COPII coat proteins (SEC23, SEC24, and SEC13) fused with fluorescent proteins have been reported to mark puncta associated with the Golgi stacks, without signals independent from the Golgi. The COPII signals moved always with the associated Golgi stacks (daSilva *et al.*, 2004; Stefano *et al.*, 2006; Hanton *et al.*, 2007; Hanton *et al.*, 2008; Hanton *et al.*, 2009). The punctate signals of YFP-SEC24 increased in number and become more definite by expression of the cargo with COPII-dependent ER export motif, indicating the involvement of the puncta of YFP-SEC24 in ER export (Hanton *et al.*, 2007). Moreover, fluorescence recovery after photobleaching (FRAP) analysis

showed that ER-to-Golgi protein transport can occur while the Golgi stacks are moving (daSilva *et al.*, 2004). Therefore, the “secretory unit” model was suggested: the Golgi stacks and the ERES are continuously associated and ER-to-Golgi transport continues during rapid movement (Figure 25B).

My observation demonstrated that SEC13-YFP expressed in BY-2 cells labels many puncta outnumbering the Golgi stacks, and some of them are associated with the Golgi in ring-like shapes surrounding the Golgi rims. Moreover, the SEC13-YFP signals move together with the associated Golgi stacks. From these results, I suggest that the truth is in between the two extreme models (hybrid model, Figure 25C). Some of the ERES are continuously associated with the Golgi stacks, and the others are not. Because the SEC13-YFP puncta without associated Golgi stacks were smaller and extremely mobile independently of actin filaments, I speculate that they become stable and active when they encounter the Golgi stacks.

There is a report suggesting that the COPII signal is not on the ER but in the small gap between the ER and the Golgi in tobacco leaf epidermal cells, which represents the COPII vesicles accumulating at the *cis*-face of the Golgi, not the ERES (Langhans *et al.*, 2012). Therefore, Langhans *et al.* (2012) proposed a difficulty to observe the ERES by using the COPII coat proteins as the markers. However, a most recent study has demonstrated that the localization of one of the Arabidopsis Sec16 homologs largely overlap with those of COPII coat components (Takagi *et al.*, 2013). Yeast Sec16 is a large multi-domain peripheral protein of the ER membrane, and binds to the

COPII components through independent domains for each subunit (Espenshade *et al.*, 1995; Gimeno *et al.*, 1996; Shaywitz *et al.*, 1997). It localizes to the ERES, and is speculated to act as the scaffold for COPII coat assembly at the ERES (Yorimitsu and Sato, 2012). Therefore, I conclude that it is reasonable to use COPII coat components as the ERES marker in plant cells.

Golgi regeneration and intra-Golgi traffic

Golgi regeneration after BFA removal has attracted attention in mammalian research, especially to reveal the mechanisms of Golgi biogenesis and reassembly after mitosis (Seemann *et al.*, 2000; Puri and Linstedt, 2003; Glick and Nakano, 2009). With plants, attempts also have been made by electron microscopy and live-cell imaging to observe the Golgi after BFA removal (Ritzenthaler *et al.*, 2002; Langhans *et al.*, 2007; Schoberer *et al.*, 2010), but time-dependent regeneration processes of the Golgi stacks have not been sufficiently described.

In this study, I performed multicolor time-lapse live-cell imaging with short intervals, which enabled me to analyze detailed behaviors of multiple Golgi membrane proteins in the same cells with the passage of time. From time-lapse confocal images, I found that the punctate structures of the *cis*-Golgi marker GFP-SYP31 gather first, and the *trans*-Golgi marker ST-mRFP concentrates later during Golgi stack regeneration after BFA removal. Furthermore, YFP-AtCASP, which is found by tricolor fluorescence imaging to localize mainly at the cisternae between SYP31 and ST, begins

to concentrate before ST-mRFP does. These results suggest that the Golgi stacks regenerate in the *cis*-to-*trans* order, as reported before in mammalian cells and tobacco leaf epidermal cells (Alcalde *et al.*, 1992; Puri and Linstedt, 2003; Schoberer *et al.*, 2010). This is consistent with the cisternal maturation model, in which a new cisterna is formed at the *cis*-side of the stack by ER-derived carriers and progress from the *cis*- to the *trans*-Golgi pole as it matures (Glick and Nakano, 2009; Nakano and Luini, 2010; Glick and Luini, 2011). The vesicles with SYP31 observed by TIRFM in BFA-treated cells might well be the ER-derived COPII vesicles to form the first cisternae.

The SYP31/RER1B compartment acts as the scaffold for Golgi regeneration

As described here, there are two types of *cis*-Golgi proteins; upon BFA treatment, one (SYP31 and RER1B) localizes to the punctate structures and the other (ERD2) to the ER membrane. By super-high-resolution 3D analysis with SCLIM, I conclude that the punctate structures of SYP31 are in the very close vicinity of the ERES but not the ERES themselves. Because these structures reassemble first to regenerate *cis*-Golgi cisternae after BFA removal, I propose that they function as "seeds" of the Golgi stacks by receiving the materials for *cis*-cisternae. Moreover, because the proteins that localize to the punctate structures upon BFA treatment appear to localize at the *cis*-most cisternae in the steady state, I suggest that the *cis*-most cisternae of the plant Golgi stacks have different BFA sensitivity compared to the later cisternae, which might indicate their special features

and functions (Ito *et al.*, 2012).

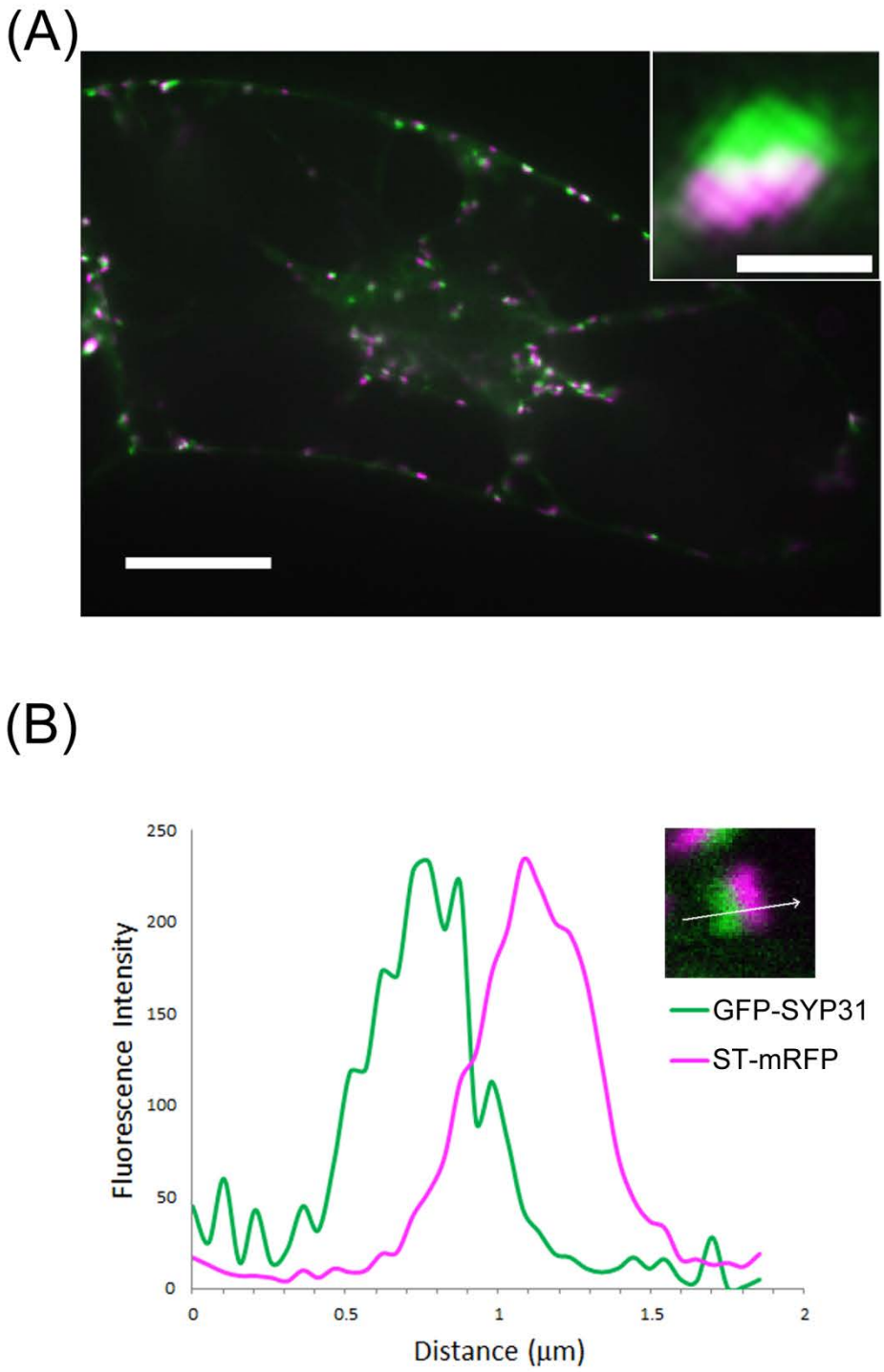

Figure 3. Visualization of the plant Golgi stacks in living cells.

(A) Confocal image of a tobacco BY-2 cell expressing GFP-SYP31 (*cis*-Golgi, green) and ST-mRFP (*trans*-Golgi, magenta). Double-colored dot-like structures represent the Golgi stacks. The insert image shows a higher magnification of a single stack. Scale bar = 20 μm (in the insert; 1 μm).

(B) The fluorescence profile along the arrow across a Golgi stack.

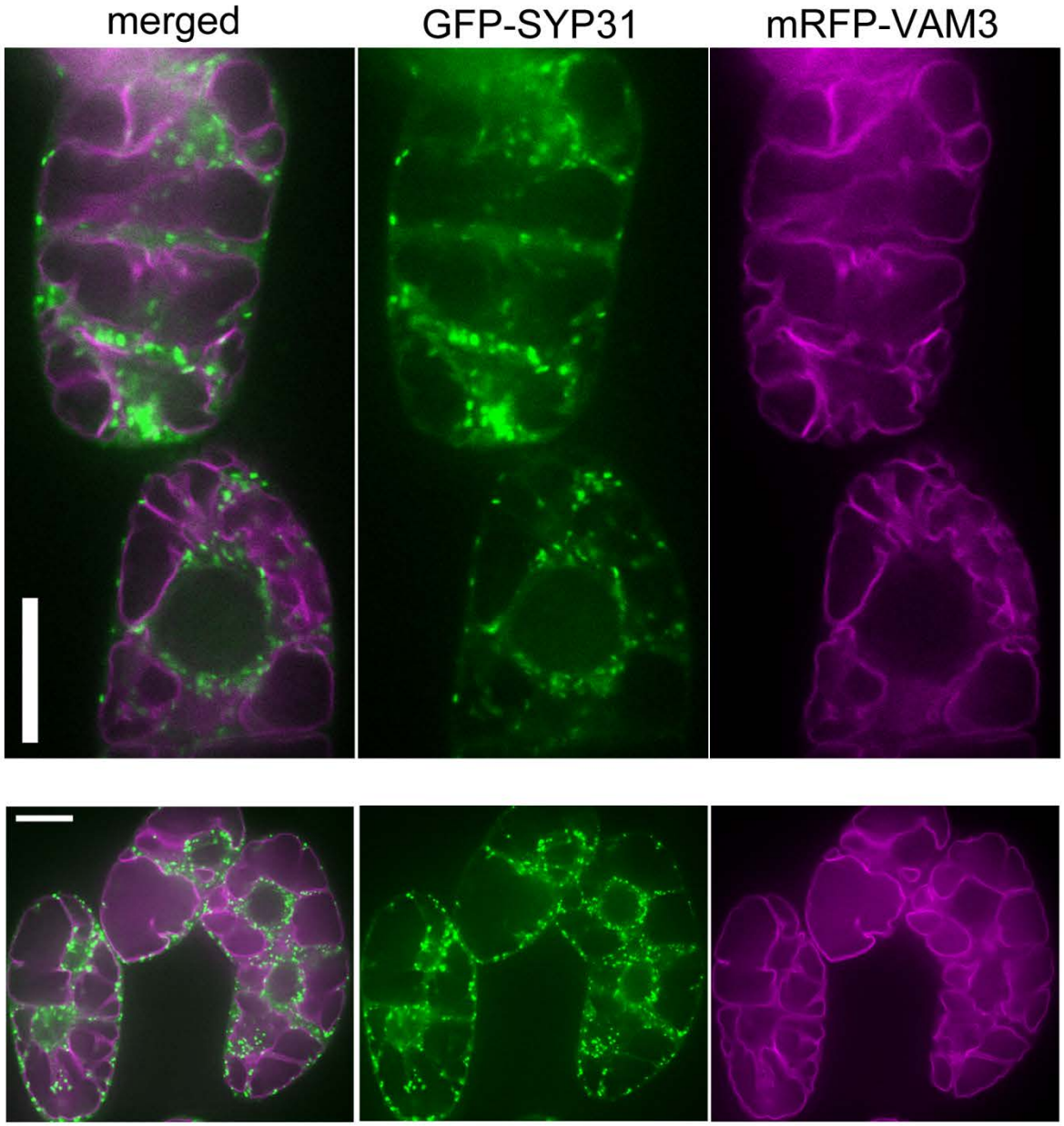

Figure 4. Expression of GFP-SYP31 and the localization of a vacuolar membrane protein.
Confocal images of BY-2 cells expressing GFP-SYP31 (*cis*, green) and mRFP-VAM3 (vacuole, magenta). Scale bars = 20 μm.

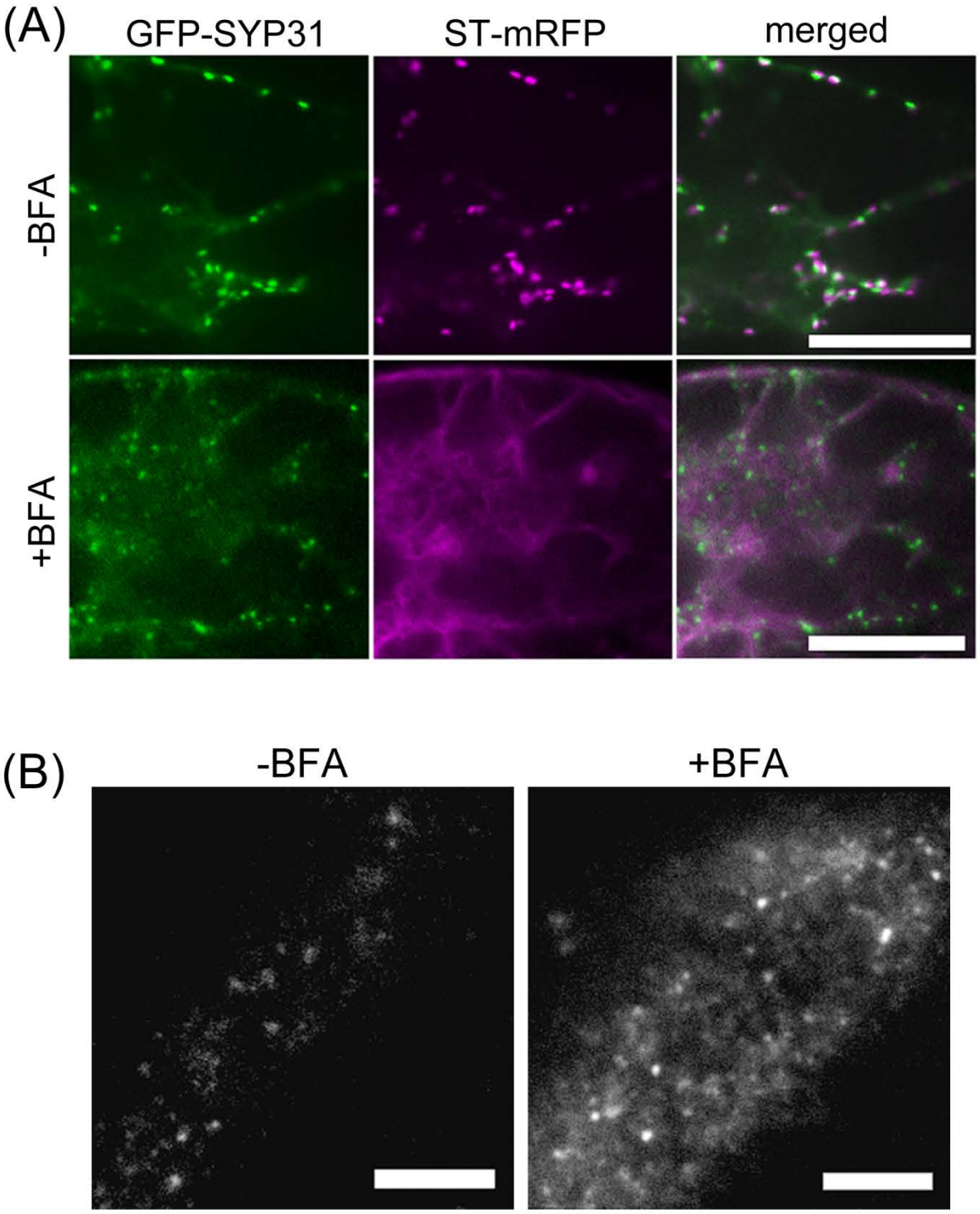

Figure 5. Effects of BFA on GFP-SYP31 and ST-mRFP.

(A) Confocal images of BY-2 cells expressing GFP-SYP31 (*cis*, green) and ST-mRFP (*trans*, magenta). Before BFA treatment (-BFA) and after 2 h of 50 μM BFA treatment (+BFA). Scale bars = 20 μm.

(B) GFP signals in BY-2 cells expressing GFP-SYP31 (*cis*) and ST-mRFP (*trans*) were observed by TIRFM. (Left) Without BFA treatment. (Right) 50 μM BFA treatment for 2 h. Scale bars = 10 μm.

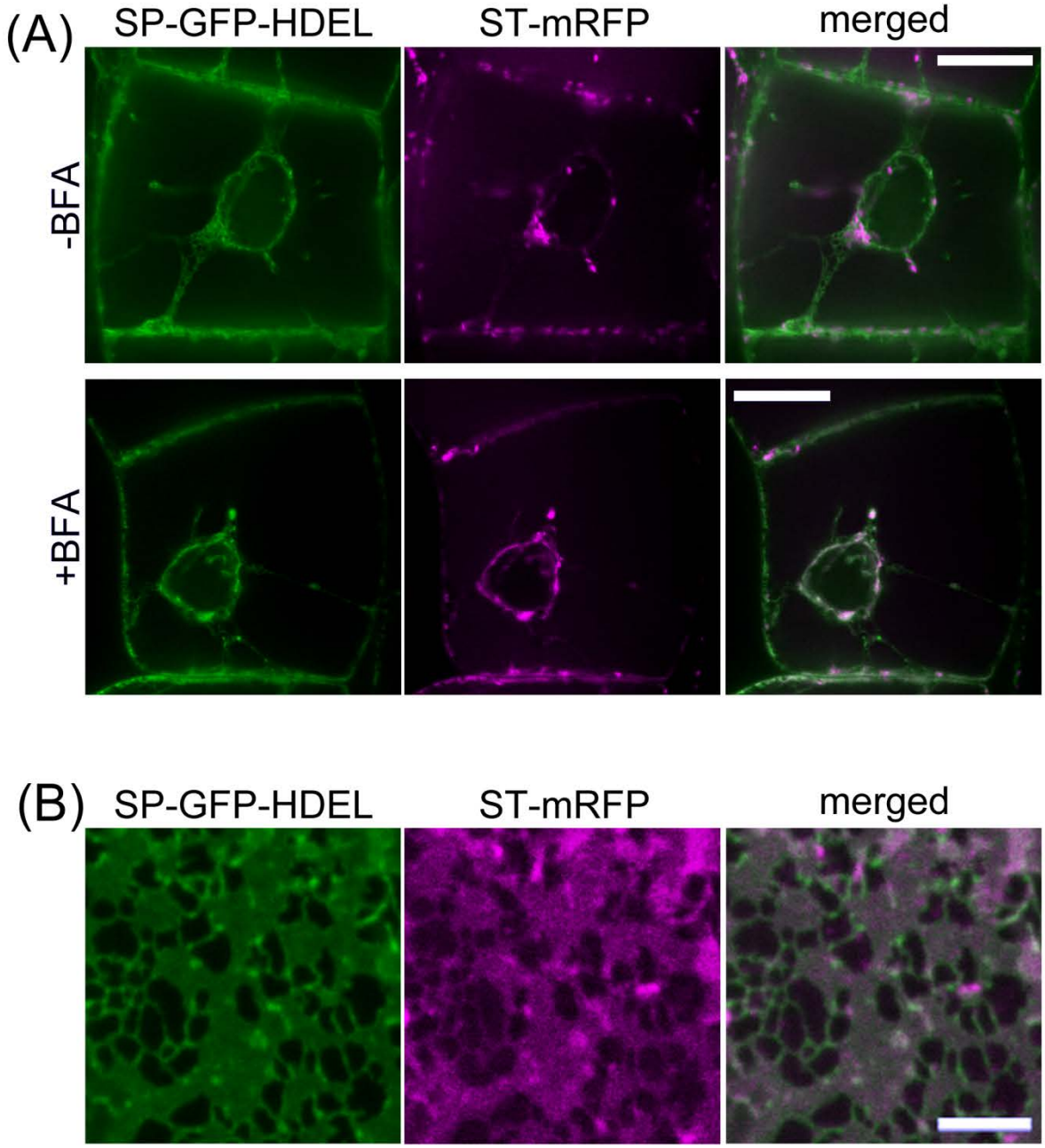

Figure 6. Relocalization of ST-mRFP to the ER.
BY-2 cells expressing SP-GFP-HDEL (ER lumen, green) and ST-mRFP (*trans*, magenta).
(A) Without BFA treatment (-BFA) and with 50 μM BFA treatment for 1.5 h (+BFA). Scale bars = 20 μm.
(B) Confocal image of a BFA treated cell at cell periphery. Scale bar = 5 μm.

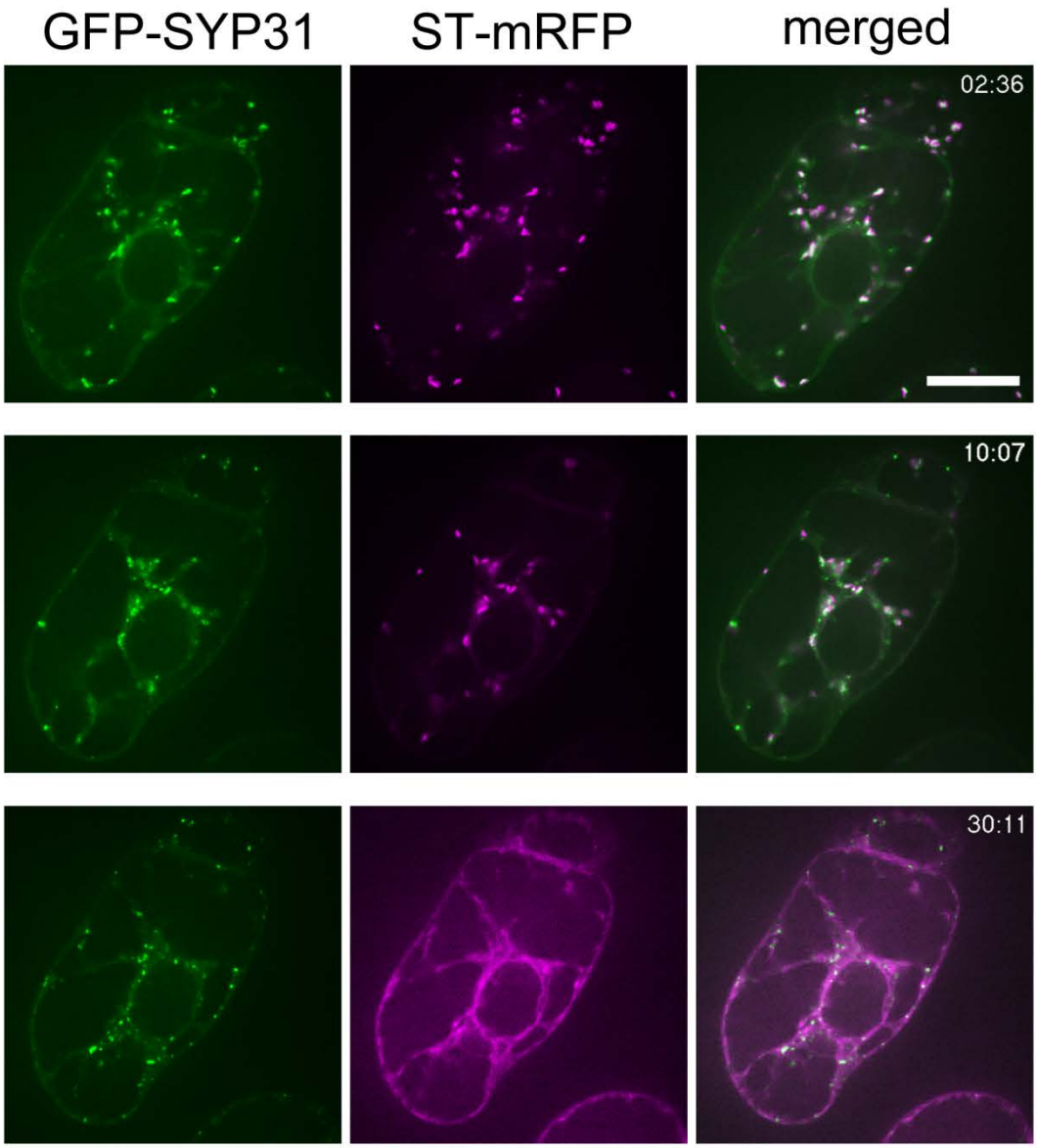

Figure 7. Effects of cycloheximide during BFA treatment.
Time-lapse observations of BY-2 cells expressing GFP-SYP31 (*cis*, green) and ST-mRFP (*trans*, magenta) during BFA treatment. The cells were treated with 100 μM cycloheximide for 30 min prior to the addition of BFA at 50 μM. The indicated times mean the elapsed time after BFA addition (minute:second). Scale bar = 20 μm.

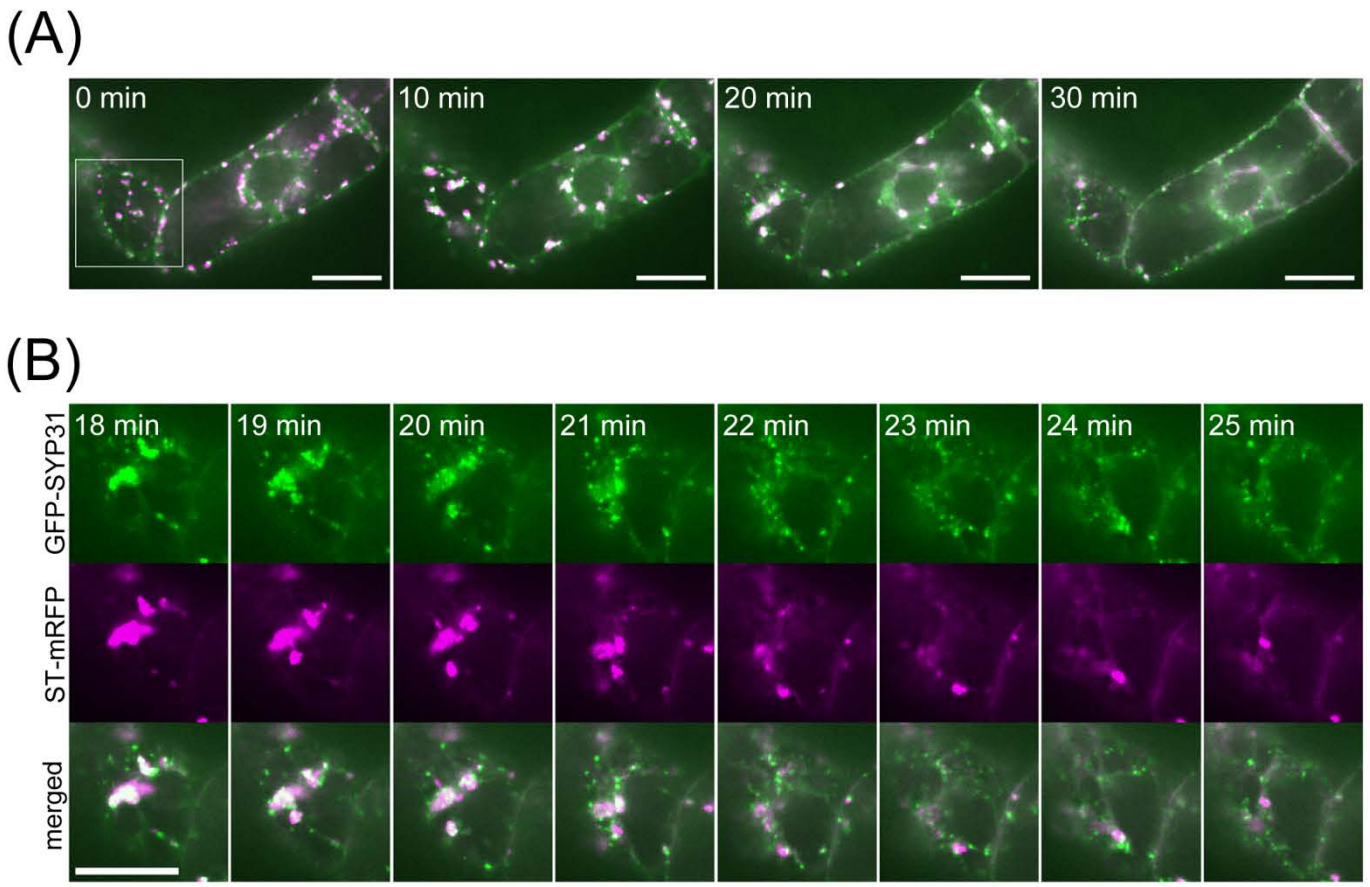

Figure 8. Time-lapse observation of the Golgi disassembly during BFA treatment.

(A) Time-lapse images of BY-2 cells expressing GFP-SYP31 (*cis*, green) and ST-mRFP (*trans*, magenta) during BFA treatment. BY-2 cells were treated with 50 μM BFA, and the fluorescent images were captured at 1-min intervals from just after the addition of BFA. The indicated times mean the elapsed time after the observation was started.

(B) Magnified images of the boxed region in (A).

Scale bars = 20 μm.

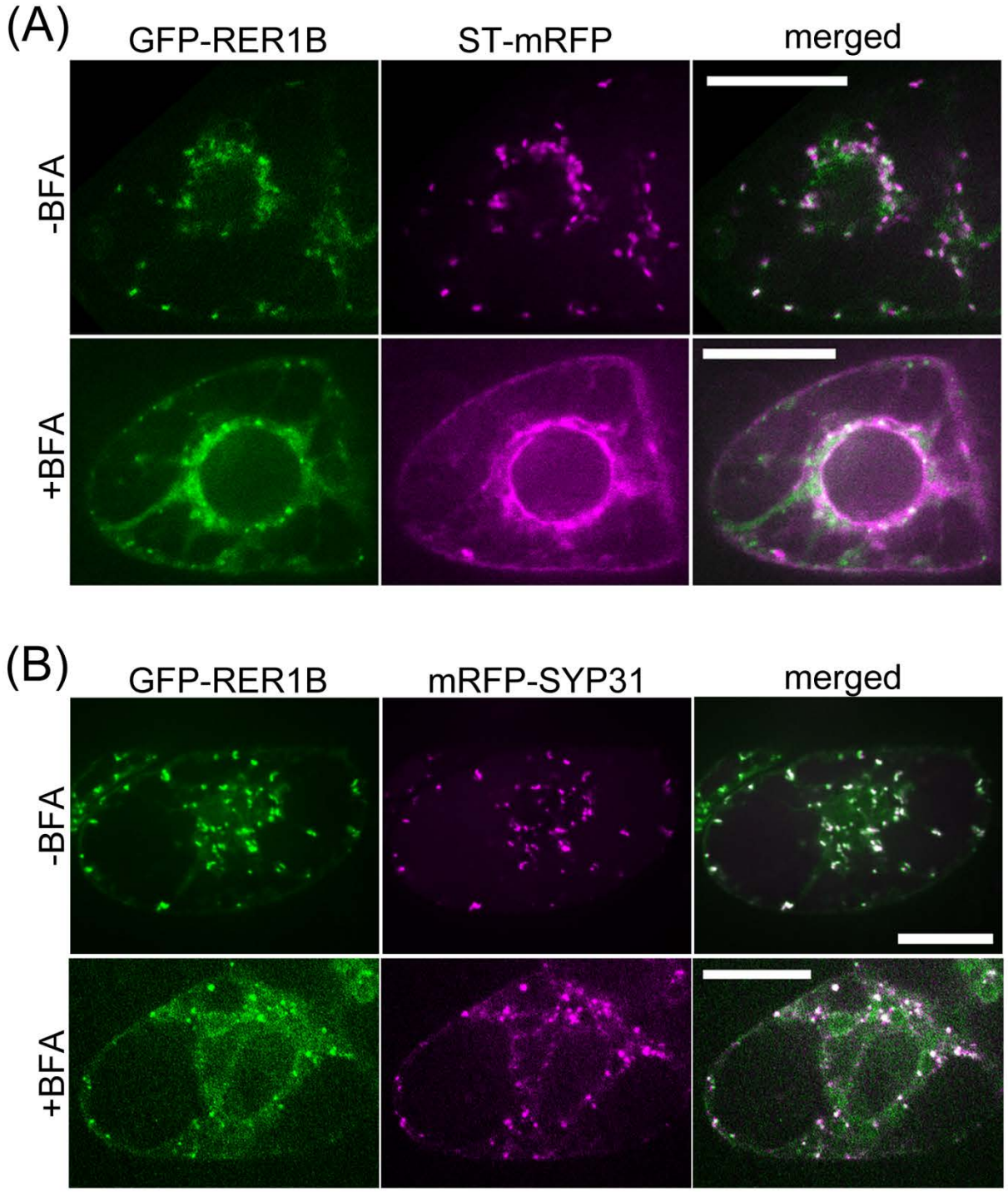

Figure 9. Effects of BFA on GFP-RER1B.

(A) BY-2 cells expressing GFP-RER1B (*cis*, green) and ST-mRFP (*trans*, magenta). Before BFA treatment (-BFA) and after 1.5 h of 50 μM BFA treatment (+BFA).

(B) BY-2 cells expressing GFP-RER1B (*cis*, green) and mRFP-SYP31 (*cis*, magenta). Before BFA treatment (-BFA) and after 1.5 h of 50 μM BFA treatment (+BFA).

Scale bars = 20 μm.

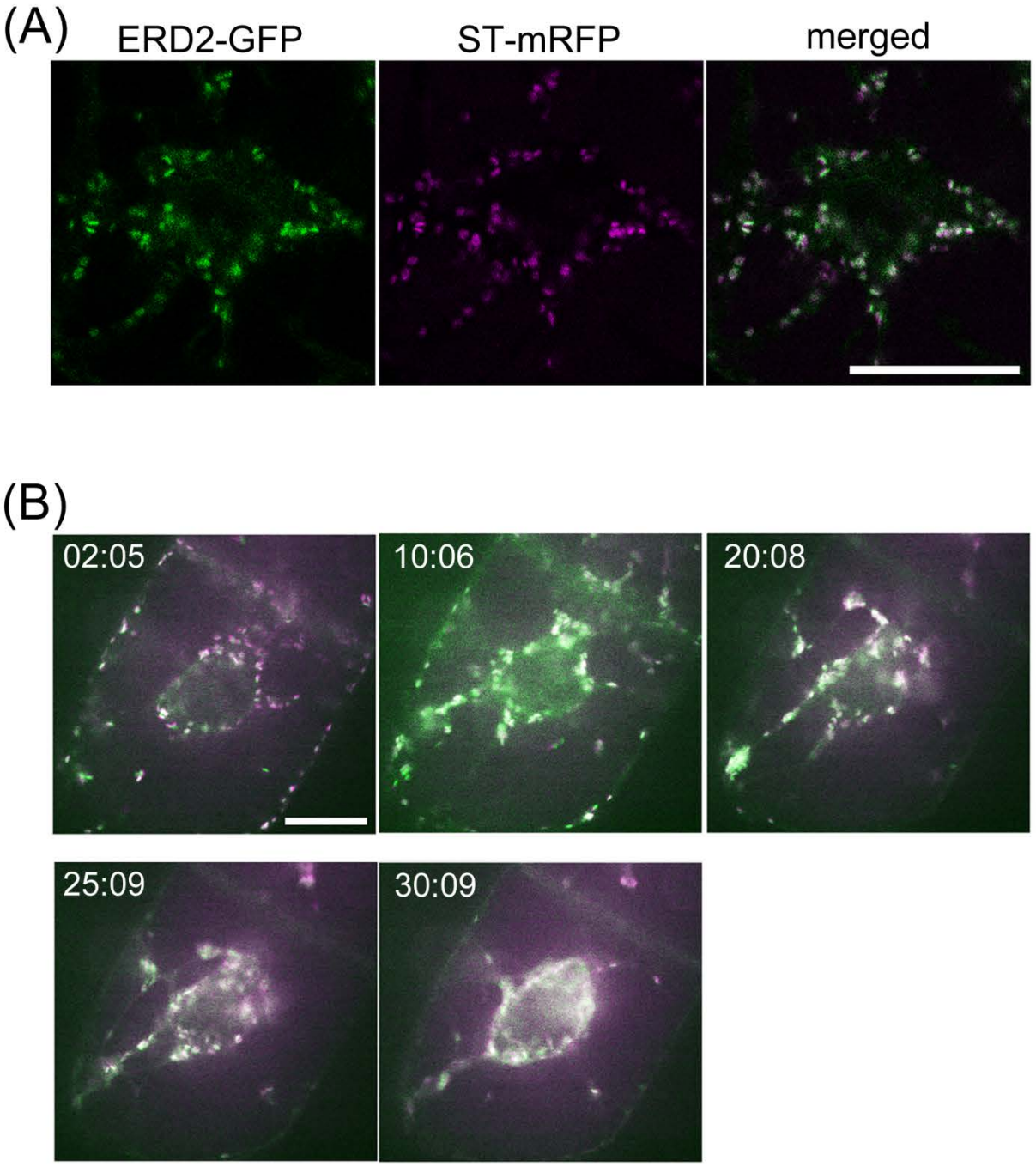

Figure 10. Effects of BFA on ERD2-GFP.

(A) BY-2 cells expressing ERD2-GFP (*cis*, green) and ST-mRFP (*trans*, magenta).

(B) Time-lapse observation of the cells expressing ERD2-GFP and ST-mRFP during BFA treatment. The cells were treated with 50 μM BFA, and the fluorescent images were captured at 30-sec intervals after BFA addition. The indicated times mean the elapsed time after BFA addition (minute:second).

Scale bars = 20 μm.

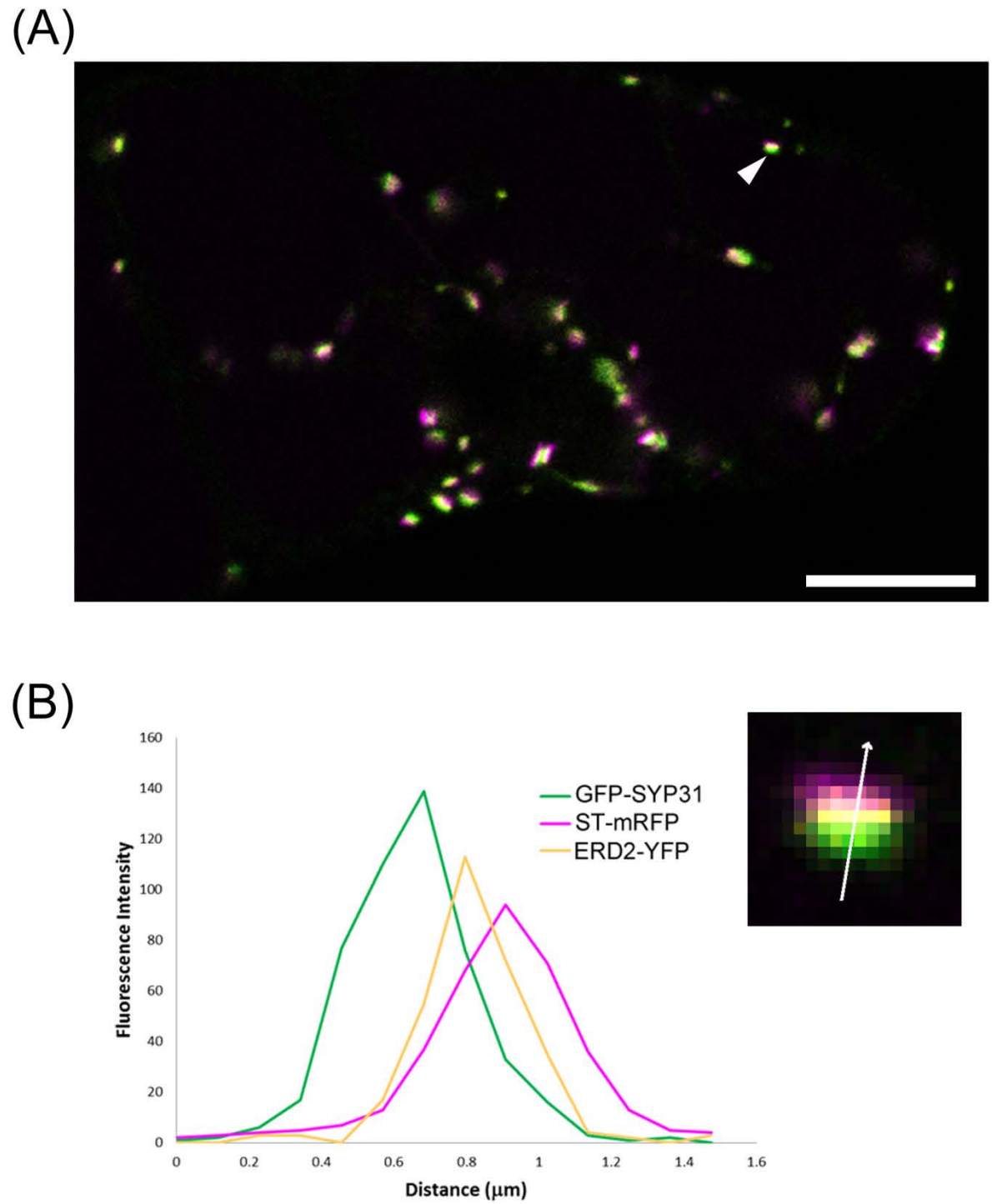

Figure 11. Intra-Golgi localization of ERD2.

(A) A BY-2 cell expressing GFP-SYP31 (*cis*, green), ST-mRFP (*trans*, magenta), and ERD2-YFP (yellow). Scale bar = 20 μm.

(B) The fluorescence profile along the arrow across a Golgi stack.

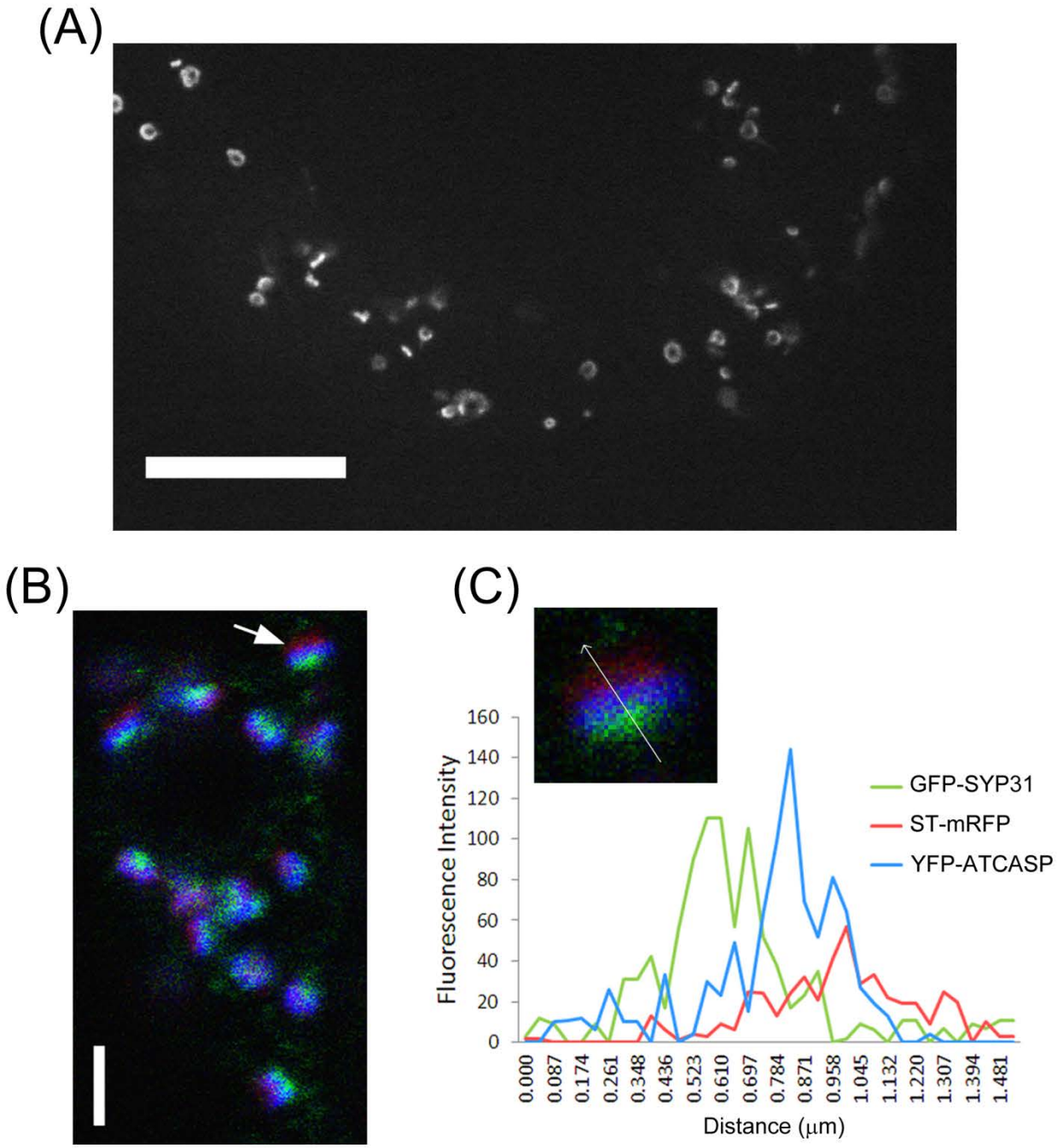

Figure 12. Intra-Golgi localization of AtCASP.

(A) Confocal image of BY-2 cells expressing YFP-AtCASP. Scale bar = 20 μm

(B) Confocal image of a BY-2 cell expressing GFP-SYP31 (*cis*, green), ST-mRFP (*trans*, red) and YFP-AtCASP (blue). The arrow indicates the Golgi stack used for the analysis in (C). Scale bar = 2 μm.

(C) The fluorescent profile along the arrow across a Golgi stack.

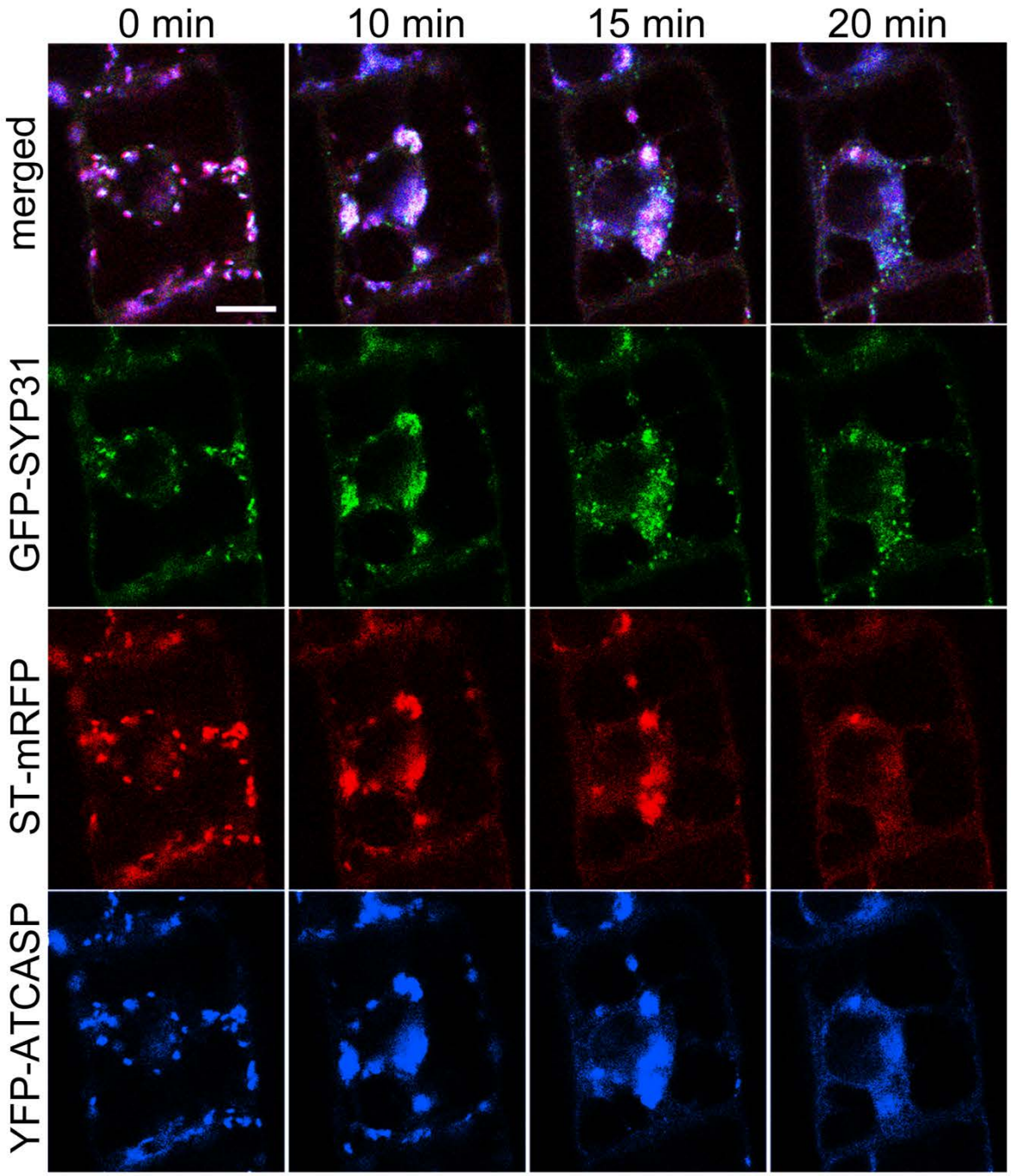

Figure 13. BFA treatment of AtCASP.
Time-lapse observation of BY-2 cells expressing GFP-SYP31 (*cis*, green), ST-mRFP (*trans*, red) and YFP-AtCASP (blue) during BFA treatment. Cells were treated with 50 μM BFA, and the fluorescent images were captured at 30-sec intervals after the addition of BFA. The indicated times mean the elapsed time after BFA addition. Scale bar = 10 μm.

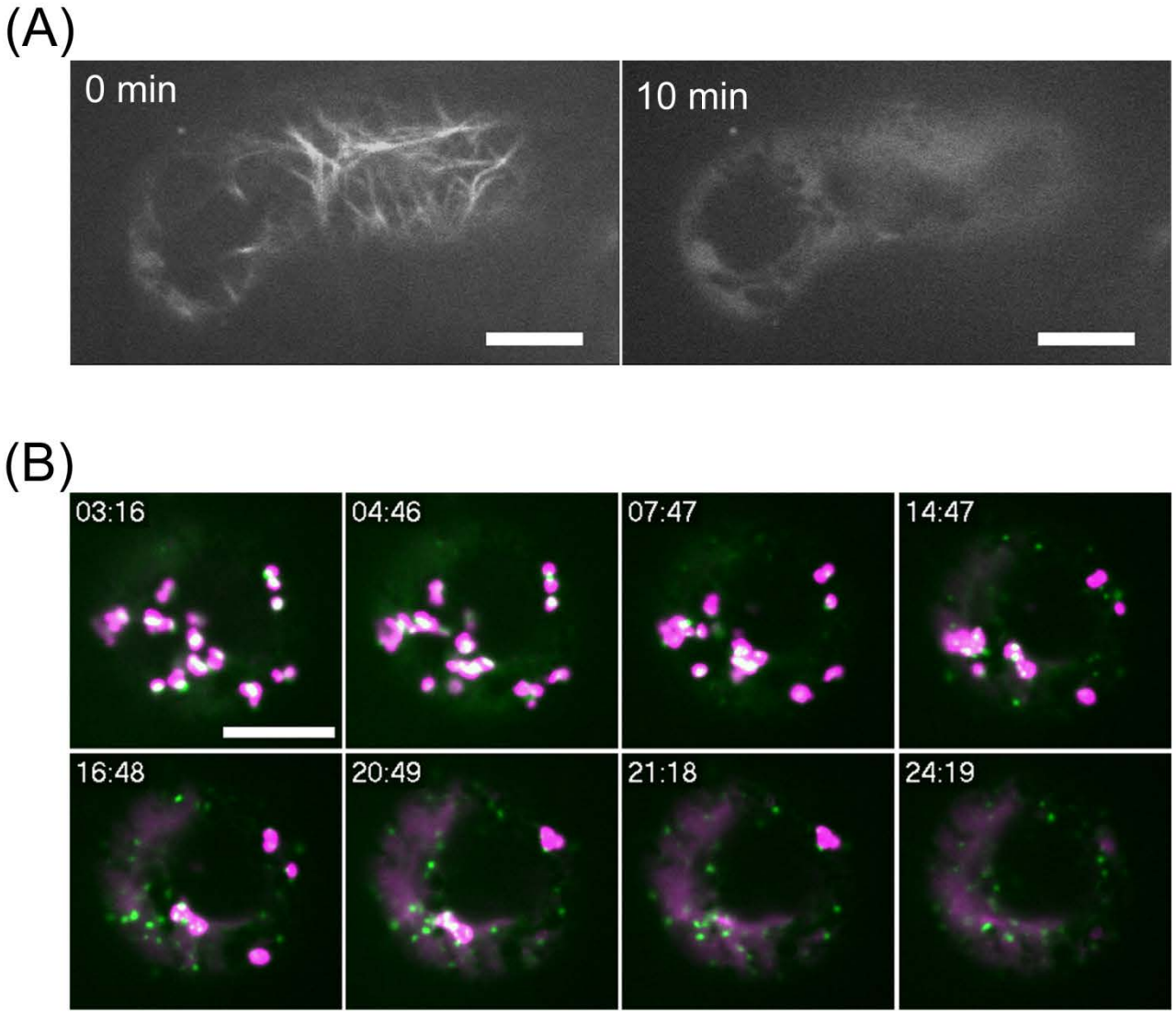

Figure 14. Effects of LatB during BFA treatment.

(A) Time-lapse observation of a BY-2 cell expressing Lifeact-Venus during LatB treatment. The indicated times represent the elapsed time after the addition of LatB at 2 μM.

(B) Time-lapse observation of a BY-2 cell expressing GFP-SYP31 (*cis*, green) and ST-mRFP (*trans*, magenta) during BFA treatment. The cell was treated with 2 μM LatB for 30 min prior to the addition of BFA at 50 μM. The fluorescent images were captured at 30-sec intervals after BFA addition. The indicated times mean the elapsed time after BFA addition (minute:second).

Scale bars = 10 μm.

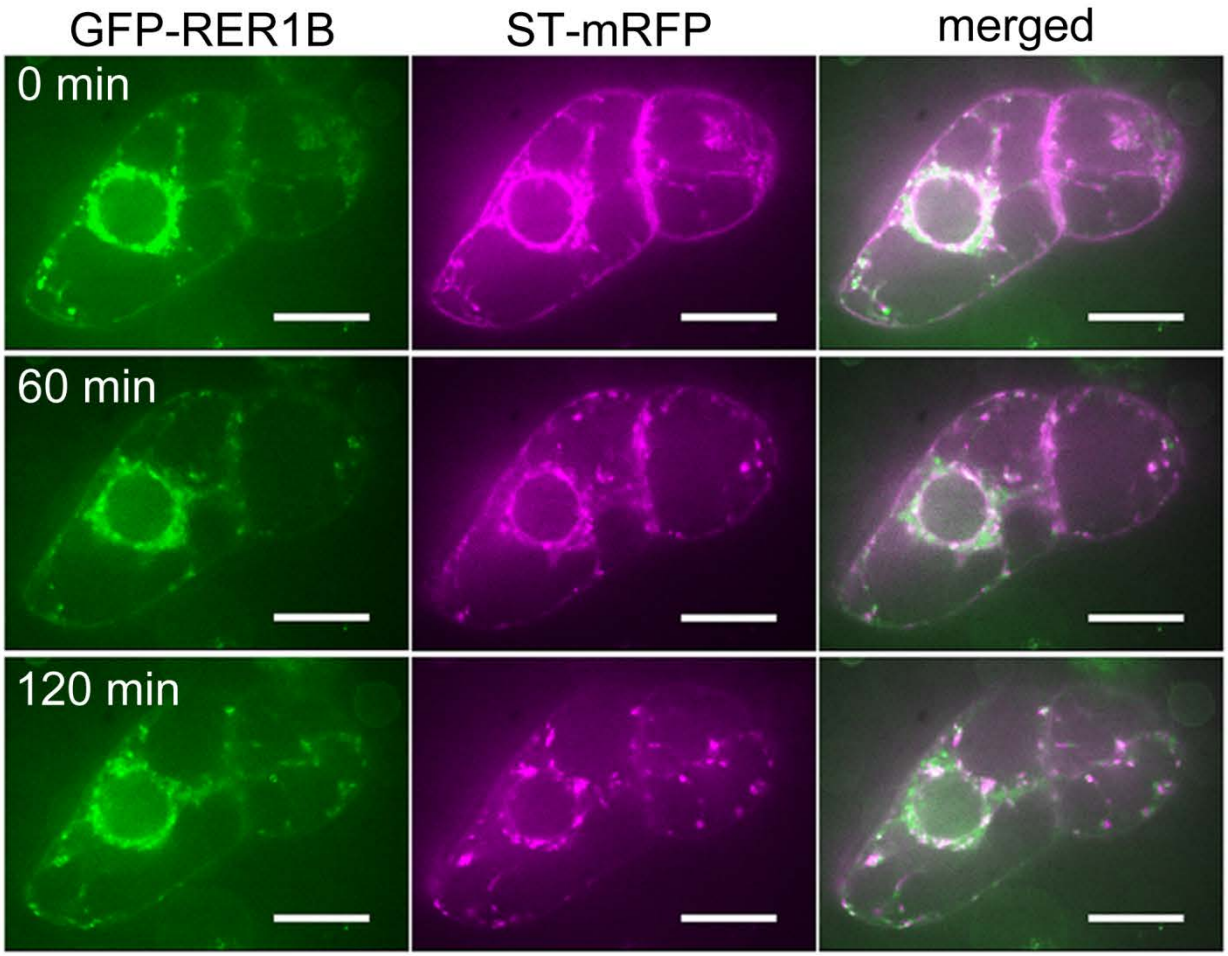

Figure 15. Golgi regeneration after BFA removal visualized by GFP-RER1B and ST-mRFP.
Time-lapse observation of BY-2 cells expressing GFP-RER1B (*cis*, green) and ST-mRFP (*trans*, magenta) after BFA removal. The cells were treated with 50 μM BFA for 2 h, and then BFA was removed. The fluorescent images were captured at 2-min intervals after BFA removal. The indicated times mean the elapsed time after the observation was started. Scale bars = 20 μm.

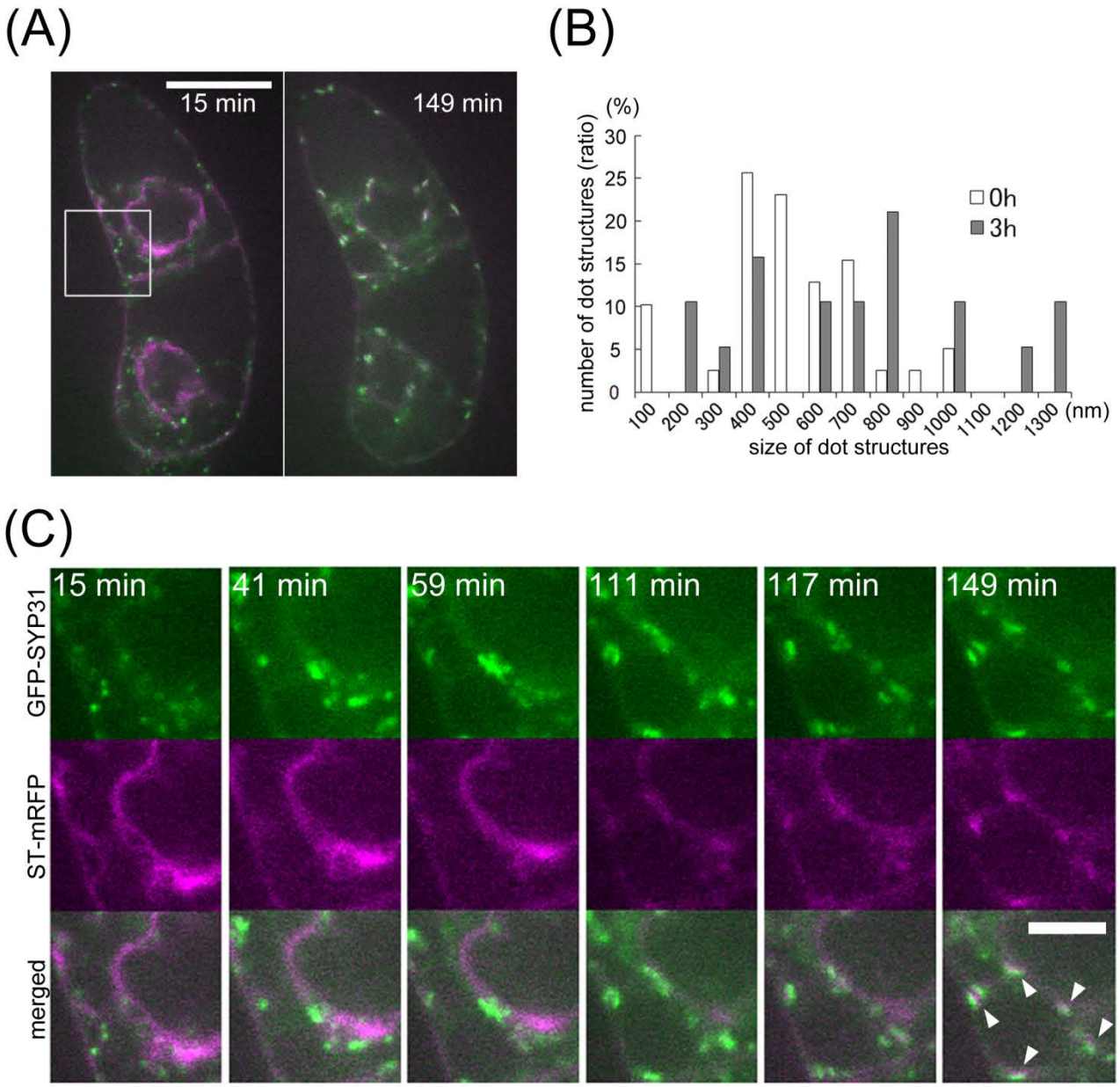

Figure 16. Golgi regeneration after BFA removal visualized by GFP-SYP31 and ST-mRFP.

(A) Time-lapse observation of BY-2 cells expressing GFP-SYP31 (*cis*, green) and ST-mRFP (*trans*, magenta) after BFA removal. The cells were treated with 50 μM BFA for 2 h, and then BFA was removed. LatB (2 μM) was added 30 min before BFA removal, and cycloheximide (100 μM) was added at the point of BFA removal. The fluorescent images were captured at 2-min interval after BFA removal. 15 min after BFA removal (left) and 149 min after BFA removal (right). Scale bar = 20 μm.

(B) Comparison of the longest diameter of each dot of GFP-SYP31 between 15 min after BFA removal (0 h, white bars) and 193 min after BFA removal (3 h, gray bars).

(C) Magnified images of the boxed region in (A). The indicated times mean the elapsed time after BFA removal. Arrowheads indicate the regenerated Golgi stacks. Scale bar = 10 μm.

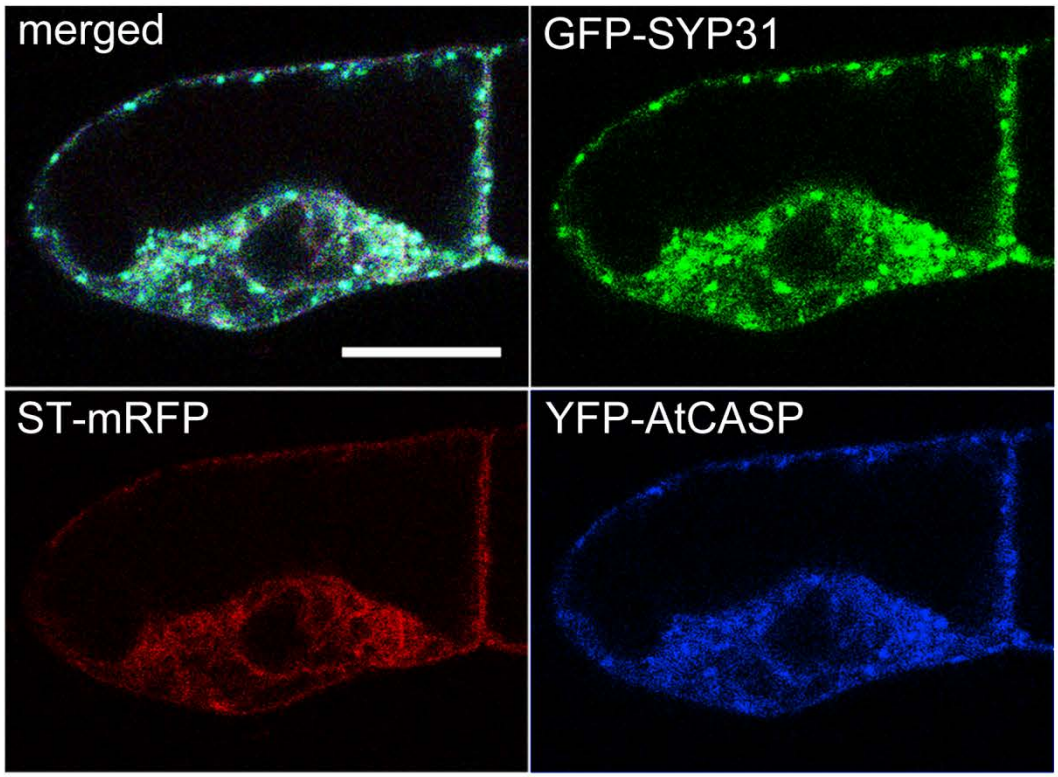

Figure 17. Golgi regeneration after BFA removal visualized by GFP-SYP31, ST-mRFP, and YFP-AtCASP.
BFA removal experiment of BY-2 cells expressing GFP-SYP31 (*cis*, green), ST-mRFP (*trans*, red), and YFP-AtCASP (blue). The cells were treated with 50 μM BFA for 2 h, and then BFA was washed out. LatB was added 30 min before BFA removal. The fluorescent image was captured 10 min after BFA removal. Scale bar = 20 μm.

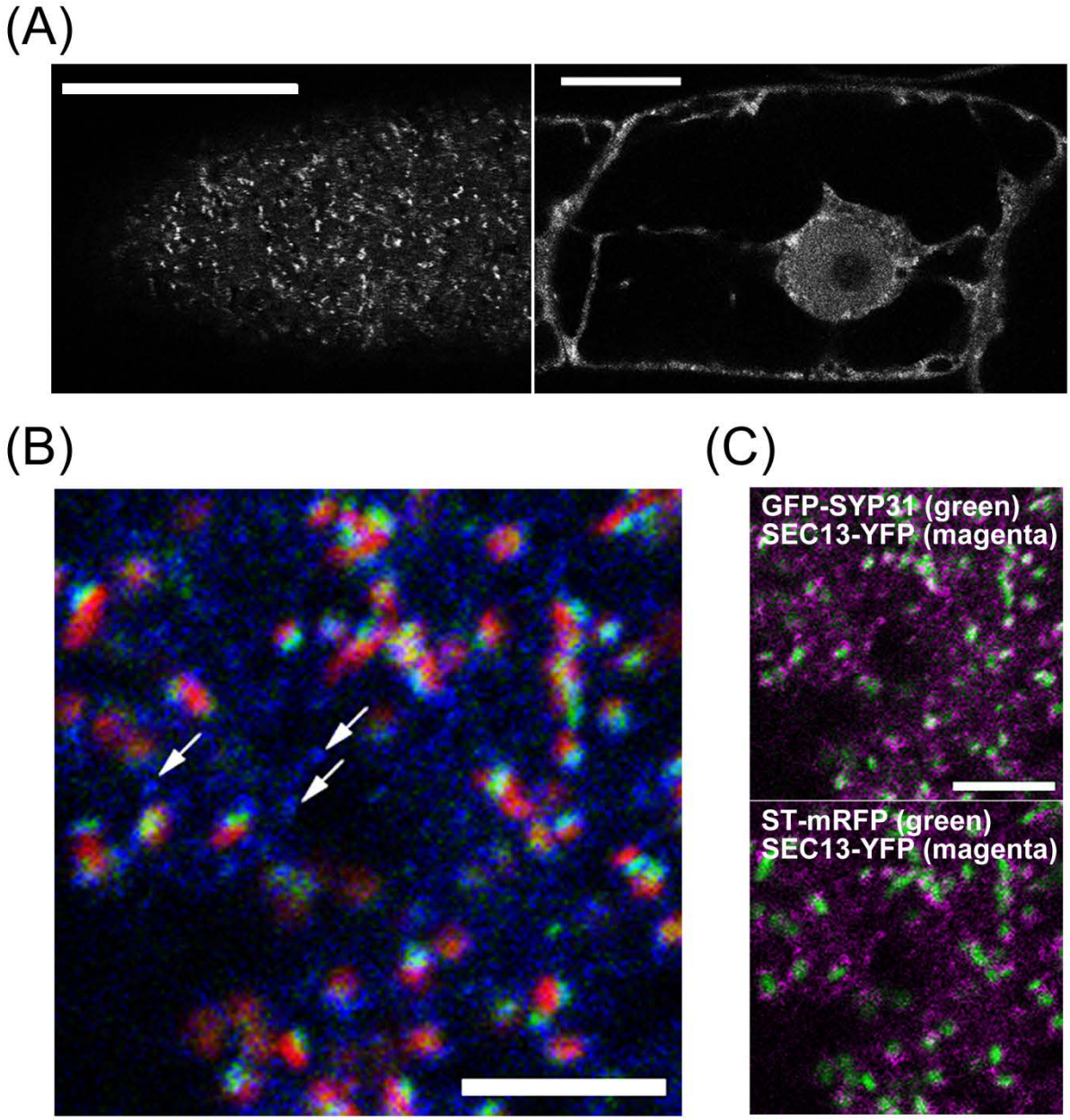

Figure 18. Relationship between the Golgi markers and the ERES.

(A) Confocal images of BY-2 cells expressing SEC13-YFP. Cell periphery (left) and the confocal plane passing through the nucleus (right). Scale bar = 20 μm

(B and C) Confocal images of BY-2 cells expressing GFP-SYP31 (*cis*), ST-mRFP (*trans*) and SEC13-YFP (ERES). Scale bars = 5 μm.

(B) Image of cell periphery. GFP-SYP31 (green), ST-mRFP (red), and SEC13-YFP (blue). Arrows indicate the ERES without partner Golgi stacks.

(C) Images of two colors extracted from (B). GFP-SYP31 (green) / SEC13-YFP (magenta) in the upper panel, and ST-mRFP (green) / SEC13-YFP (magenta) in the lower panel.

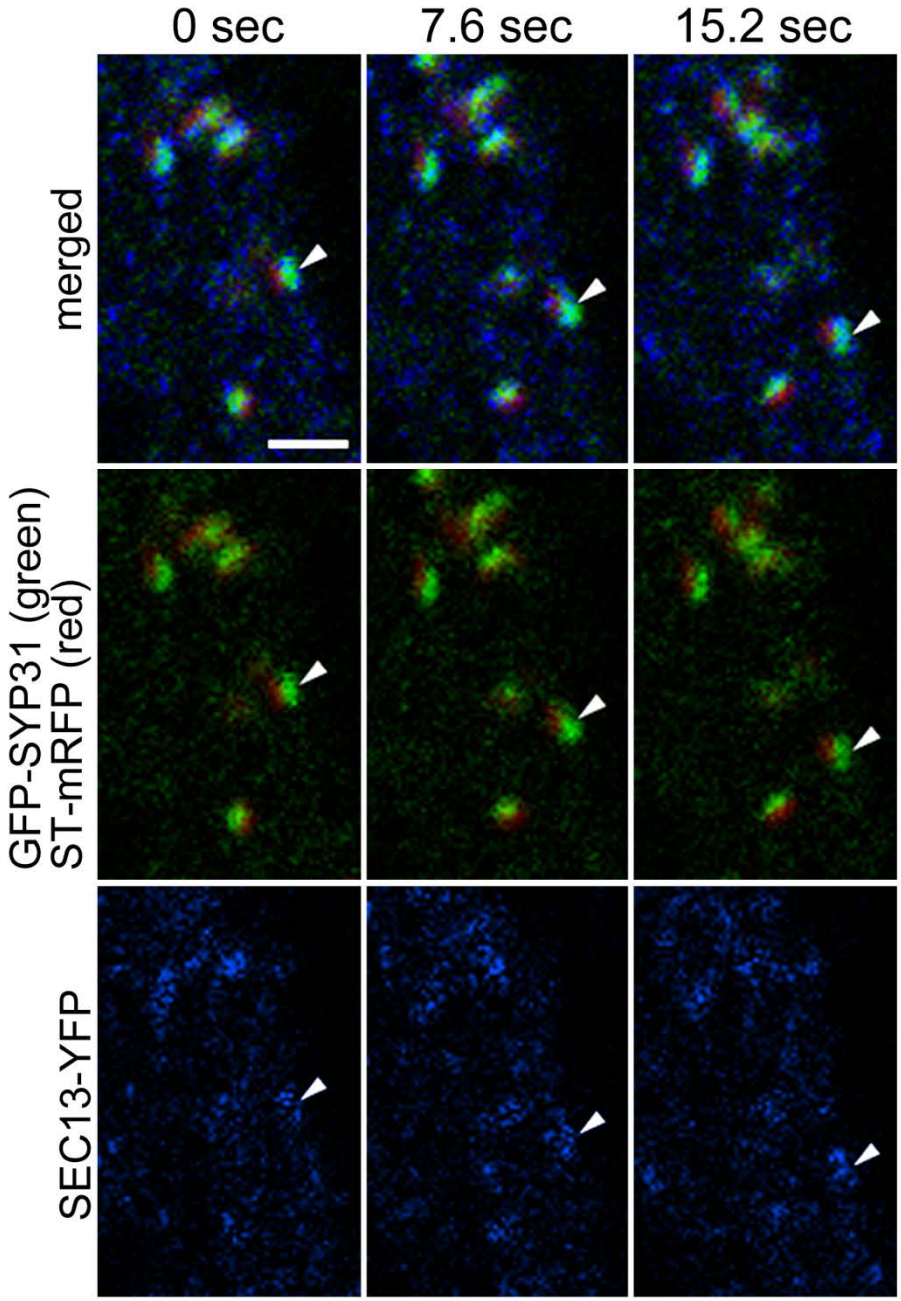

Figure 19. Movement of the Golgi stacks and the ERES.
Time-lapse images of BY-2 cells expressing GFP-SYP31 (*cis*), ST-mRFP (*trans*) and SEC13-YFP (ERES) with short-interval (7.6 sec). GFP-SYP31 (green), ST-mRFP (red), and SEC13-YFP (blue). Arrowheads indicate a unit of a Golgi stack and an ERES moving toward lower right. Scale bar = 2 μm.

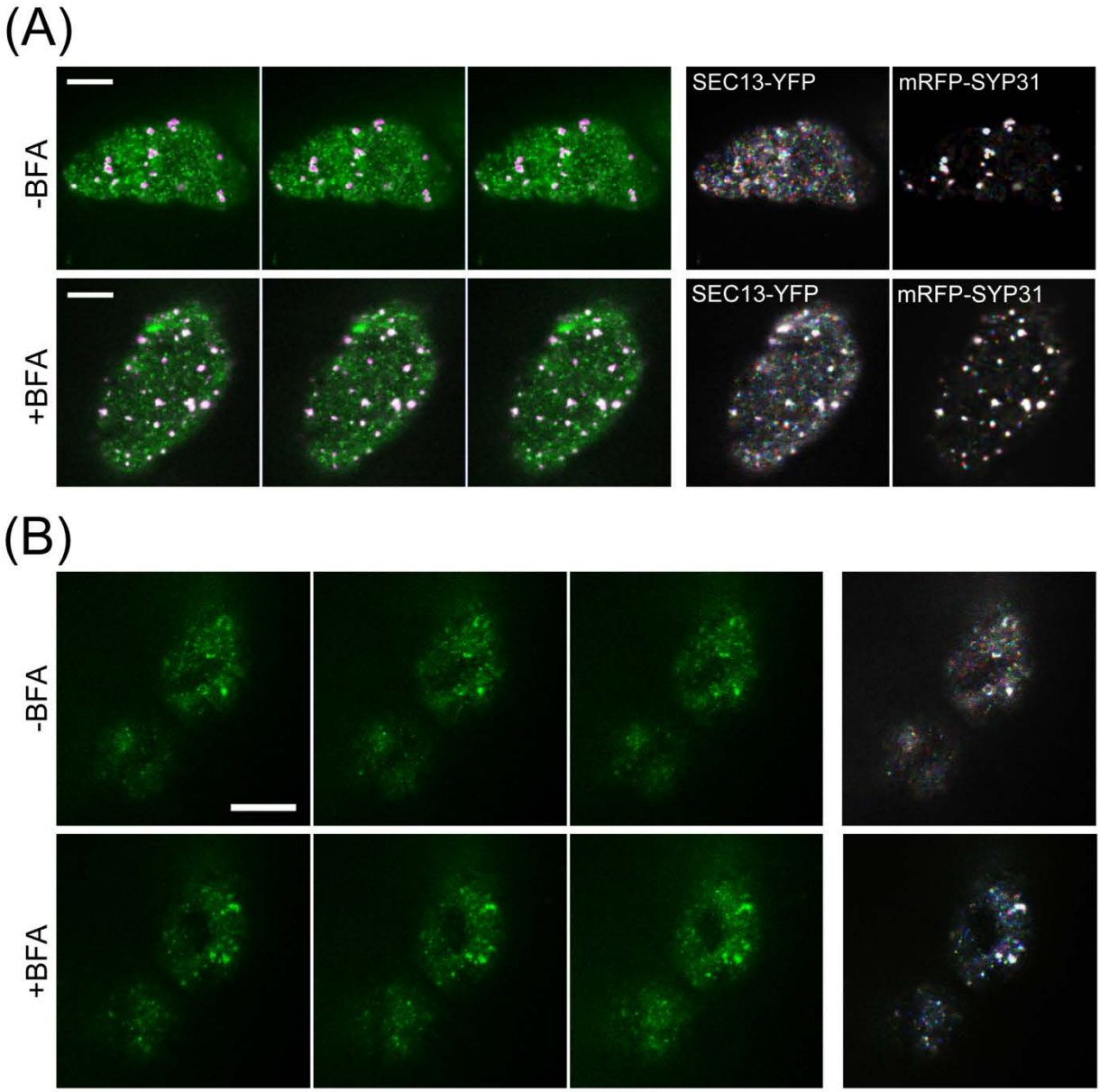

Figure 20. Relationship between SYP31 and SEC13 signals.

(A) BY-2 cells expressing SEC13-YFP (ERES, green) and mRFP-SYP31 (*cis*, magenta) were treated with 2 μM LatB for 30 min (-BFA) and 50 μM BFA for 1.5 h additionally (+BFA). Left three panels are time-lapse images with 3 sec intervals. Right two panels are maximum intensity projection (MIP) images of each marker, with pseudo-colors associated with time (0 sec: red, 3 sec: green, 6 sec: blue.)

(B) Time-lapse observation of BY-2 cells expressing SEC13-YFP alone. The cells were treated with 2 μM LatB for 30 min prior to the addition of BFA at 50 μM. Just after BFA addition (-BFA) and 1.5 h after BFA addition (+BFA). Left three panels are time-lapse images with 3 sec intervals. Rightmost panels are MIP images with the pseudo-colors same as (A).

Scale bars = 10 μm.

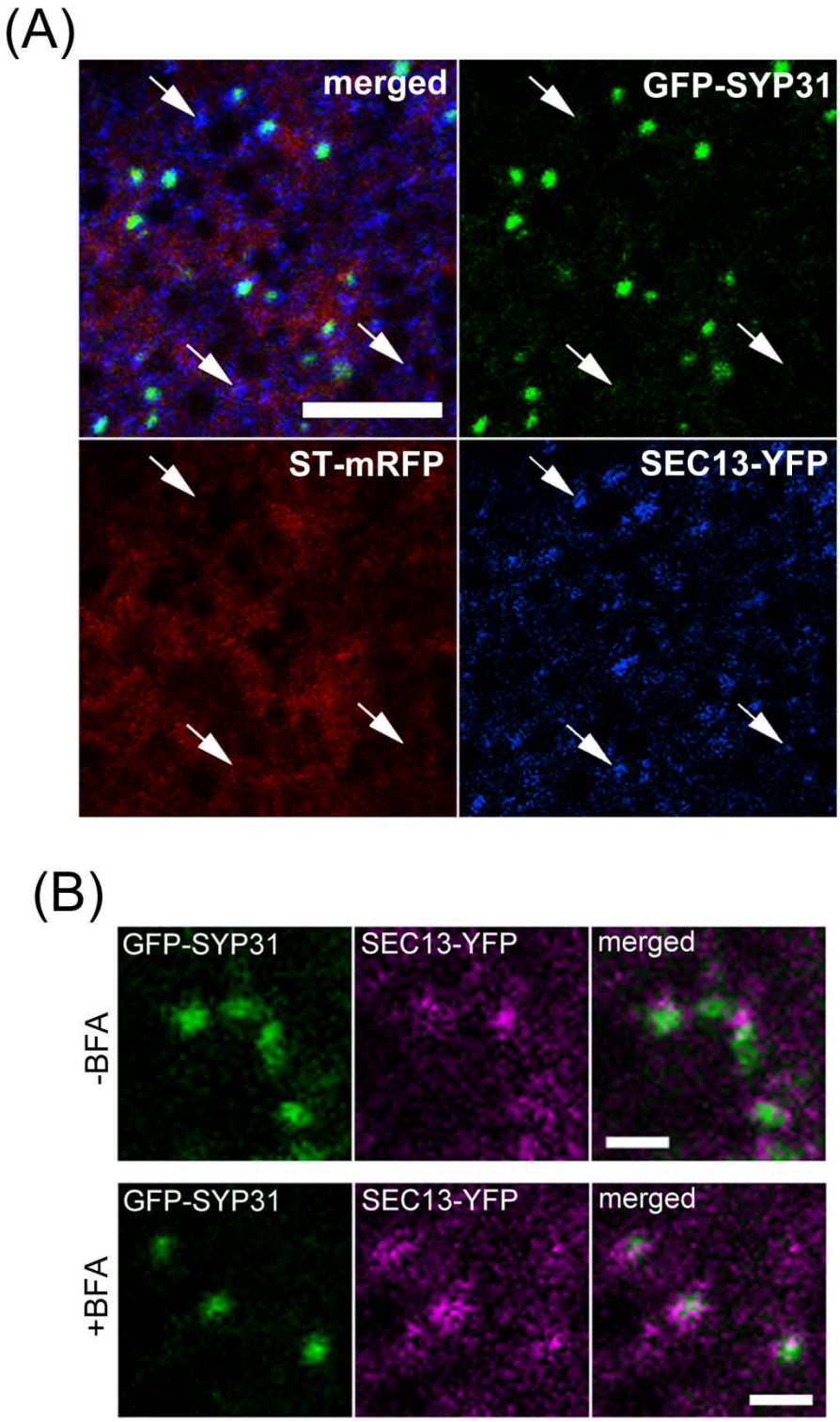

Figure 21. BFA treatment of the Golgi stacks and the ERES.

Confocal images of BY-2 cells expressing GFP-SYP31 (*cis*), ST-mRFP (*trans*) and SEC13-YFP (ERES).

(A) Effects of BFA treatment. GFP-SYP31 (green), ST-mRFP (red), and SEC13-YFP (blue). The cells were treated with 50 μM BFA for 150 min. Arrows indicate the dots of SEC13-YFP without partner GFP-SYP31 signal. Scale bar = 5 μm

(B) Comparison of positional relationship between GFP-SYP31 (green) and SEC13-YFP (magenta) signals before and after BFA treatment. Scale bar = 1 μm.

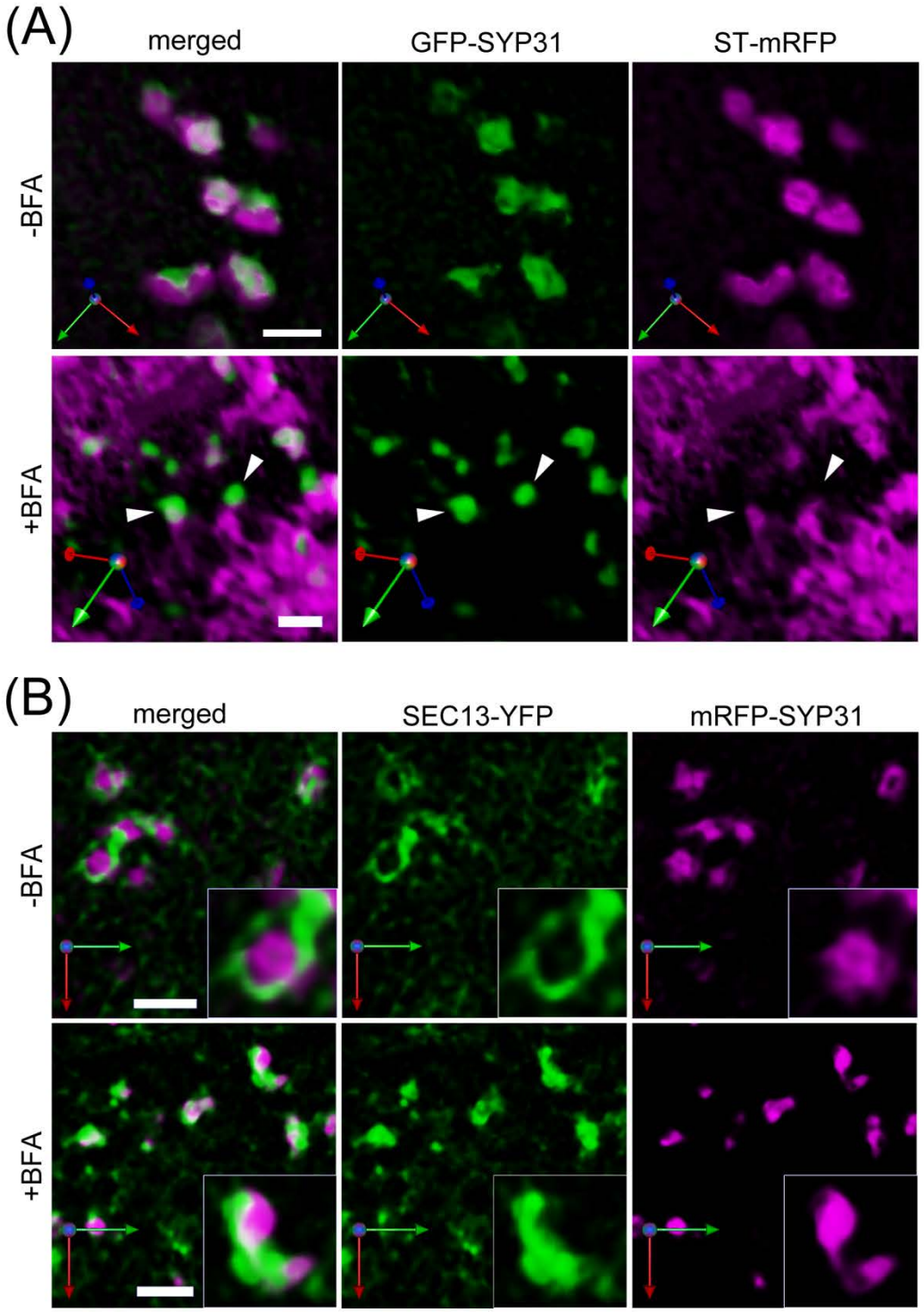

Figure 22. Three-dimensional deconvolution observations of the Golgi markers and the ERES.
BY-2 cells were observed by SCLIM with optical slices 0.2 μm apart in the Z axis. 3D images were reconstructed, deconvolved by parameters optimized for the Yokogawa spinning-disk confocal scanner.
(A) GFP-SYP31 (*cis*, green) and ST-mRFP (*trans*, magenta). Before BFA treatment (-BFA) and after 2 h of 50 μM BFA treatment (+BFA). Arrowheads indicate the punctate compartments of GFP-SYP31 on the tips of the tubular ER.
(B) SEC13-YFP (ERES, green) and mRFP-SYP31 (*cis*, magenta). Before BFA treatment (-BFA) and after 1.5 h of 50 μM BFA treatment (+BFA).
Scale bars = 2 μm.

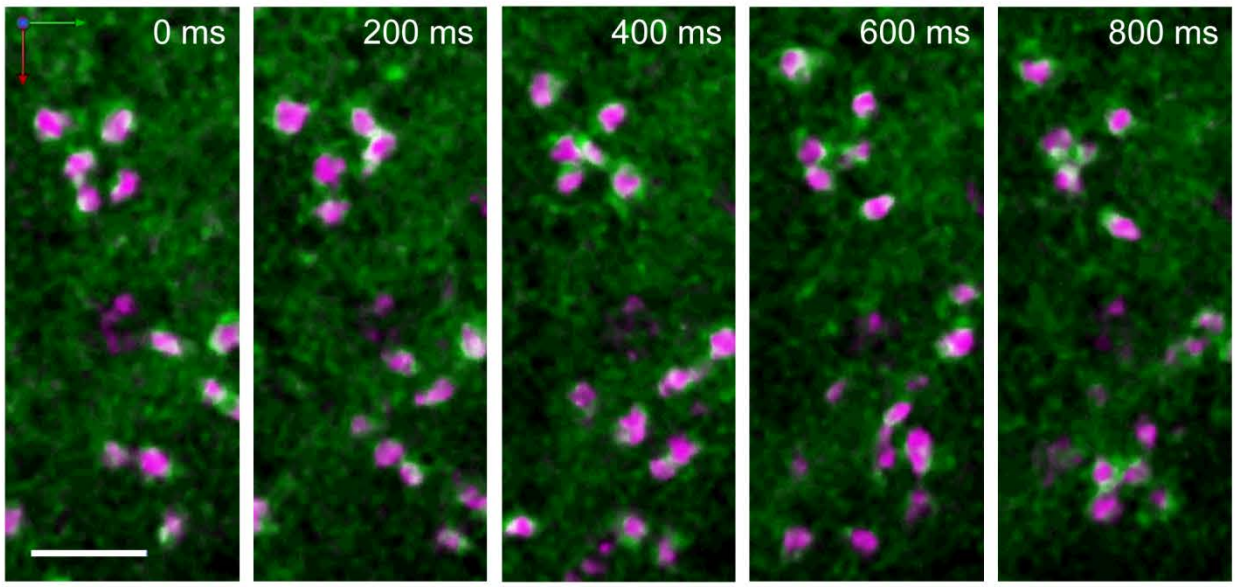

Figure 23. Three-dimensional observation of the movement of the Golgi stacks and the ERES.
A BY-2 cell was observed by SCLIM with optical slices 0.2 μm apart in the Z axis with 200 ms intervals. 3D images were reconstructed, deconvolved by parameters optimized for the Yokogawa spinning-disk confocal scanner. SEC13-YFP (ERES, green) and mRFP-SYP31 (*cis*, magenta). Scale bar = 3 μm.

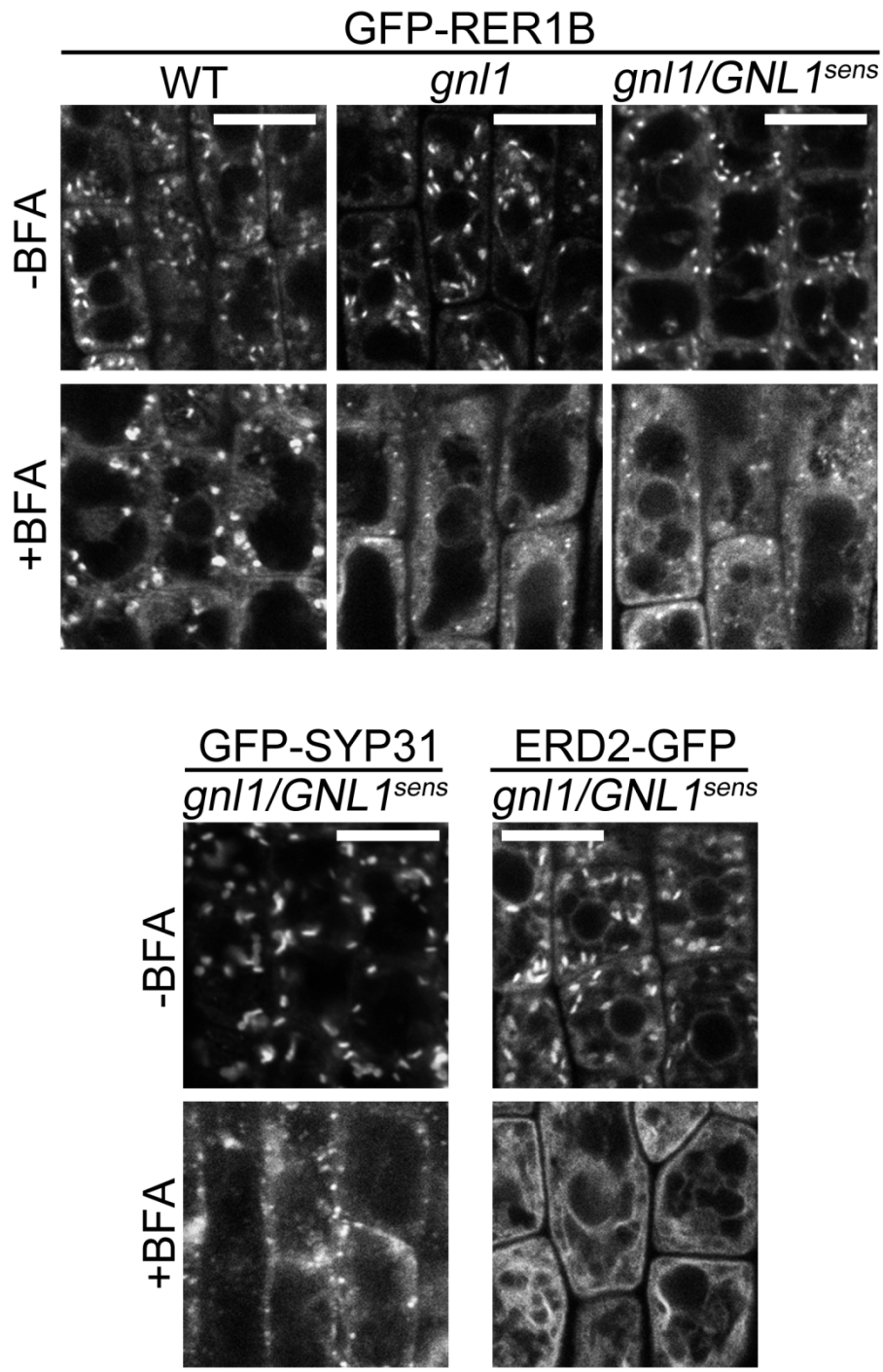

Figure 24. Effects of BFA on the *cis*-Golgi proteins in Arabidopsis root cells.
Confocal images of Arabidopsis root cells. GFP-RER1B was introduced into the wild type, the *gnl1* mutant, and the *gnl1* mutant complemented by BFA sensitive *GNL1* (*gnl1/GNL1*^{sens}). Similarly, GFP-SYP31 and ERD2-GFP were expressed in *gnl1/GNL1*^{sens} plants. The plants 5 days after germination were observed. Without BFA treatment (-BFA) and after 50 μM BFA treatment for 1.5-2 h. Scale bars = 10 μm.

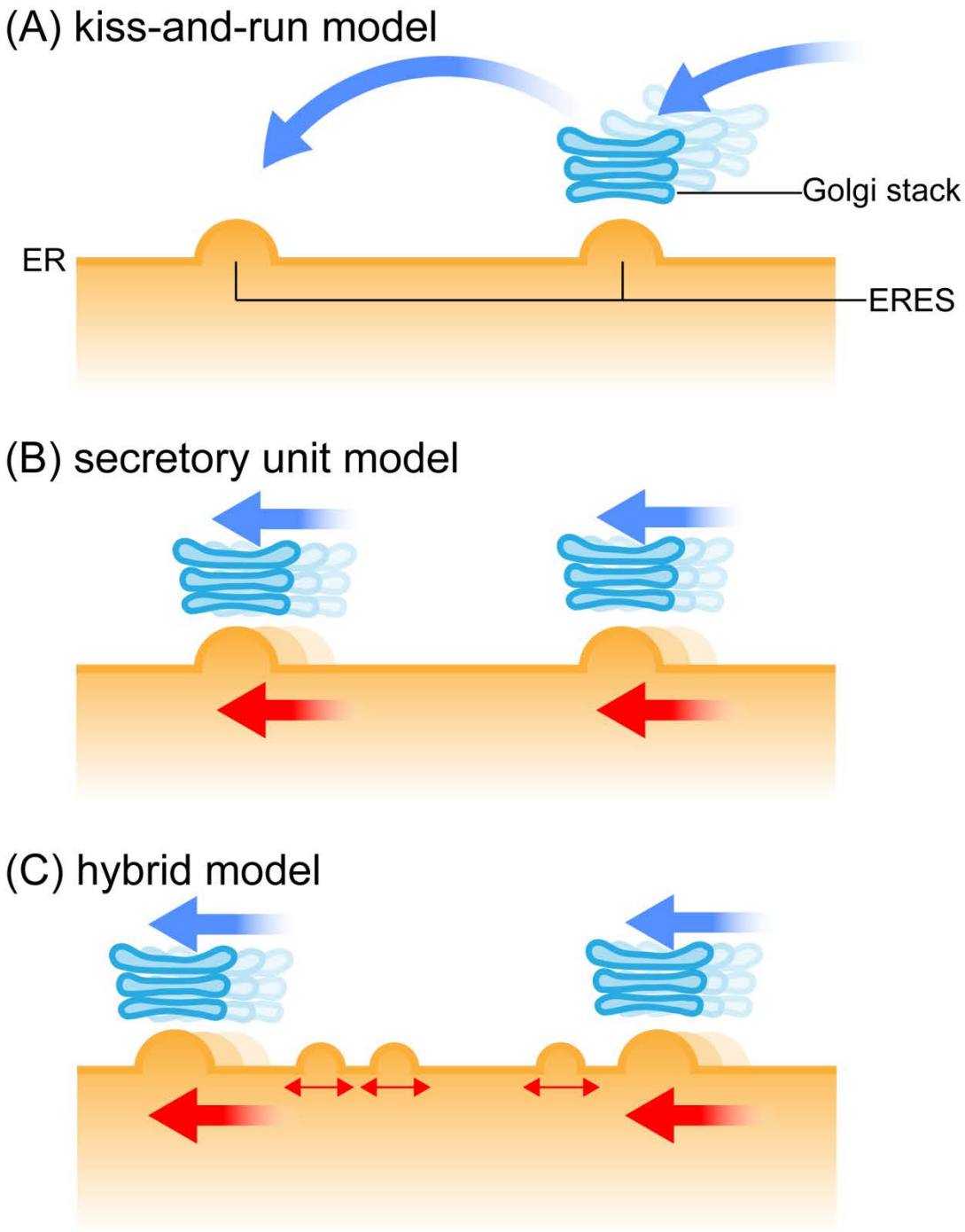

Figure 25. Models for ERES-Golgi organization in plants cells.
(A)The kiss-and-run model. In this model, the ERES are relatively stable, and the Golgi stacks travel from one ERES to another. ER-to-Golgi transport takes place during the temporal association of the Golgi stacks and the ERES. (B) The secretory unit model. In this model, the Golgi stacks and the ERES are continuously associated and move together. ER-to-Golgi transport occurs not only during their pauses but also during rapid movement. (C) The hybrid model. In this model, some of the ERES are continuously associated with the Golgi stacks similarly to the secretory unit model, but the others are not. The ERES without associated Golgi stacks are smaller and move independently from the Golgi stacks. They get stable and active when they encounter the Golgi stacks.

Chapter 3

Regeneration of the TGN starts independently of the Golgi apparatus but is followed by association with each other in tobacco cells

Introduction

The *trans*-Golgi network (TGN) was first defined as a specialized compartment composed of tubular networks on the *trans*-side of the Golgi apparatus in mammalian cells (Roth *et al.*, 1985; Griffiths and Simons, 1986; Taatjes and Roth, 1986). Similarly to the Golgi cisternae, the TGN also contains many resident enzymes for cargo processing (Rabouille *et al.*, 1995). However, in addition to function as the sequel to the cargo processing line of the Golgi, the TGN sorts cargo proteins destined for the plasma membrane and endosomes (Keller and Simons, 1997). The Golgi cisternae and the TGN can be distinguished by the vesicles they form, because the Golgi cisternae generate COPI vesicles but not clathrin-coated vesicles, and the opposite is true for the TGN (Ladinsky *et al.*, 2002).

In plant cells, the TGN was first identified as “partially coated reticulum,” a vesiculo-tubular compartment with clathrin-coated buds (Pesacreta and Lucas, 1985), and later the word TGN was applied from mammalian studies (Staehelin *et al.*, 1990). Similarly to the mammalian TGN, clathrin-coated vesicles are formed from the TGN, but not from the Golgi cisternae in plant cells (Donohoe *et al.*, 2007). Recently, the plant TGN is suggested to act not only in the secretory pathway, but also in the endocytic pathway in plant cells. An endocytosis tracer FM4-64 has been demonstrated to localize at the TGN before late endosomes, indicating that the

TGN functions as an early endosome (Dettmer *et al.*, 2006). This is also supported by the observations by time-lapse imaging and immunoelectron microscopy, which have shown that the plasma membrane proteins internalized by endocytosis pass through the TGN (Viotti *et al.*, 2010). Thus, the TGN acts as the trafficking hub that both the secretory and endocytic pathways pass through.

In addition to the functional difference, dynamic behavior of the TGN is distinct from the Golgi cisternae. By electron tomography in Arabidopsis cells, the TGN seems to get separated from the Golgi (Staehelin and Kang, 2008). Further observation by spinning disc confocal microscopy has revealed that the plant TGN moves independently of the Golgi apparatus and transiently associates with it (Viotti *et al.*, 2010; Uemura and Nakano, 2013; Uemura *et al*., in press). Such differences between the Golgi apparatus and the TGN may reflect their protein composition. Now it is becoming possible to isolate and characterize the Golgi and the TGN proteins separately, and a recent study suggests that almost 30% of the proteins identified in the Arabidopsis TGN are non-Golgi proteins (Parsons *et al.*, 2013).

In this study, in order to get insights into the relationship between the Golgi apparatus and the TGN, I observed the dynamic behaviors of the TGN during BFA treatment and its removal in living plant cells. I have demonstrated that the TGN proteins relocalize to numerous tiny structures dispersed throughout the cytoplasm by weak BFA treatment in tobacco BY-2 cells. Furthermore,

after BFA removal, the TGN started to regenerate independently from the Golgi apparatus, but they were associated at the later stage of the regeneration. Therefore, I suggest that the TGN is not a mere extension of the Golgi maturation, whereas the association of the TGN with the Golgi stacks is indispensable.

Results

Behaviors of the TGN proteins upon BFA treatment

In order to observe the dynamic relationship between the TGN and the Golgi stacks, I visualized the two organelles by different fluorescent colors. As the TGN marker, I used SYP41, one of the Qa-SNAREs at the TGN (Bassham *et al.*, 2000; Uemura *et al.*, 2004). I established a BY-2 cell line coexpressing GFP-SYP41 and ST-mRFP. By confocal microscopy, I observed many punctate signals of GFP moving throughout the cytoplasm. Some of them were associated with the disk-shaped Golgi cisternae labeled by ST-mRFP, and the others were not (Figure 26A). Similar spatial relationship between the signals of GFP and mRFP was also observed in the cells expressing GFP-SYP31 and mRFP-SYP41 (Figure 26B). These results were similar to a previous report that visualized the Golgi and the TGN in Arabidopsis hypocotyl cells (Viotti *et al.*, 2010).

In plant cells, the TGN is known to form aggregates upon BFA treatment, while their appearances are different among species. In Arabidopsis root cells, in which the Golgi stacks do not disappear by BFA, the TGN forms large aggregates called BFA bodies (or BFA compartments) with endosomal components (Langhans *et al.*, 2011; Uemura and Nakano, 2013). On the other hand, in tobacco leaf protoplasts, in which the Golgi stacks fuse and get absorbed into the ER upon BFA treatment, the TGN forms what look like BFA bodies, which are much smaller than those in

Arabidopsis root cells (Langhans *et al.*, 2011). This difference may be because the Golgi maturation continues and supplies materials to the TGN in the presence of BFA in Arabidopsis cells but not in tobacco cells.

In the BY-2 cells expressing GFP-SYP41 and ST-mRFP, ST-mRFP was absorbed into the ER and GFP-SYP41 localized to some aggregates upon 50 μM BFA treatment, as previously reported in protoplasts (Figure 27A). Similar fluorescent pattern was obtained in the same cell line with 25 μM BFA (Figure 28). Time-lapse observation during 50 μM BFA treatment revealed that the TGN and the Golgi stacks formed aggregates together, and subsequently ST-mRFP mostly relocated to the ER, whereas GFP-SYP41 remained in the clumps (Figure 27A).

On the other hand, with 10 μM BFA, I found that most of the signal of GFP-SYP41 seemed to be dispersed in the cytosol, and punctate structures or aggregates were rarely observed (Figure 27B). Although GFP-SYP41 behaved differently between the two BFA concentrations, ST-mRFP relocalized to the ER by 10 μM BFA treatment similarly to when treated with 50 μM BFA (Figure 27B). Similar relocalization of the two markers was also observed upon 5 μM BFA treatment (Figure 28). By time-lapse observation during 10 μM BFA treatment, I could observe that the TGN formed aggregates with the Golgi stacks at the early stage, however, they became dispersed at the later stage when the Golgi stacks disassembled (Figure 27B). These results indicated that the TGN proteins behaved differently depending on the BFA concentration.

In order to examine the behavior of non-SNARE TGN protein upon BFA treatment with a low concentration, I established a cell line expressing VHA-a1-GFP. VHA-a1 is a subunit of V-ATPase, and has been demonstrated to localize at the TGN and colocalize with SYP41 (Dettmer *et al.*, 2006). In tobacco BY-2 cells, VHA-a1-GFP labeled many punctate structures (Figure 29). After 10 μM BFA treatment, VHA-a1-GFP exhibited cytosol-like localization with few punctate structures left, similarly to SYP41 (Figure 29).

Moreover, I confirmed the behavior of the Golgi proteins upon weak BFA treatment. In the cells coexpressing GFP-SYP31 and ST-mRFP, GFP-SYP31 localized at small punctate structures, and ST-mRFP was absorbed into the ER membrane upon 10 μM or 5 μM BFA treatment (Figure 30). This result was almost identical to what I observed with 50 μM BFA as described in the chapter 2 (Figure 5A).

Localization of SYP41 upon weak BFA treatment

Because SYP41 and VHA-a1 are transmembrane proteins, it is highly unlikely that they become soluble and disperse into the cytosol. Therefore, I considered that their cytosolic localization patterns upon weak BFA treatment represented that they localized to numerous tiny membrane vesicles that could not be distinguished by normal confocal microscopy.

To test this hypothesis, I performed TIRFM observation of GFP-SYP41. Without BFA

treatment, I observed that GFP-SYP41 localized to punctate structures (Figure 31A). Some of them were much larger than the others (Figure 31A, arrowhead). Time-lapse observation with short intervals revealed that the smaller structures moved rapidly but the larger ones were relatively stable (Figure 31B). I presumed that the larger structures were the TGN, which could be observed by confocal microscopy, according to their size. The smaller structures were likely to be vesicles or small clusters of vesicles.

Upon weak BFA treatment, the larger structures disappeared as was observed by confocal microscopy. Instead, the number of the smaller structures significantly increased compared to the control cells (Figure 31A). By time-lapse observation, these small dot-like structures were revealed to move very actively (Figure 31B). These results indicated that the cytosolic signal of GFP-SYP41 upon weak BFA treatment was not from the protein solubilized in the cytosol, but from the protein localizing on many small vesicle-like structures.

Uptake of FM4-64 in the presence of weak BFA

Recently, plant TGN is suggested to act as the early endosome in the endocytic pathway (Dettmer *et al.*, 2006; Viotti *et al.*, 2010). To examine the effects of weak BFA treatment on the endocytic pathway, I observed internalization of FM4-64, which is well known as an endocytosis tracer. Without BFA treatment, FM4-64 was gradually internalized from the plasma membrane, and

many punctate structures were labeled (Figure 32). Later, I could observe the vacuolar membrane clearly, which indicated that FM4-64 had been transported through the endocytic pathway and reached the vacuole (Figure 32, 4 h). On the other hand, with 10 μM BFA treatment, FM4-64 internalized into the cytoplasm exhibited cytosolic fluorescent pattern, and punctate structures were rarely observed (Figure 32). However, it subsequently reached the vacuole similarly to the control cells (Figure 32, 4 h). This result indicated that weak BFA treatment did not affect the transport of FM4-64 from the plasma membrane to the vacuole, and moreover, that FM4-64 did not pass through any compartments that are large enough to be observed by confocal microscopy in this condition.

To examine the relationship between the vesicle-like structures with SYP41 and FM4-64 transport in the presence of BFA with a low concentration, I observed the internalization of FM4-64 in the BY-2 cells expressing GFP-SYP41. I treated the cells with 10 μM BFA for 90 min in advance, added FM4-64 to the cell suspension, and washed the cells immediately with fresh medium containing 10 μM BFA. By TIRFM, dotty signals of FM4-64 were observed, which presumably represented endosomes just beneath the plasma membrane (Figure 33). Some of the punctate signals of GFP-SYP41 were very close to some of the FM4-64 dots, however, the two signals did not overlap completely (Figure 33A, arrows). By time-lapse observation with short intervals, I observed a punctate structure of GFP-SYP41 approached a dot of FM4-64, seemed to associate briefly, and moved away (Figure 33B, arrowheads). These results suggested that FM4-64 did not pass through

the same compartments where SYP41 localized, but there was some association between the structures with FM4-64 and SYP41.

TGN regeneration after BFA removal

Next, I observed the regeneration process of the TGN in relation to that of the Golgi apparatus. The cells expressing GFP-SYP41 and ST-mRFP were treated with 10 μM of BFA, and time-lapse observation was performed after BFA removal. Similarly to the experiment described in the chapter 2, I added LatB and cycloheximide to stop the movement of the organelles and inhibit the synthesis of the marker proteins. Confocal microscopy revealed that bright punctate structures of GFP-SYP41 appeared very early after BFA removal (Figure 34, 0 min). The number of the structures gradually increased as time elapsed, whereas ST-mRFP still mainly localized at the ER (Figure 34, 30 min). ST-mRFP became punctate much later than GFP-SYP41 (Figure 34, 90-180 min). This indicated that the TGN began to regenerate before the *trans*-Golgi cisternae did.

To examine the relationship between the regeneration of the TGN and the punctate structures of *cis*-Golgi proteins, I also performed regeneration experiment with the cells expressing GFP-SYP31 and mRFP-SYP41. At the early stage of the regeneration, the punctate structures of GFP-SYP31 and the regenerated puncta of mRFP-SYP41 seemed independent from each other (Figure 35, 09:44). Subsequently, however, as the punctate structures of GFP-SYP31 gathered to

form larger clumps, the puncta of mRFP-SYP41 also gathered together (Figure 35, 27:45-91:48). The two signals kept associated while the regeneration proceeded. After regeneration, almost all the Golgi stacks and the TGN were in pairs (Figure 35, 121:49). From these results, I suggest that the TGN starts to regenerate independently from the Golgi stacks, but the association between the two organelles might be indispensable to complete their regeneration.

Discussion

Distinct behaviors of the TGN proteins dependent on BFA concentration

The plant TGN has been known to form aggregates with endosomal components by BFA treatment (Langhans *et al.*, 2011; Uemura and Nakano, 2013). Also in this study, I confirmed that a TGN marker SYP41 aggregates in BY-2 cells upon 25-50 μM BFA treatment. However, I have also shown that SYP41 behaves differently in the same cell line only by decreasing the BFA concentration to 5-10 μM; it does not localize to any recognizable structures but exhibits hazy cytosolic pattern. Another TGN marker VHA-a1 responds similarly to weak BFA treatment. Because Golgi markers including Qa-SNARE SYP31 do not show different behaviors by decreasing the BFA concentration, such concentration dependency is not shared between the Golgi and the TGN, neither among Qa-SNAREs. TIRFM observation has revealed that SYP41 localizes at numerous small punctate structures upon weak BFA treatment, indicating that the cytosolic signal comes from these punctate structures, which are too small to be distinguished by normal confocal microscopy. SYP41 is a transmembrane protein, thus the small structures are presumed to be membrane-bounded compartments such as vesicles (Figure 36B).

Unlike the Golgi cisternae, the TGN produces clathrin-coated vesicles (Ladinsky *et al.*, 2002; Donohoe *et al.*, 2007), and their formation step is regulated by ARF1 (Memon, 2004;

Robinson *et al.*, 2011). Because BFA inhibits the GEFs for ARF1, the formation of clathrin-coated vesicles at the TGN is thought to be inhibited by BFA treatment (Ritzenthaler *et al.*, 2002; Langhans *et al.*, 2011). However, the causal relationship between such transport inhibition and the formation of aggregates is unknown. In this study, I have found that the TGN gathers with the Golgi stacks at the very early stage of weak BFA treatment, but the aggregates do not remain until the later stage. From these facts, I suggest that formation and retention of the aggregates of the TGN are different steps with different BFA sensitivity. Both steps are caused by strong BFA, but weak BFA cause only the former step. It might be because these two steps are regulated by different GEFs with different sensitivity to BFA.

What occurs during weak BFA treatment?

There are several possibilities about what occurs when SYP41 disperses throughout the cytoplasm localizing on the small vesicle-like structures. It has been reported that SCAMP2, which mostly colocalizes with SYP41, relocalizes to the plasma membrane by 5 μg/mL (about 18 μM) BFA treatment in BY-2 cells (Toyooka *et al.*, 2009). Therefore, SYP41 might also be once transported to the plasma membrane and rapidly internalized by endocytosis, or excluded from the compartments where SCAMP2 localizes (secretory vesicle clusters: SVCs) before they reach the plasma membrane. On the other hand, the plant TGN is recently suggested to mature into multivesicular endosomes

(MVEs) along the endocytic pathway (Scheuring *et al.*, 2011; Choi *et al.*, 2013). In this context, SYP41 might be excluded from the TGN during the maturation into MVE. It is also possible that the TGN itself becomes fragmented into small vesicles.

In any case, the vesicle-like compartments do not gather to form larger structures in the presence of a low concentration of BFA. Is it because the Golgi stacks have disappeared and there is no target to fuse with? After BFA removal, SYP41 started to localize at larger structures very rapidly before the Golgi stacks complete their regeneration (see discussion later). This result indicates that the small structures can assemble without the Golgi stacks. Therefore, I suggest that there are scaffolding or tethering proteins that collect the vesicles independently of the Golgi apparatus, and their function is inhibited by weak BFA treatment. One candidate of such proteins is AtGRIP. In animal cells, some of the long coiled-coil tethering factors have a GRIP domain and localize at the TGN (McConville *et al.*, 2002; Goud and Gleeson, 2010). An Arabidopsis GRIP domain protein AtGRIP has been shown to localize at the far *trans* side of the Golgi stacks and the TGN (Gilson *et al.*, 2004; Latijnhouwers *et al.*, 2005; Latijnhouwers *et al.*, 2007; Osterrieder, 2012). This localization of AtGRIP to the membranes depends on the direct interaction with a small GTPase ARF-LIKE 1 (ARL1; Latijnhouwers *et al.*, 2005), whose homologs are known to be inhibited by BFA in mammalian cells (Lowe *et al.*, 1996; Man *et al.*, 2011).

Transport from the plasma membrane to the vacuole with weak BFA

Because the plant TGN is suggested to act as the early endosome in the endocytic pathway, I first thought that the transport from the plasma membrane to the vacuole would be inhibited when the TGN proteins do not show normal localization upon weak BFA treatment. However, uptake and transport of FM4-64 from the plasma membrane to the vacuolar membrane were not affected. This might indicate that the small vesicle-like structures with the TGN proteins can achieve the function as the early endosome. It is also possible that the transport route via the TGN is blocked but those do not pass through the TGN remain unaffected. Nevertheless, I have observed the association between the vesicle-like structures with FM4-64 and SYP41, although they did not colocalize completely. Whether such association has physiological significance is unknown. The behaviors of the cargo proteins that are transported along the endocytic pathway via the TGN should be examined.

Moreover, FM4-64 rarely labeled recognizable structures before the vacuole in the presence of a low concentration of BFA. This might indicate that the late endosomes are also fragmented into small structures. It is important to visualize the late endosomes and examine their responses to weak BFA.

TGN regeneration and its relationship with the Golgi stacks

In this study, I have demonstrated that the regeneration of the TGN begins very early after

BFA removal. Regeneration of the *trans*-Golgi cisternae is significantly later than the start of TGN regeneration. In addition, at the early stage of regeneration, the punctate TGN appears to be formed independently of the punctate structures of *cis*-Golgi protein, which act as the scaffold for Golgi regeneration (Figure 36C). In the chapter 2, I have shown that the regeneration of the Golgi stacks proceeds in the *cis*-to-*trans* order, and this is consistent with the cisternal maturation model. If the TGN is formed completely by cisternal maturation that continues from the Golgi apparatus, it would start to regenerate near the Golgi scaffold after the *trans*-Golgi cisternae have been completed. Therefore, I suggest that the plant TGN is not just the sequel to the Golgi maturation; at least a portion of its components can reassemble without supply from the Golgi.

Furthermore, I have found that almost all the Golgi stacks and the TGN are associated in pairs after regeneration. This is different from the untreated cells, in which significant proportion of the two organelles are apart from each other. Time-lapse observation has revealed that the TGN, which has started to regenerate independently from the Golgi, gets associated with the Golgi stacks at the later stage of the regeneration (Figure 36D). The previously regenerated part of the TGN without Golgi might receive materials from the associated Golgi.

From the results above, I propose that the TGN does not fully depend on the Golgi, but the association between the two organelles is indispensable step for their regeneration.

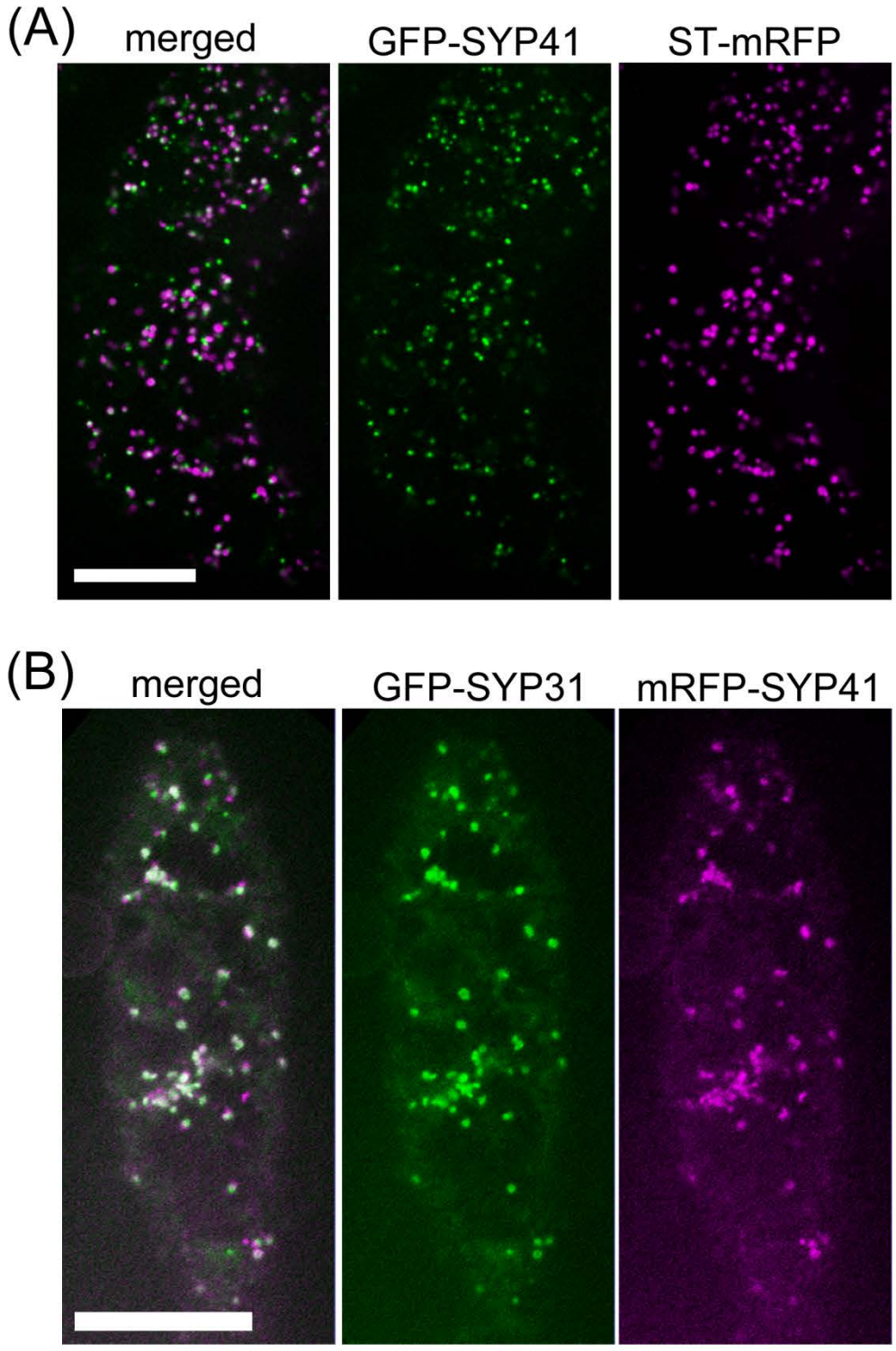

Figure26. Visualization of the TGN with the Golgi stacks in BY-2 cells.

(A) Confocal image of BY-2 cells expressing GFP-SYP41 (TGN, green) and ST-mRFP (*trans*-Golgi, magenta).

(B) Confocal image of BY-2 cells expressing GFP-SYP31 (*cis*-Golgi, green) and mRFP-SYP41 (TGN, magenta).

Scale bars = 20 μm.

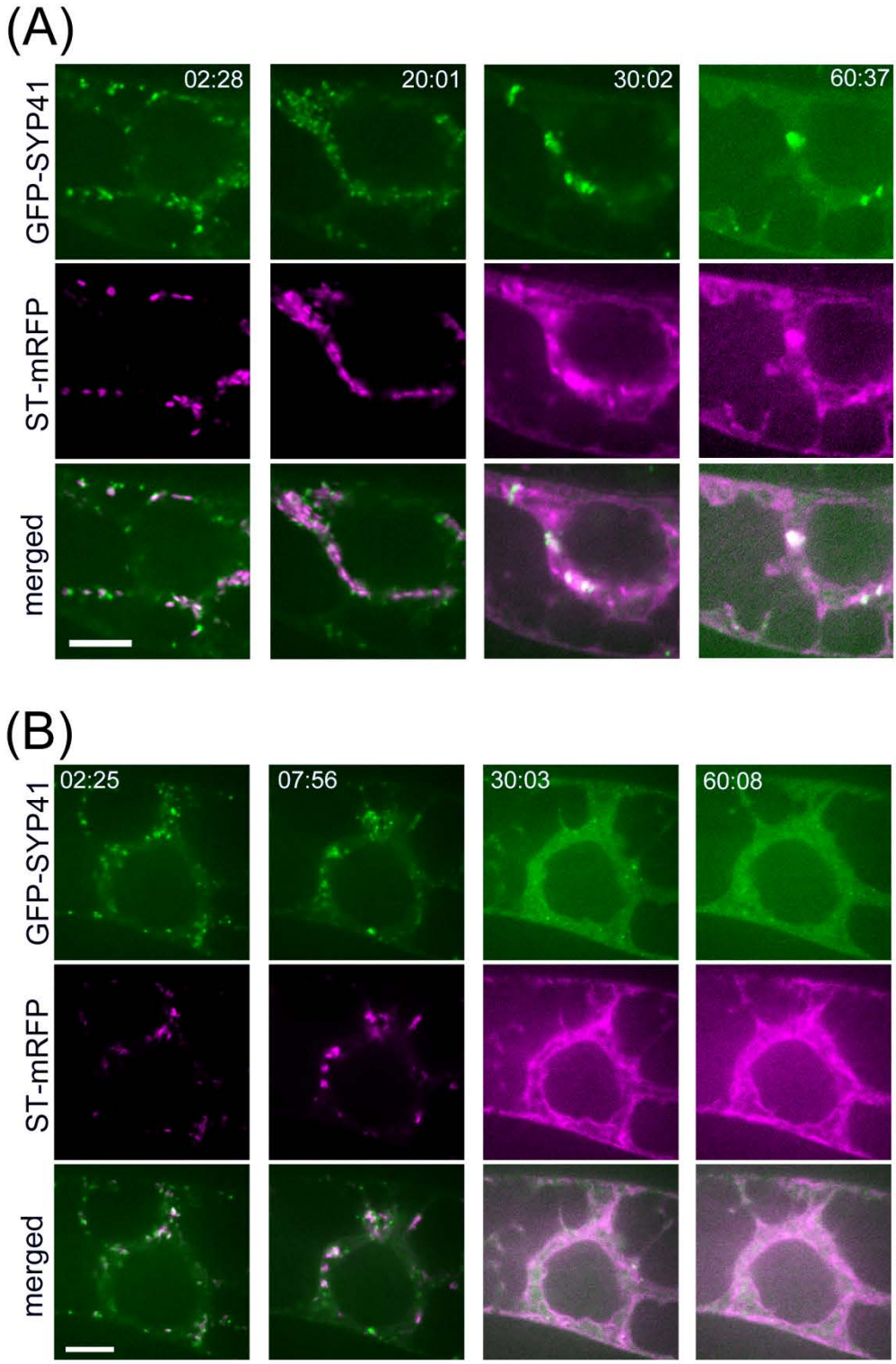

Figure27. Behaviors of SYP41 upon BFA treatment with 50 μM or 10 μM.
Time-lapse images of BY-2 cells expressing GFP-SYP41 (TGN, green) and ST-mRFP (*trans*-Golgi, magenta) during BFA treatment. The indicated times mean the elapsed time after BFA addition (minute:second). (A) 50 μM BFA. (B) 10 μM BFA. Scale bars = 10 μm.

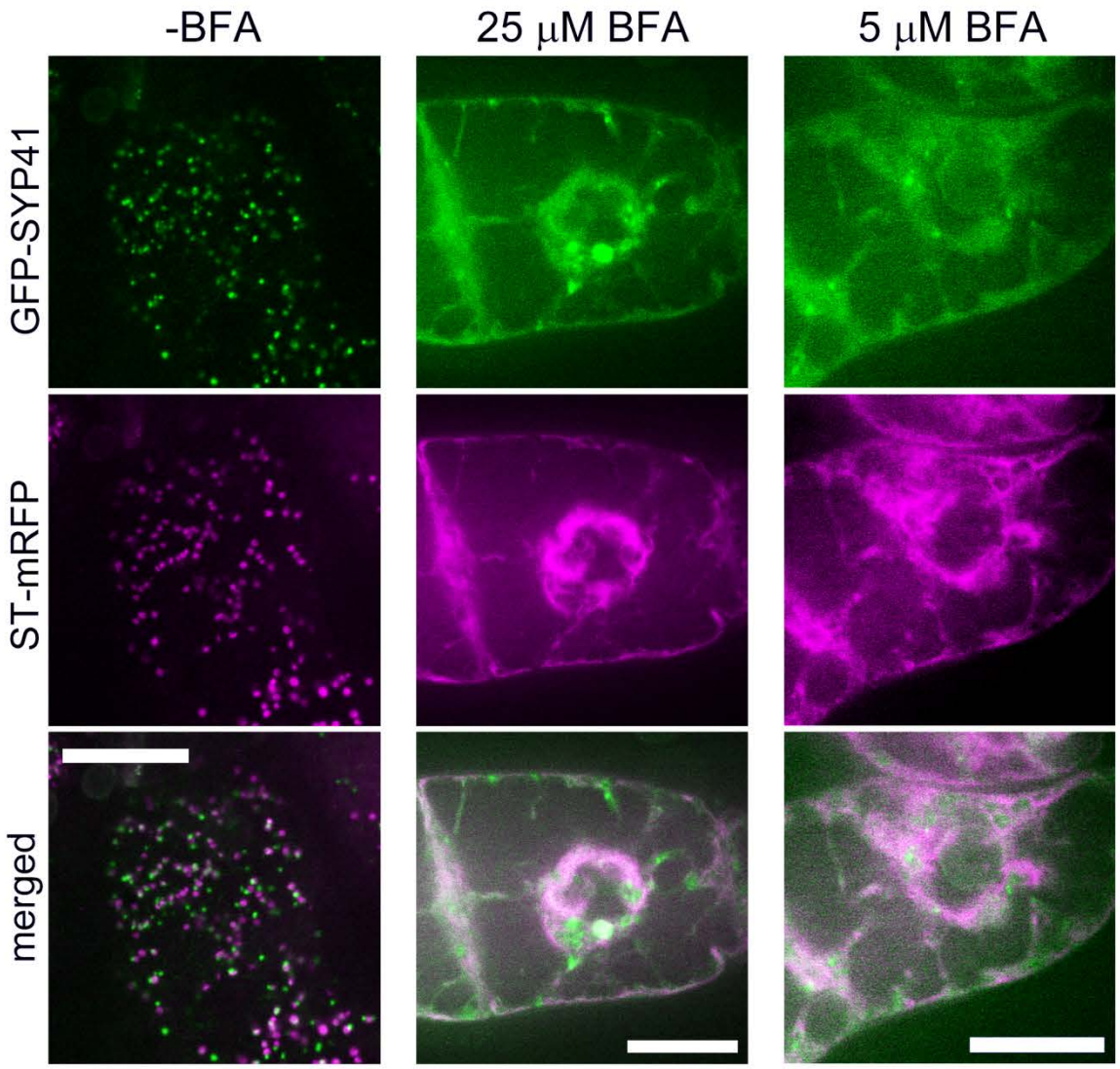

Figure28. Behaviors of SYP41 upon BFA treatment with 25 μM or 5 μM.
Confocal images of BY-2 cells expressing GFP-SYP41 (TGN, green) and ST-mRFP (*trans*-Golgi, magenta). Without BFA treatment, and after 25 μM or 5 μM BFA treatment for 1.5 h. Scale bars = 20 μm.

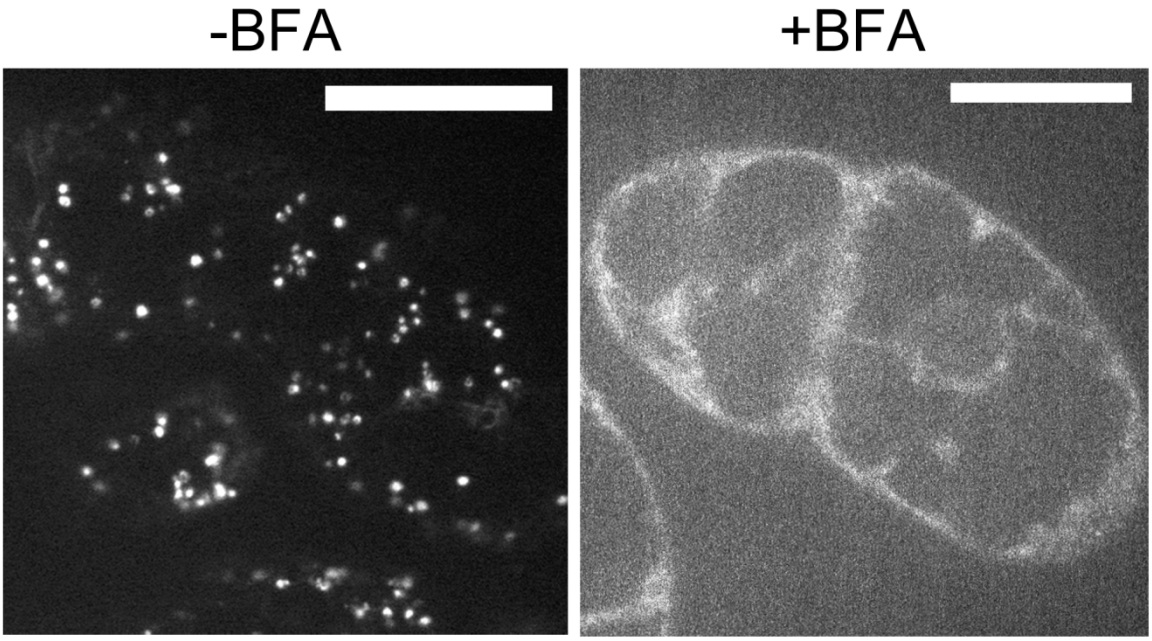

Figure29. Weak BFA treatment of VHA-a1-GFP.
Confocal images of BY-2 cells expressing VHA-a1-GFP. Without BFA treatment (-BFA) and after 10 μM BFA treatment for 1.5 h (+BFA). Scale bars = 20 μm.

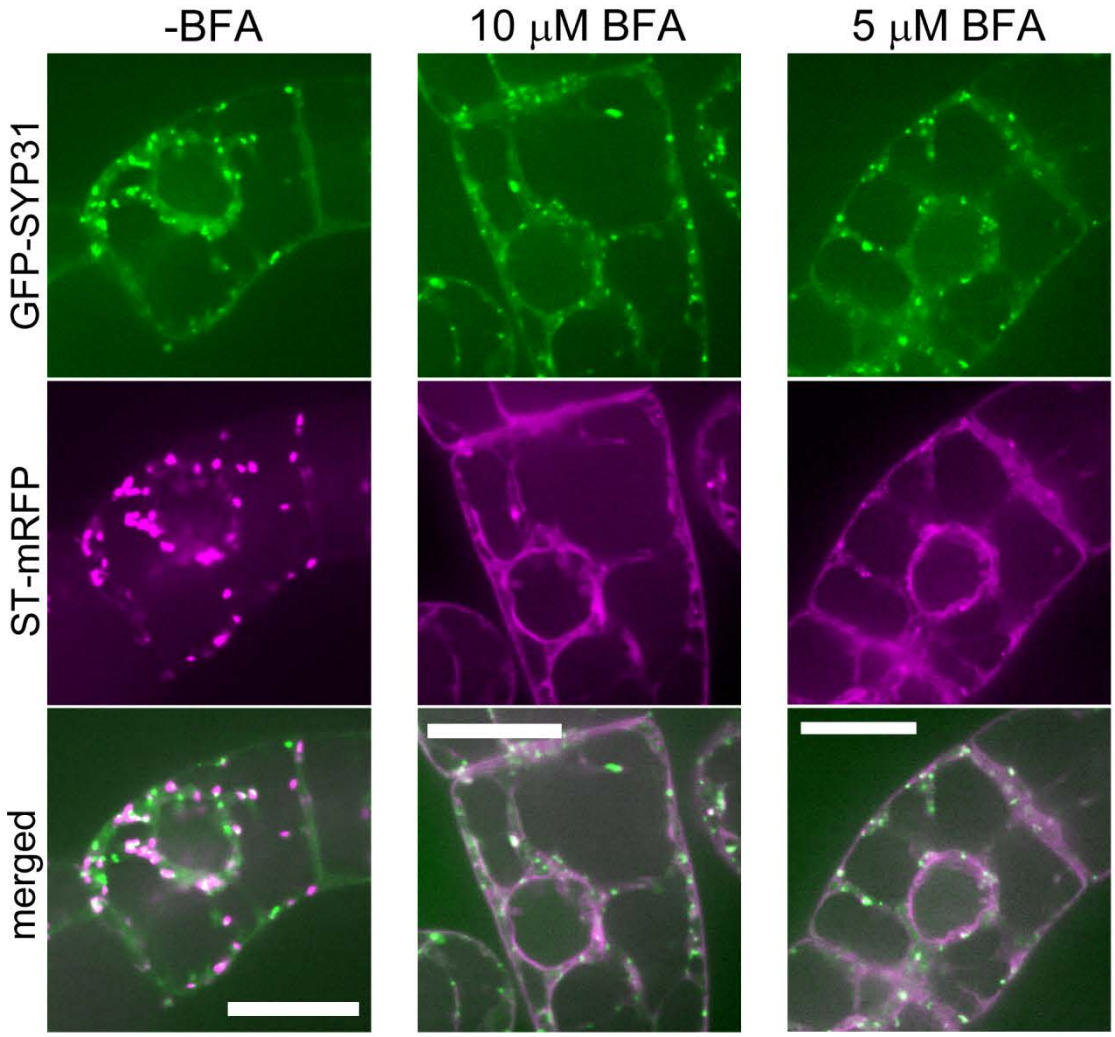

Figure 30. Effects of weak BFA on SYP31.
Confocal images of BY-2 cells expressing GFP-SYP31 (*cis*, green) and ST-mRFP (*trans*, magenta). Without BFA treatment, and after 10 μM or 5 μM BFA treatment for 2 h. Scale bars = 20 μm.

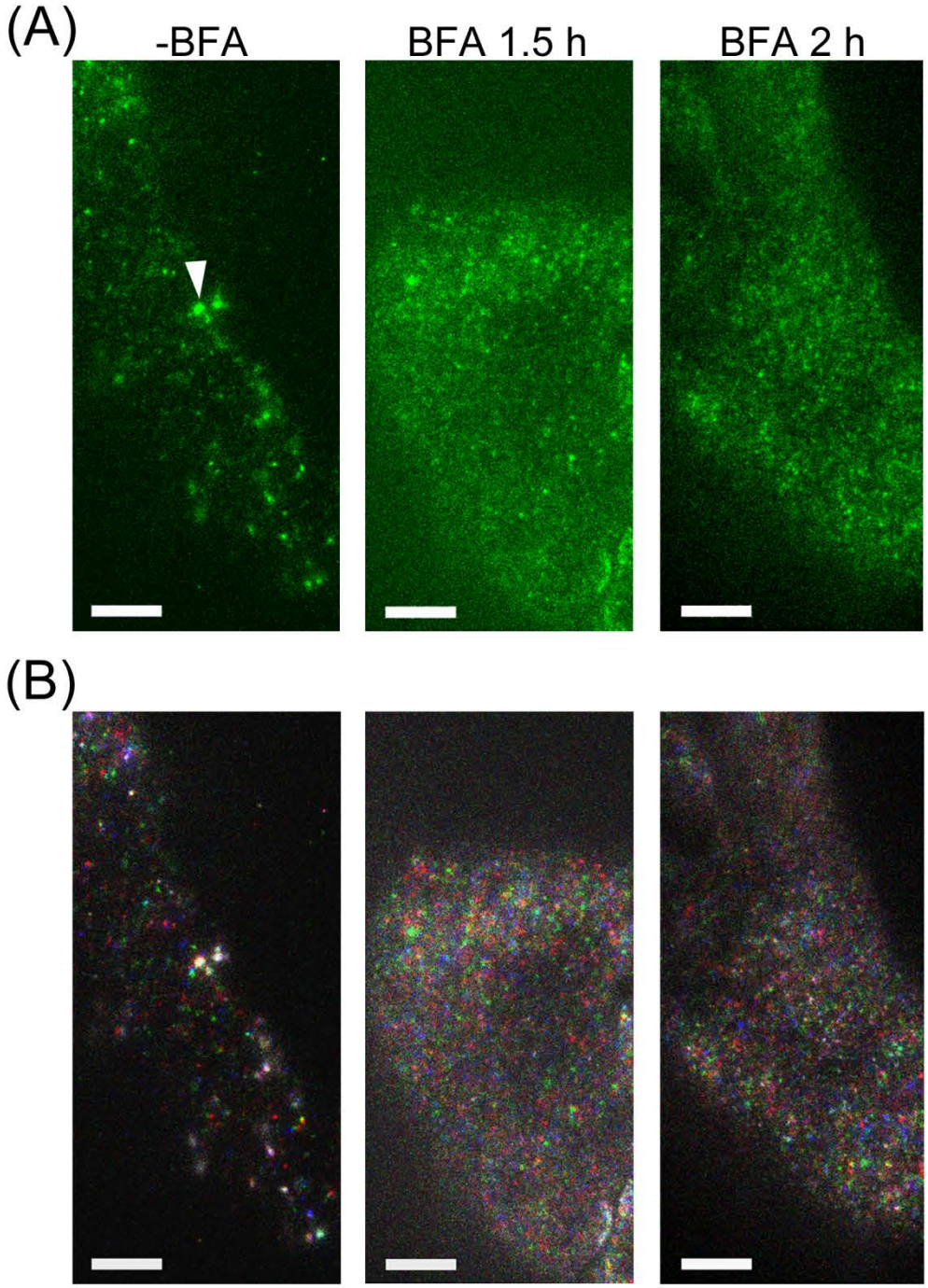

Figure 31. TIRFM observation of SYP41 upon weak BFA treatment.

(A) TIRFM images of the GFP signal of BY-2 cells expressing GFP-SYP41 (TGN) and ST-mRFP (*trans*). Without BFA treatment (-BFA), and after 10 μM BFA treatment for 1.5 or 2 h. The arrowhead indicates the larger structure, which is presumed to be the TGN.

(B) Maximum intensity projection of the time-lapse images of the same cells in (A) with pseudo-colors associated with time (0 sec: red, 1 sec: green, 2 sec: blue.)

Scale bars = 10 μm.

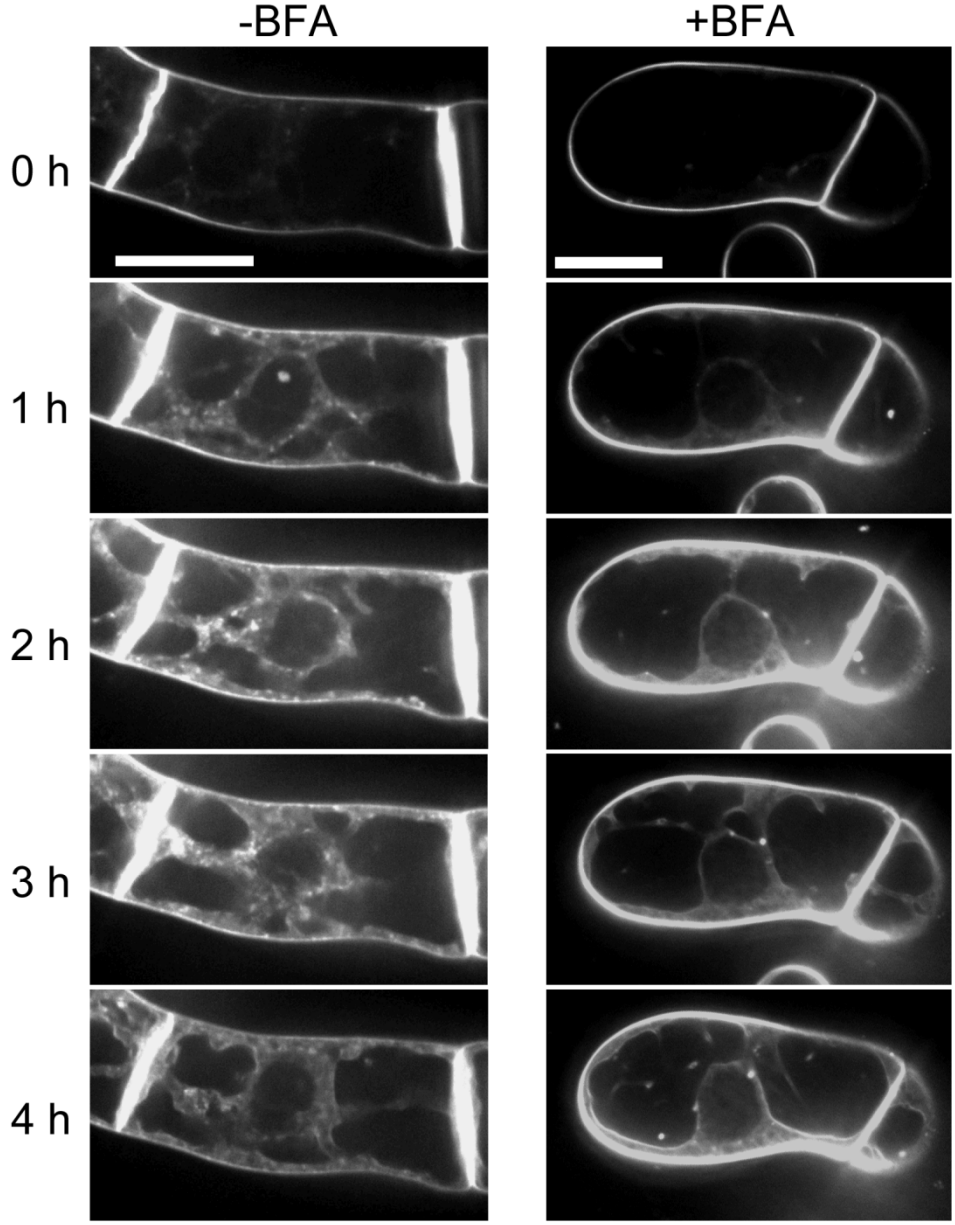

Figure 32. Uptake of FM4-64 with under the presence of weak BFA.
Time-lapse images of BY-2 cells treated with 10 μg/ml FM4-64. Without BFA treatment (-BFA) and the cells treated with 10 μM BFA for 30 min prior to FM4-64 addition (+BFA). The indicated times mean the elapsed time after FM4-64 addition. Scale bars = 20 μm.

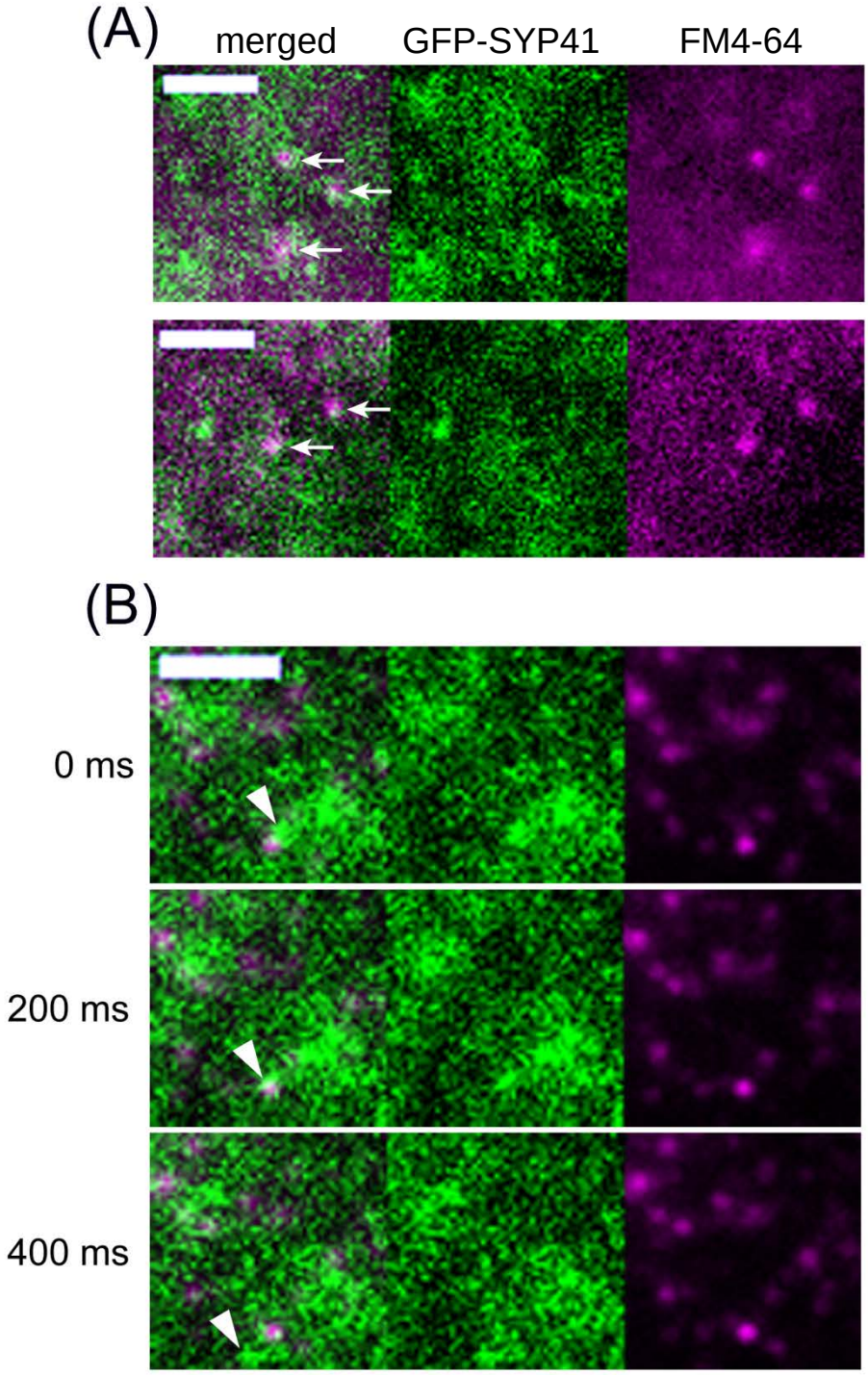

Figure 33. TIRFM observation of SYP41 and FM4-64 upon weak BFA treatment.
BY-2 cells expressing GFP-SYP41 (TGN, green) were treated with 10 μM BFA for 90 min prior to brief FM4-64 treatment (magenta), and washed by fresh medium containing BFA.
(A) TIRFM images. Arrows indicate the partial colocalization of GFP and FM4-64 signals.
(B) Time-lapse images by TIRFM. Arrowheads indicate a punctate signal of GFP that moves toward a FM4-64 dot, seems to associate briefly, and goes away.
Scale bars = 3 μm.

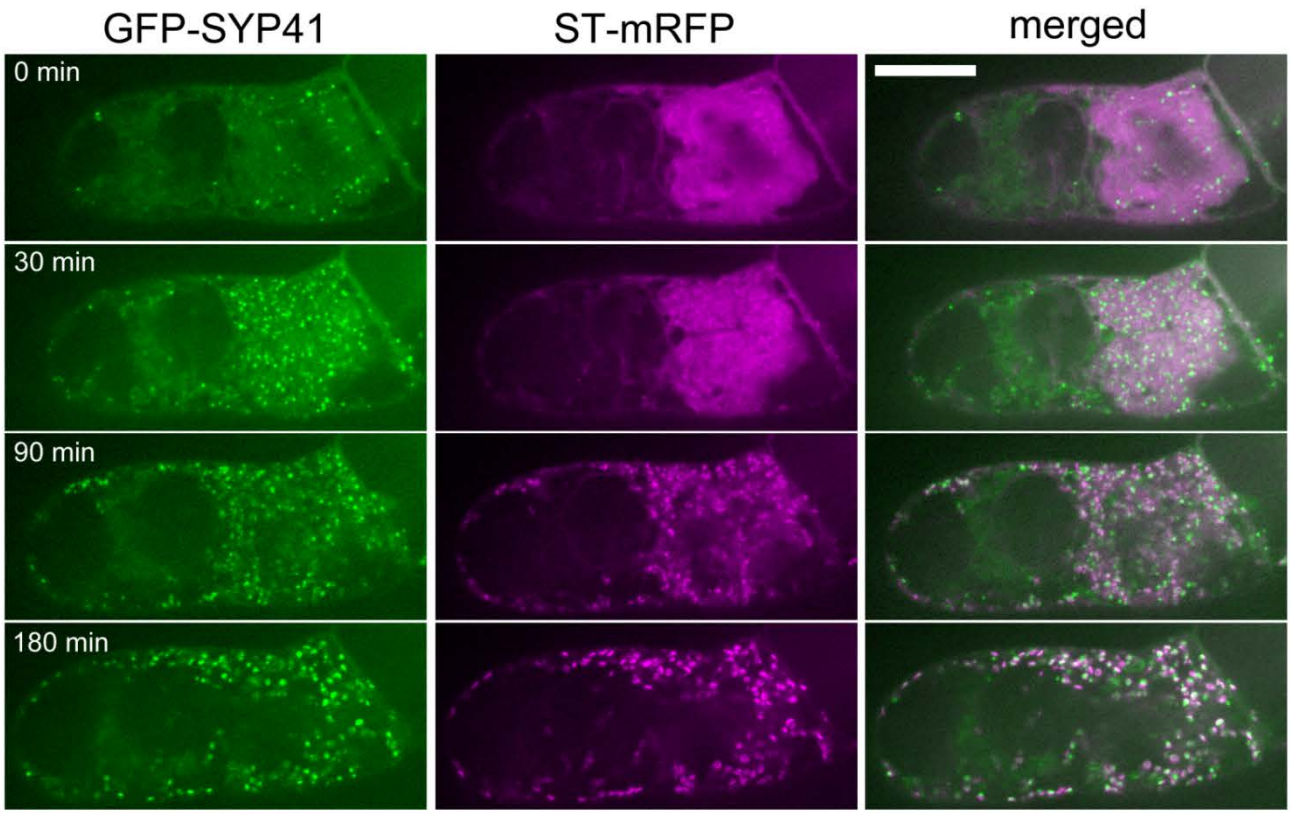

Figure 34. Regeneration of the TGN and *trans*-Golgi after BFA removal.
Time-lapse images of BY-2 cells expressing GFP-SYP41 (TGN, green) and ST-mRFP (*trans*-Golgi, magenta) after BFA removal. The cells were treated with 10 μM BFA for 2 h, and then BFA was removed. LatB (2 μM) was added 30 min before BFA removal, and cycloheximide (100 μM) was added at the point of BFA removal. The indicated times mean the elapsed time after the observation was started. Scale bar = 20 μm.

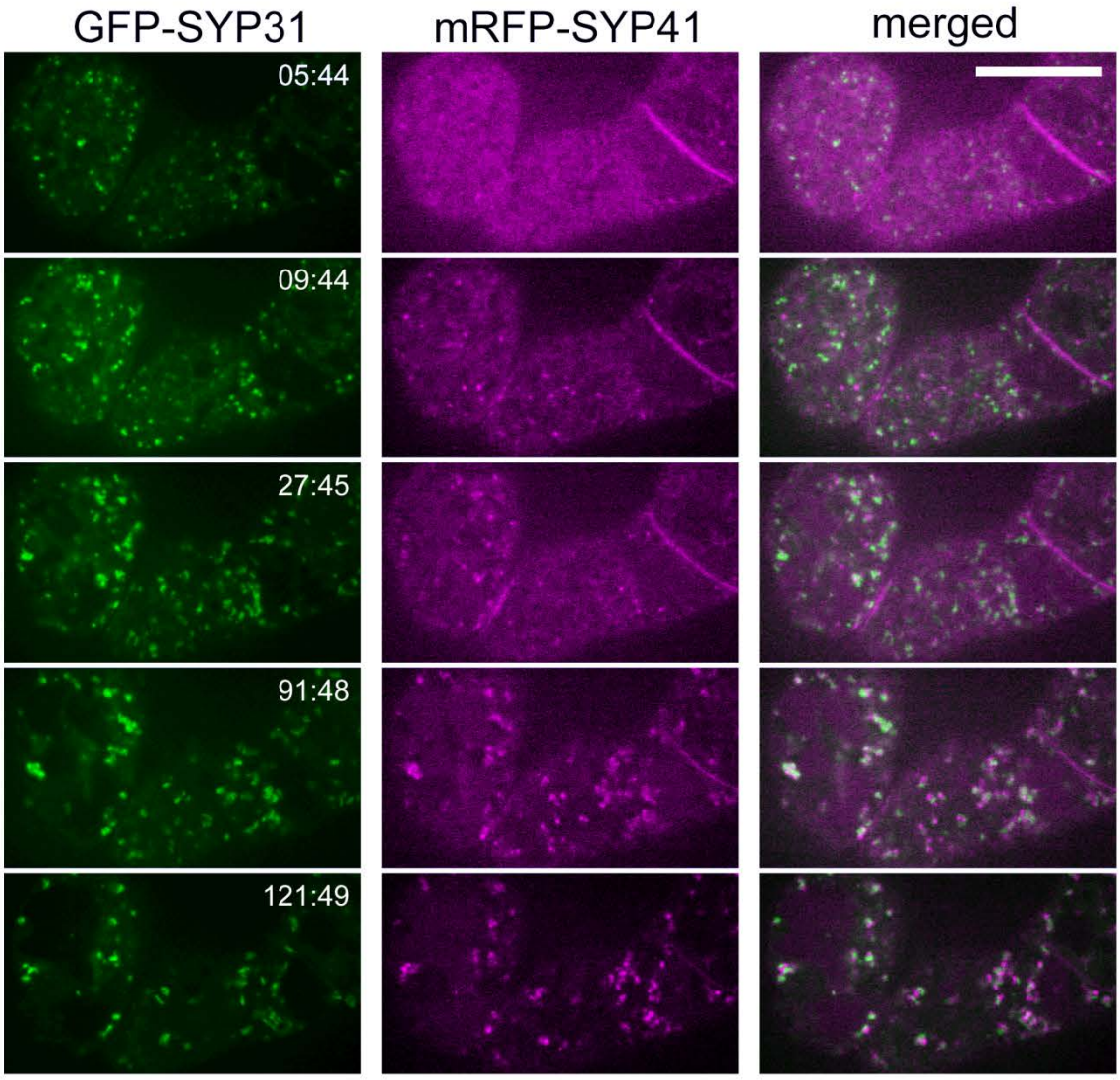

Figure 35. Regeneration of the TGN and *cis*-Golgi after BFA removal.
Time-lapse images of BY-2 cells expressing GFP-SYP31 (*cis*-Golgi, green) and mRFP-SYP41 (TGN, magenta) after BFA removal. The cells were treated with 10 μM BFA for 2 h, and then BFA was removed. LatB (2 μM) was added 30 min before BFA removal, and cycloheximide (100 μM) was added at the point of BFA removal. The indicated times mean the elapsed time after BFA removal. Scale bar = 20 μm.

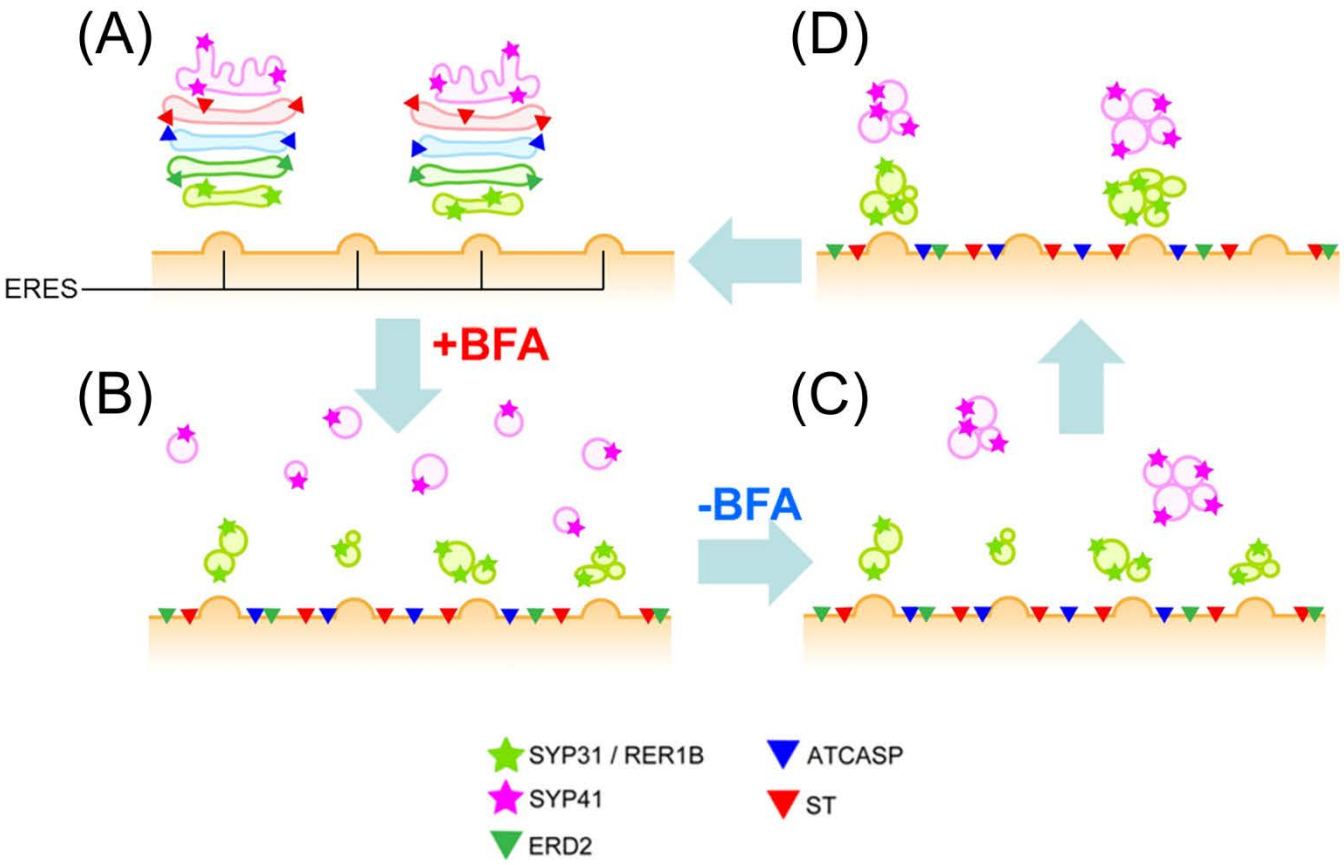

Figure 36. A model for the behaviors of the Golgi apparatus and the TGN upon BFA treatment and removal in plant cells.

(A) The Golgi stacks are located near the ERES, and there might be some ERES without associated Golgi.

(B) By BFA treatment, the proteins of the *cis*-most cisternae localize to the punctate compartments closely associated to the ERES, while other *cis*-, medial-, and *trans*-Golgi proteins relocate to the ER membrane. Some of the TGN proteins relocalize to small vesicle-like structures dispersed throughout the cytoplasm.

(C) After BFA removal, the TGN proteins begin to localize at larger structures, which are not related to the ERES or the punctate compartments of *cis*-Golgi proteins.

(D) The punctate compartments with *cis*-Golgi proteins gather to form the *cis*-most cisternae. The regenerating TGN associates with them. The Golgi stacks reassemble from the regenerated *cis*-most cisternae in the *cis*-to-*trans* order (back to A).

Chapter 4

General Discussion and Perspectives

BFA has been used as a nice tool to investigate Golgi organization especially in mammalian cells in order to know whether the Golgi biogenesis occurs *de novo* from the ER or requires preexisting templates. Those studies have revealed that a subset of Golgi proteins including some *cis*-Golgi components (mammalian homologs of SYP31, RER1, and ERD2) are segregated from other Golgi components including Golgi enzymes by BFA treatment. Such proteins localize at punctate structures adjacent to the ERES, whereas the others are absorbed into the ER (Tang *et al.*, 1993; Nakamura *et al.*, 1995; Füllekrug *et al.*, 1997a; Füllekrug *et al.*, 1997b; Seemann *et al.*, 2000). These structures are often called “Golgi remnants” because they appear to be left behind after the Golgi absorption into the ER. However, it is not evident whether these structures are indeed left behind or are re-formed after fusion with the ER.

Compared to plants, fungi, and invertebrates, the Golgi apparatus is far from the ERES in mammalian cells because the Golgi is concentrated near the nucleus. In order to achieve this long-distance transport, mammalian cells have the specialized compartment called ERGIC (ER-Golgi intermediate compartment). In the ERGIC, sorting and concentration of anterograde and retrograde cargoes by COPI vesicles are thought to take place (Martínez-Menárguez *et al.*, 1999). ERGIC consists of vesiculo-tubular clusters, and is marked by a lectin ERGIC-53 (Schweizer *et al.*, 1990; Appenzeller-Herzog and Hauri, 2006). Similarly to some Golgi proteins, ERGIC-53 is known to localize at the Golgi remnants upon BFA treatment (Lippincott-Schwartz *et al.*, 1990). In the

organisms with discrete Golgi, the Golgi stacks are frequently found in the vicinity of the ERES, thus they have been believed to have no ERGIC. However, a recent report on *C. elegans* Golgi suggests that an ERGIC-like compartment also exists in invertebrate cells, in the region sandwiched between the ERES and the Golgi stack (Witte *et al.*, 2011).

The punctate structures of *cis*-Golgi proteins I have discovered in plant cells upon BFA treatment are very similar to the Golgi remnants in mammalian cells. From this similarity, and moreover from the result that the proteins which localize to the punctate structures seem to originally localize at the *cis*-most cisternae without BFA, I propose that the *cis*-most cisternae of the plant Golgi stacks have the properties equivalent to both the ERGIC and the *cis*-Golgi in mammalian cells. A recent report by electron tomography which suggests that the *cis*-most cisternae in plant cells are biosynthetically inactive supports this idea (Donohoe *et al.*, 2013).

Among the proteins that localize at the Golgi remnants upon BFA treatment, some are suggested to be the candidates for the “Golgi stacking factors”; GRASP65, GRASP55, and GM130 (Seemann *et al.*, 2000). GRASP65 was identified as the major target of a compound that prevents Golgi reassembly after mitosis (Barr *et al.*, 1997), and its homolog GRASP55 was also revealed to have a similar nature (Shorter *et al.*, 1999). Both of them are Golgi matrix proteins, and were shown to interact with another Golgi matrix protein GM130 (Barr *et al.*, 1998; Shorter *et al.*, 1999).

GRASPs are suggested to function after tethering by GM130 (Shorter and Warren, 1999; Puthenveedu *et al.*, 2006; Marra *et al.*, 2007). However, although *in vitro* inhibition of GRASP65 after Golgi disassembly led to the formation of single cisternae without stacking upon reassembly (Barr *et al.*, 1997), *in vivo* inhibition of either GRASP65 or GRASP55 caused only Golgi ribbon fragmentation into ministacks and did not affect the stacked structure (Puthenveedu *et al.*, 2006; Feinstein and Linstedt, 2008). Because double depletion of GRASPs *in vivo* resulted in significant reduction of stacked structure of the Golgi apparatus, mammalian GRASPs are suggested to act in Golgi stacking redundantly, but independently in Golgi ribbon formation (Xiang and Wang, 2010).

However, in spite of their prominent roles in the Golgi structure formation in mammalian cells, the function of GRASP homologs as the “Golgi stacking protein” is not very obvious in other organisms without the Golgi ribbon. Deletion of the only GRASP homolog Grh1 in *P. pastoris* has no significant effect on the Golgi structure (Levi *et al.*, 2010). *S. cerevisiae* also has a GRASP homolog, which localizes to the *cis*-Golgi membrane, in spite of the unstacked Golgi (Behnia *et al.*, 2007). On top of them, GRASP and GM130 are lacking in plants (Latijnhouwers *et al.*, 2007; Klute *et al.*, 2011). Green algae also lack GRASP but red algae have it, indicating the secondary loss of GARSP in the chloroplastida stem lineage (Klute *et al.*, 2011). Whether conservation of the genes involved is too low or completely different components substitute GRASP and GM130 in plants remain obscure. Considering the close relation between the Golgi stacking and the Golgi ribbon

formation in mammalian cells, the organisms with the Golgi ribbon might have developed a different system to maintain the Golgi structure.

From the similarity between the punctate structures in this study and the Golgi remnants in mammalian cells, I speculate that the “Golgi stacking factors” localize at the structures in plant cells. Because I have confirmed that the similar structures can be observed not only in tobacco cells but also in Arabidopsis root cells, now the way to genetical analyses is open. Identification of the components that localize at the structures should contribute to reveal the molecular mechanisms for Golgi biogenesis and maintenance.

Also in this study, the TGN has been revealed to have a special feature different from the other Golgi cisternae. Although the cisternal maturation model appears to be widely accepted now, some conflicting data have been reported. One of them is about the export kinetics of cargo proteins from the Golgi apparatus. In mammalian cells, it has been demonstrated that both big and small secretory cargoes exit the Golgi with exponential kinetics (Patterson *et al.*, 2008). However, in the cisternal maturation model, the cargoes are predicted to exit the Golgi with linear kinetics. The problem can be avoided by modifying the model to include a post-Golgi organelle as a compartment that does not transport the cargoes only by its maturation. From the results I have obtained in this study, I suggest that there is a border of the simple cisternal maturation between the *trans*-Golgi and

the TGN in plant cells. Further investigation of cargo transport not only within the Golgi but also between the Golgi and the TGN will provide more insights.

Although the plant Golgi stacks are believed to double in number prior to cytokinesis (Garcia-Herdugo *et al.*, 1988; Seguí-Simarro and Staehelin, 2006), the Golgi biogenesis around mitosis has never been observed in living cells, mostly because of the technical problems (Nebenführ *et al.*, 2000). From this study using BFA treatment, I speculate that the *cis*-most cisternae might play a key role in Golgi biogenesis around mitosis. Moreover, because the TGN is not likely to be formed only from the Golgi apparatus, the biogenesis process of the TGN might be different from that of the Golgi stacks. I believe that the discoveries in this study will contribute to the future analyses of the biogenesis of plant Golgi and TGN, which would be realized soon by the advance in live imaging techniques.

Experimental Procedures

Construction of plasmids

The dual site Gateway vectors harboring *GFP-SYP31* and *ST-mRFP* (GFP-SYP31/ST-mRFP), *GFP-SYP31* and *mRFP-SYP41* (GFP-SYP31/mRFP-SYP41), and *GFP-SYP41* and *ST-mRFP* (GFP-SYP41/ST-mRFP) were kindly provided by Dr. T. Uemura (The University of Tokyo). *mRFP-SYP31* cloned in pDD301, *ST-mRFP* cloned in pDD302, *mRFP-VAM3* cloned in pGWB1, and *GFP-SYP31* cloned in pGWB1 were also presented by Dr. T. Uemura. The DNA fragment coding P_{35S}-*GFP-RER1B*-T_{NOS} was digested from *RER1B*/pSKP1 (Takeuchi *et al.*, 2000) by *Sal*I and *Not*I and entered into pENTR1A. P_{35S}-*GFP-RER1B*-T_{NOS} in pENTER1A and *mRFP-SYP31* in pDD301 or *ST-mRFP* in pDD302 were recombined into pGWB3501 (kindly gifted by Dr. T. Nakagawa, Shimane University) by LR clonase (Invitrogen), and resulting plasmids were designated as GFP-RER1B/ST-mRFP and GFP-RER1B/mRFP-SYP31, respectively. P_{35S}-*GFP-RER1B*-T_{NOS} in pENTER1A was also used for the LR reaction to generate *GFP-RER1B* in pGWB1.

To generate *ERD2-GFP* in pGWB1, the DNA fragment coding P_{35S}-*ERD2-GFP*-T_{NOS} was amplified by PCR using a primer set (5'-CACC-GATTAGCCTTTTCAATTTCAGAAAG-3' and 5'-TTGCGGGACTCTAATCATAA-3'). The fragment was cloned into pENTR/D-TOPO

(Invitrogen) and recombined into pGWB1 by LR clonase. For the construction of *ERD2-YFP*, the DNA fragment coding *ERD2* was amplified by PCR by using a primer set (5'-CACC-ATGAATATCTTTAGATTTGCTGGCG-3' and 5'-AGCCGGAAGCTTAAGTTTGG-3'), cloned into pENTR/D-TOPO, and recombined into pK7YWG2 (Karimi *et al.*, 2005). The DNA fragment coding *ST* was amplified by PCR using a primer set (5'-CACC-ATGATTCATACCAACTTGAAGAAAAAGTTC-3' and 5'-CATGGCCACTTTCTCCTGG-3'), cloned into pENTR/D-TOPO, and recombined into pH7RWG2 (Karimi *et al*., 2005). *GFP-SYP31* and *mRFP-SYP31* cloned in pENTR/D-TOPO (gifted by Dr. T. Uemura) were recombined into pHGW (Karimi *et al*., 2002) similarly.

For the construction of SEC13-YFP and YFP-ATCASP, each cDNA was amplified by PCR and cloned into pENTR/D-TOPO. The primer sets (5'-CACCATGCCTCCTCAGAAGATTGA-3' and 5'-TGGCTCAACAACAGTCACTT-3' for *SEC13*) and (5'-CACCATGGAGGTTTCGCAAGATGG-3' and 5'-TTAAAGACCGTGAGGAAGGTTT-3' for *ATCASP*) were used. The entry clones of *SEC13* and *ATCASP* were then recombined with pK7YWG2 and pK7WGY2, respectively (Karimi *et al.*, 2005).

SP-GFP-HDEL, *Lifeact-Venus*, and *VHA-a1-GFP* have been already described in Takeuchi *et al*. (2000), Era *et al.* (2009), and Dettmer *et al.* (2006), respectively.

Establishment of transgenic BY-2 cell lines

WT bright yellow-2 (BY-2) tobacco (*Nicotiana tabacum*) cell suspension cultures were grown in modified Murashige and Skoog medium enriched with 0.2 mg l^{-1} 2-4-D and were maintained as described in previous study (Nagata *et al.*, 1992). Three- and four-day-old BY-2 cells were used for the microscopic observations.

Ti plasmids were individually transformed into *Agrobacterium tumefaciens* strain EHA105. Three 5 ml aliquots of 3-day-old BY-2 cells were incubated with 40 μl, 100 μl and 400 μl of the overnight culture of the transformed *A. tumefaciens* as the method described previously (An, 1985). After 48 h incubation at 28 ^{o}C, cells were washed three times in 5 ml of modified MS medium, and resuspended in modified MS medium containing 200 mg l^{-1} claforan with suitable antibiotics for selection: 50 mg l^{-1} hygromycin for ST-mRFP, mRFP-SYP31, GFP-SYP31, GFP-SYP31/ST-mRFP, GFP-RER1B/ST-mRFP, GFP-RER1B/mRFP-SYP31, GFP-SYP31/mRFP-SYP41, and GFP-SYP41/ST-mRFP; 50 mg l^{-1} kanamycin for Lifeact-Venus, SEC13-YFP, and VHA-a1-GFP. Then, the suspended cells were plated onto solid modified MS medium containing the same antibiotics as the medium used for suspension (excluding claforan). After about 3 weeks, selected calli were transferred onto new plates and cultured for about 2 weeks additionally. As each callus reached a size of 1-2 cm in diameter, suitable lines expressing marker proteins at the appropriate level for microscopic observation were selected. Each selected line was transferred to 30 ml of new

modified MS medium, and cultured with continuous shaking similarly to WT cells.

Transgenic BY-2 cells expressing SEC13-YFP/GFP-SYP31/ST-mRFP were established by introducing the SEC13-YFP into the cell line expressing GFP-SYP31/ST-mRFP as the method described above with the *A. tumefaciens* EHA105 with Ti plasmids harboring *SEC13-YFP*. Transformants were suspended in modified MS medium containing 200 mg l^{-1} claforan with 50 mg l^{-1} kanamycin, and selected on plates of solid modified MS medium containing 50 mg l^{-1} kanamycin. The selected calli were transferred onto plates of modified MS medium containing 25 mg l^{-1} hygromycin and 25 mg l^{-1} kanamycin. Transgenic BY-2 cells expressing ERD2-YFP/GFP-SYP31/ST-mRFP or YFP-ATCASP/GFP-SYP31/ST-mRFP were established similarly by using Ti plasmids harboring *ERD2-YFP* or *YFP-ATCASP*, respectively. Transgenic BY-2 cell lines expressing ERD2-GFP/ST-mRFP and SP-GFP-HDEL/ST-mRFP were also established similarly by introducing ERD2-GFP or SP-GFP-HDEL into the cell line expressing ST-mRFP with Ti plasmids harboring *ERD2-GFP* or *SP-GFP-HDEL*, respectively. BY-2 cells expressing GFP-SYP31/mRFP-VAM3 were also established similarly by introducing mRFP-VAM3 into the cell line expressing GFP-SYP31. BY-2 cells expressing SEC13-YFP/mRFP-SYP31 was also established by introducing SEC13-YFP into the cell line expressing mRFP-SYP31.

Transformation and growth conditions of Arabidopsis plants

GFP-RER1B in pGWB1 was used for transforming wild type (Col-0), *gnl1*, and *gnl1/GNL1*^{sens} Arabidopsis plants (Richter *et al.*, 2007). Transformation was performed by floral dipping (Clough and Bent, 1998) using *Agrobacterium tumefaciens* strain GV3101::pMP90. GFP-SYP31 in pGWB1 and ERD2-GFP in pGWB1 were also used for transforming *gnl1/GNL1*^{sens} plants similarly.

Arabidopsis seeds were sterilized and planted on 0.3% agar plates containing half-strength Murashige and Skoog medium, 1% w/v sucrose and vitamins (pH 6.3). Plants were growth in a climate chamber at 23°C under the continuous light.

BFA treatment and removal

50 mM Brefeldin A (BFA; Sigma-Aldrich) diluted in DMSO was prepared as stock solution. Aliquots of stock solution were added to suspension cultures at 50 μM in the final concentration. For Golgi regeneration experiments, BY-2 cells treated with BFA were washed twice by fresh modified MS medium (BFA-free), and resuspended in the modified MS medium containing drugs indicated in the figure legends.

Drug treatments

To depolymerize actin filaments, 2 μM of latrunculin B (LatB; Sigma-Aldrich, stock solution was prepared at 2 mM in DMSO) was added to suspension cultures. To inhibit the protein synthesis, 100 μM of cycloheximide (Sigma-Aldrich, stock solution was prepared at 100 mM in DMSO) was used. The timings when these drugs were added are indicated in the figure legends.

Confocal microscopy

For 2D observation of BY-2 cells expressing fluorescent proteins, two microscopic settings were used: 1) Olympus IX81-ZDC fluorescence microscope equipped with a confocal scanner unit (model CSU10, Yokogawa Electric) and a cooled digital CCD camera (model ORCA-R2, Hamamatsu Photonics) and 2) confocal laser scanning microscope (model LSM710; Zeiss). The latter was also used for confocal observation of Arabidopsis root cells. For long time-lapse observations of BY-2, cells were placed on 35 mm glass bottom dishes with PLL coat (Matsunami). Images were processed and analyzed with MetaMorph (Molecular Devices), ImageJ 1.43 (National Institutes of Health) and Photoshop CS5 (Adobe Systems).

For high-resolution 3D imaging, Super-resolution Confocal Live Imaging Microscopy (SCLIM) was employed. In the SCLIM system we developed (Matsuura-Tokita *et al.*, 2006; Nakano and Luini, 2010; Kurokawa *et al.*, 2013), Olympus IX-70 microscope was equipped with a

custom-made, super-low-noise and high-speed confocal scanner (Yokogawa Electric), custom-made, cooled image intensifiers (Hamamatsu Photonics) and high-speed and high-sensitivity EM-CCD cameras (Hamamatsu Photonics). The objective lens was oscillated vertically to the cover slip by a custom-made, high-speed and low-vibration piezo actuator system (Yokogawa Electric). Data were oversampled and subjected to a deconvolution analysis with Volocity (Improvision) by using the point-spread function optimized for the Yokogawa spinning-disk confocal system.

References

Akkerman, M., Overdijk, E.J.R., Schel, J.H.N., Emons, A.M.C., and Ketelaar, T. (2011). Golgi Body Motility in the Plant Cell Cortex Correlates with Actin Cytoskeleton Organization. Plant Cell Physiol. *52*, 1844-1855.

Alber, F., Dokudovskaya, S., Veenhoff, L.M., Zhang, W., Kipper, J., Devos, D., Suprapto, A., Karni-Schmidt, O., Williams, R., Chait, B.T., Sali, A., and Rout, M.P. (2007). The molecular architecture of the nuclear pore complex. Nature *450*, 695-701.

Alcalde, J., Bonay, P., Roa, A., Vilaro, S., and Sandoval, I.V. (1992). Assembly and disassembly of the Golgi complex: two processes arranged in a *cis-trans* direction. J. Cell Biol. *116*, 69-83.

Appenzeller-Herzog, C., and Hauri, H.-P. (2006). The ER-Golgi intermediate compartment (ERGIC): in search of its identity and function. J. Cell Sci. *119*, 2173-2183.

Axelsson, M.A.B., and Warren, G. (2004). Rapid, endoplasmic reticulum-independent diffusion of the mitotic Golgi haze. Mol. Cell. Biol. *15*, 1843-1852.

Barr, F.A., Nakamura, N., and Warren, G. (1998). Mapping the interaction between GRASP65 and GM130, components of a protein complex involved in the stacking of Golgi cisternae. EMBO J. *17*, 3258-3268.

Barr, F.A., Puype, M., Vandekerckhove, J., and Warren, G. (1997). GRASP65, a Protein Involved in the Stacking of Golgi Cisternae. Cell *91*, 253-262.

Bassham, D.C., Sanderfoot, A.A., Kovaleva, V., Zheng, H., and Raikhel, N.V. (2000). AtVPS45 Complex Formation at the trans-Golgi Network. Mol. Cell. Biol. *11*, 2251-2265.

Beams, H.W., and Kessel, R.G. (1968). The Golgi Apparatus: Structure and Function. In: Int. Rev. Cytol., vol. Volume 23, eds. J.F.D. G.H. Bourne and K.W. Jeon: Academic Press, 209-276.

Beams, H.W., Tahmisian, T.N., Devine, R.L., and Anderson, E. (1956). ELECTRON MICROSCOPE STUDIES ON THE DICTYOSOMES AND ACROBLASTS IN THE MALE GERM CELLS OF THE CRICKET. J. Biophys. Biochem. Cytol. *2*, 123-128.

Behnia, R., Barr, F.A., Flanagan, J.J., Barlowe, C., and Munro, S. (2007). The yeast orthologue of GRASP65 forms a complex with a coiled-coil protein that contributes to ER to Golgi traffic. J. Cell Biol. *176*, 255-261.

Benchimol, M., Consort Ribeiro, K., Meyer Mariante, R., and Alderete, J.F. (2001). Structure and division of the Golgi complex in *Trichomonas vaginalis* and *Tritrichomonas foetus*. Eur. J. Cell Biol. *80*, 593-607.

Bentivoglio, M. (1998). 1898: The Golgi apparatus emerges from nerve cells. Trends Neurosci. *21*, 195-200.

Boevink, P., Oparka, K., Cruz, S.S., Martin, B., Betteridge, A., and Hawes, C. (1998). Stacks on tracks: the plant Golgi apparatus traffics on an actin/ER network. Plant J. *15*, 441-447.

Brandizzi, F., and Barlowe, C. (2013). Organization of the ER-Golgi interface for membrane traffic control. Nat. Rev. Mol. Cell Biol. *14*, 382-392.

Bubeck, J., Scheuring, D., Hummel, E., Langhans, M., Viotti, C., Foresti, O., Denecke, J., Banfield, D.K., and Robinson, D.G. (2008). The syntaxins SYP31 and SYP81 control ER–Golgi trafficking in the plant secretory pathway. Traffic *9*, 1629-1652.

Cavalier-Smith, T. (1987). Eukaryotes with no mitochondria. Nature *326*, 332-333.

Chardin, P., and McCormick, F. (1999). Brefeldin A: the advantage of being uncompetitive. Cell *97*, 153-155.

Choi, S.-w., Tamaki, T., Ebine, K., Uemura, T., Ueda, T., and Nakano, A. (2013). RABA Members Act in Distinct Steps of Subcellular Trafficking of the FLAGELLIN SENSING2 Receptor. Plant Cell *25*, 1174-1187.

Clough, S.J., and Bent, A.F. (1998). Floral dip: a simplified method forAgrobacterium-mediated transformation ofArabidopsis thaliana. Plant J. *16*, 735-743.

Cosson, P., Amherdt, M., Rothman, J.E., and Orci, L. (2002). A resident Golgi protein is excluded from peri-Golgi vesicles in NRK cells. Proc. Natl. Acad. Sci. USA *99*, 12831-12834.

Dalton, A.J. (1951). Observations of the Golgi Substance with the Electron Microscope. Nature *168*, 244-245.

Dalton, A.J., and Felix, M.D. (1954). Cytologic and cytochemical characteristics of the Golgi substance of epithelial cells of the epididymis–in situ, in homogenates and after isolation. Am. J. Anat. *94*, 171-207.

daSilva, L.L., Snapp, E.L., Denecke, J., Lippincott-Schwartz, J., Hawes, C., and Brandizzi, F. (2004).

Endoplasmic reticulum export sites and Golgi bodies behave as single mobile secretory units in plant cells. Plant Cell *16*, 1753-1771.

Dettmer, J., Hong-Hermesdorf, A., Stierhof, Y.D., and Schumacher, K. (2006). Vacuolar H^+-ATPase activity is required for endocytic and secretory trafficking in *Arabidopsis*. Plant Cell *18*, 715-730.

Donaldson, J.G., Finazzi, D., and Klausner, R.D. (1992). Brefeldin A inhibits Golgi membrane-catalysed exchange of guanine nucleotide onto ARF protein. Nature *360*, 350-352.

Donaldson, J.G., Lippincott-Schwartz, J., Bloom, G.S., Kreis, T.E., and Klausner, R.D. (1990). Dissociation of a 110-kD peripheral membrane protein from the Golgi apparatus is an early event in brefeldin A action. J. Cell Biol. *111*, 2295-2306.

Donohoe, B.S., Kang, B.-H., Gerl, M.J., Gergely, Z.R., McMichael, C.M., Bednarek, S.Y., and Staehelin, L.A. (2013). *Cis*-Golgi Cisternal Assembly and Biosynthetic Activation Occur Sequentially in Plants and Algae. Traffic *14*, 551-567.

Donohoe, B.S., Kang, B.-H., and Staehelin, L.A. (2007). Identification and characterization of COPIa- and COPIb-type vesicle classes associated with plant and algal Golgi. Proc. Natl. Acad. Sci. USA *104*, 163-168.

Dunphy, W.G., and Rothman, J.E. (1985). Compartmental organization of the Golgi stack. Cell *42*, 13-21.

Dupree, P., and Sherrier, D.J. (1998). The plant Golgi apparatus. BBA-Mol. Cell. Res. *1404*, 259-270.

Era, A., Tominaga, M., Ebine, K., Awai, C., Saito, C., Ishizaki, K., Yamato, K.T., Kohchi, T., Nakano, A., and Ueda, T. (2009). Application of Lifeact reveals F-actin dynamics in *Arabidopsis thaliana* and the liverwort, *Marchantia polymorpha*. Plant Cell Physiol. *50*, 1041-1048.

Espenshade, P., Gimeno, R.E., Holzmacher, E., Teung, P., and Kaiser, C.A. (1995). Yeast SEC16 gene encodes a multidomain vesicle coat protein that interacts with Sec23p. J. Cell Biol. *131*, 311-324.

Füllekrug, J., Boehm, J., Röttger, S., Nilsson, T., Mieskes, G., and Schmitt, H.D. (1997a). Human Rer1 is localized to the Golgi apparatus and complements the deletion of the homologous Rer1 protein of Saccharomyces cerevisiae. Eur. J. Cell Biol. *74*, 31-40.

Füllekrug, J., Sönnichsen, B., Schäfer, U., Nguyen Van, P., Söling, H.D., and Mieskes, G. (1997b). Characterization of brefeldin A induced vesicular structures containing cycling proteins of the intermediate compartment/cis-Golgi network. FEBS Lett. *404*, 75-81.

Feinstein, T.N., and Linstedt, A.D. (2008). GRASP55 Regulates Golgi Ribbon Formation. Mol. Cell. Biol. *19*, 2696-2707.

Fujimoto, M., Arimura, S., Nakazono, M., and Tsutsumi, N. (2007). Imaging of plant dynamin-related proteins and clathrin around the plasma membrane by variable incidence angle fluorescence microscopy. Plant Biotechnol. *24*, 449-455.

Fujiwara, T., Oda, K., Yokota, S., Takatsuki, A., and Ikehara, Y. (1988). Brefeldin A causes disassembly of the Golgi complex and accumulation of secretory proteins in the endoplasmic reticulum. J. Biol. Chem. *263*, 18545-18552.

Garcia-Herdugo, G., González-Reyes, J.A., Gracia-Navarro, F., and Navas, P. (1988). Growth kinetics of the Golgi apparatus during the cell cycle in onion root meristems. Planta *175*, 305-312.

Gaynor, E.C., and Emr, S.D. (1997). COPI-independent anterograde transport: cargo-selective ER to Golgi protein transport in yeast COPI mutants. J. Cell Biol. *136*, 789-802.

Gilson, P., Vergara, C., Kjer-Nielsen, L., Teasdale, R., Bacic, A., and Gleeson, P. (2004). Identification of a Golgi-localised GRIP domain protein from Arabidopsis thaliana. Planta *219*, 1050-1056.

Gimeno, R.E., Espenshade, P., and Kaiser, C.A. (1996). COPII coat subunit interactions: Sec24p and Sec23p bind to adjacent regions of Sec16p. Mol. Cell. Biol. *7*, 1815-1823.

Glick, B.S., and Luini, A. (2011). Models for Golgi Traffic: A Critical Assessment. Cold Spring Harbor Perspectives in Biology *3*, a005215.

Glick, B.S., and Nakano, A. (2009). Membrane traffic within the Golgi apparatus. Annu. Rev. Cell. Dev. Biol. *25*, 113-132.

Golgi, C. (1898). Sur la structure des cellules nerveuses. Arch. Ital. Biol. *30*, 60-71.

Goud, B., and Gleeson, P.A. (2010). TGN golgins, Rabs and cytoskeleton: regulating the Golgi trafficking highways. Trends Cell Biol. *20*, 329-336.

Griffiths, G., and Simons, K. (1986). The *trans* Golgi network: sorting at the exit site of the Golgi complex. Science *234*, 438-443.

Hammond, A.T., and Glick, B.S. (2000). Dynamics of Transitional Endoplasmic Reticulum Sites in Vertebrate Cells. Mol. Cell. Biol. *11*, 3013-3030.

Hanton, S., Chatre, L., Matheson, L., Rossi, M., Held, M., and Brandizzi, F. (2008). Plant Sar1 isoforms with near-identical protein sequences exhibit different localisations and effects on secretion. Plant Mol. Biol. *67*, 283-294.

Hanton, S.L., Chatre, L., Renna, L., Matheson, L.A., and Brandizzi, F. (2007). De Novo Formation of Plant Endoplasmic Reticulum Export Sites Is Membrane Cargo Induced and Signal Mediated. Plant Physiol. *143*, 1640-1650.

Hanton, S.L., Matheson, L.A., Chatre, L., and Brandizzi, F. (2009). Dynamic organization of COPII coat proteins at endoplasmic reticulum export sites in plant cells. Plant J. *57*, 963-974.

He, C.Y., Ho, H.H., Malsam, J., Chalouni, C., West, C.M., Ullu, E., Toomre, D., and Warren, G. (2004). Golgi duplication in *Trypanosoma brucei*. J. Cell Biol. *165*, 313-321.

Helms, J.B., and Rothman, J.E. (1992). Inhibition by brefeldin A of a Golgi membrane enzyme that catalyses exchange of guanine nucleotide bound to ARF. Nature *360*, 352-354.

Horton, A.C., and Ehlers, M.D. (2003). Dual Modes of Endoplasmic Reticulum-to-Golgi Transport in Dendrites Revealed by Live-Cell Imaging. J. Neurosci. *23*, 6188-6199.

Ito, Y., Uemura, T., and Nakano, A. Formation and maintenance of the plant Golgi apparatus. Int. Rev. Cell Mol. Biol. in press.

Ito, Y., Uemura, T., Shoda, K., Fujimoto, M., Ueda, T., and Nakano, A. (2012). *cis*-Golgi proteins

accumulate near the ER exit sites and act as the scaffold for Golgi regeneration after brefeldin A treatment in tobacco BY-2 cells. Mol. Cell. Biol. *23*, 3203-3214.

Jékely, G. (2008). Evolution of the Golgi complex. In: The Golgi Apparatus, eds. A. Mironov and M. Pavelka: Springer Vienna, 675-691.

Jackson, C.L., and Casanova, J.E. (2000). Turning on ARF: the Sec7 family of guanine-nucleotide-exchange factors. Trends Cell Biol. *10*, 60-67.

Karimi, M., De Meyer, B., and Hilson, P. (2005). Modular cloning in plant cells. Trends Plant Sci. *10*, 103-105.

Keller, P., and Simons, K. (1997). Post-Golgi biosynthetic trafficking. J. Cell Sci. *110*, 3001-3009.

Klute, M.J., Melançon, P., and Dacks, J.B. (2011). Evolution and Diversity of the Golgi. Cold Spring Harbor Perspectives in Biology *3*, a007849.

Kondylis, V., and Rabouille, C. (2009). The Golgi apparatus: Lessons from Drosophila. FEBS Lett. *583*, 3827-3838.

Konopka, C.A., and Bednarek, S.Y. (2008). Variable‐angle epifluorescence microscopy: a new way to look at protein dynamics in the plant cell cortex. Plant J. *53*, 186-196.

Kuge, O., Dascher, C., Orci, L., Rowe, T., Amherdt, M., Plutner, H., Ravazzola, M., Tanigawa, G., Rothman, J.E., and Balch, W.E. (1994). Sar1 promotes vesicle budding from the endoplasmic reticulum but not Golgi compartments. J. Cell Biol. *125*, 51-65.

Kurokawa, K., Ishii, M., Suda, Y., Ichihara, A., and Nakano, A. (2013). Live Cell Visualization of Golgi Membrane Dynamics by Super-resolution Confocal Live Imaging Microscopy. In: Methods Cell Biol., vol. Volume 118, eds. P. Franck and J.S. David: Academic Press, 235-242.

Kweon, H.-S., Beznoussenko, G.V., Micaroni, M., Polishchuk, R.S., Trucco, A., Martella, O., Di Giandomenico, D., Marra, P., Fusella, A., Di Pentima, A., Berger, E.G., Geerts, W.J.C., Koster, A.J., Burger, K.N.J., Luini, A., and Mironov, A.A. (2004). Golgi Enzymes Are Enriched in Perforated Zones of Golgi Cisternae but Are Depleted in COPI Vesicles. Mol. Cell. Biol. *15*, 4710-4724.

Ladinsky, M.S., Wu, C.C., McIntosh, S., McIntosh, J.R., and Howell, K.E. (2002). Structure of the Golgi and Distribution of Reporter Molecules at 20°C Reveals the Complexity of the Exit Compartments. Mol. Cell. Biol. *13*, 2810-2825.

Langhans, M., Förster, S., Helmchen, G., and Robinson, D.G. (2011). Differential effects of the brefeldin A analogue (6R)-hydroxy-BFA in tobacco and Arabidopsis. J. Exp. Bot. *62*, 2949-2957.

Langhans, M., Hawes, C., Hillmer, S., Hummel, E., and Robinson, D.G. (2007). Golgi regeneration after brefeldin A treatment in BY-2 cells entails stack enlargement and cisternal growth followed by division. Plant Physiol. *145*, 527-538.

Langhans, M., Meckel, T., Kress, A., Lerich, A., and Robinson, D. (2012). ERES (ER exit sites) and the “Secretory Unit Concept”. J. Microsc. *247*, 48-59.

Latijnhouwers, M., Gillespie, T., Boevink, P., Kriechbaumer, V., Hawes, C., and Carvalho, C.M. (2007). Localization and domain characterization of *Arabidopsis* golgin candidates. J. Exp. Bot. *58*, 4373-4386.

Latijnhouwers, M., Hawes, C., Carvalho, C., Oparka, K., Gillingham, A.K., and Boevink, P. (2005). An Arabidopsis GRIP domain protein locates to the trans‐Golgi and binds the small GTPase ARL1. Plant J. *44*, 459-470.

Lavieu, G., Zheng, H., and Rothman, J.E. (2013). Stapled Golgi cisternae remain in place as cargo passes through the stack. eLife *2*, e00558.

Lee, H.I., Gal, S., Newman, T.C., and Raikhel, N.V. (1993). The *Arabidopsis* endoplasmic reticulum retention receptor functions in yeast. Proc. Natl. Acad. Sci. USA *90*, 11433-11437.

Levi, S.K., Bhattacharyya, D., Strack, R.L., Austin, J.R., and Glick, B.S. (2010). The Yeast GRASP Grh1 Colocalizes with COPII and Is Dispensable for Organizing the Secretory Pathway. Traffic *11*, 1168-1179.

Lewis, M.J., Sweet, D.J., and Pelham, H.R.B. (1990). The *ERD2* gene determines the specificity of the luminal ER protein retention system. Cell *61*, 1359-1363.

Lippincott-Schwartz, J., Donaldson, J.G., Schweizer, A., Berger, E.G., Hauri, H.P., Yuan, L.C., and Klausner, R.D. (1990). Microtubule-dependent retrograde transport of proteins into the ER in the presence of brefeldin A suggests an ER recycling pathway. Cell *60*, 821-836.

Lippincott-Schwartz, J., Yuan, L.C., Bonifacino, J.S., and Klausner, R.D. (1989). Rapid redistribution of Golgi proteins into the ER in cells treated with brefeldin A: Evidence for membrane cycling from Golgi to ER. Cell *56*, 801-813.

Losev, E., Reinke, C.A., Jellen, J., Strongin, D.E., Bevis, B.J., and Glick, B.S. (2006). Golgi

maturation visualized in living yeast. Nature *441*, 1002-1006.

Lowe, M. (2011). Structural organization of the Golgi apparatus. Curr. Opin. Cell Biol. *23*, 85-93.

Lowe, S.L., Wong, S.H., and Hong, W. (1996). The mammalian ARF-like protein 1 (Arl1) is associated with the Golgi complex. J. Cell Sci. *109*, 209-220.

Madison, S.L., and Nebenführ, A. (2011). Live-Cell Imaging of Dual-Labeled Golgi Stacks in Tobacco BY-2 Cells Reveals Similar Behaviors for Different Cisternae during Movement and Brefeldin A Treatment. Mol. Plant *4*, 896-908.

Man, Z., Kondo, Y., Koga, H., Umino, H., Nakayama, K., and Shin, H.-W. (2011). Arfaptins Are Localized to the trans-Golgi by Interaction with Arl1, but Not Arfs. J. Biol. Chem. *286*, 11569-11578.

Marra, P., Salvatore, L., Mironov, A., Di Campli, A., Di Tullio, G., Trucco, A., Beznoussenko, G., and De Matteis, M.A. (2007). The Biogenesis of the Golgi Ribbon: The Roles of Membrane Input from the ER and of GM130. Mol. Cell. Biol. *18*, 1595-1608.

Martínez-Menárguez, J.A., Geuze, H.J., Slot, J.W., and Klumperman, J. (1999). Vesicular Tubular Clusters between the ER and Golgi Mediate Concentration of Soluble Secretory Proteins by Exclusion from COPI-Coated Vesicles. Cell *98*, 81-90.

Matsuura-Tokita, K., Takeuchi, M., Ichihara, A., Mikuriya, K., and Nakano, A. (2006). Live imaging of yeast Golgi cisternal maturation. Nature *441*, 1007-1010.

McConville, M.J., Ilgoutz, S.C., Teasdale, R.D., Foth, B.J., Matthews, A., Mullin, K.A., and Gleeson,

P.A. (2002). Targeting of the GRIP domain to the *trans*-Golgi network is conserved from protists to animals. Eur. J. Cell Biol. *81*, 485-495.

Mellman, I., and Warren, G. (2000). The road taken: past and future foundations of membrane traffic. Cell *100*, 99-112.

Memon, A.R. (2004). The role of ADP-ribosylation factor and SAR1 in vesicular trafficking in plants. Biochim. Biophys. Acta *1664*, 9-30.

Mogelsvang, S., Gomez-Ospina, N., Soderholm, J., Glick, B.S., and Staehelin, L.A. (2003). Tomographic evidence for continuous turnover of Golgi cisternae in *Pichia pastoris*. Mol. Cell. Biol. *14*, 2277-2291.

Moore, P.J., Swords, K.M., Lynch, M.A., and Staehelin, L.A. (1991). Spatial organization of the assembly pathways of glycoproteins and complex polysaccharides in the Golgi apparatus of plants. J. Cell Biol. *112*, 589-602.

Mowbrey, K., and Dacks, J.B. (2009). Evolution and diversity of the Golgi body. FEBS Lett. *583*, 3738-3745.

Nakamura, N., Rabouille, C., Watson, R., Nilsson, T., Hui, N., Slusarewicz, P., Kreis, T.E., and Warren, G. (1995). Characterization of a *cis*-Golgi matrix protein, GM130. J. Cell Biol. *131*, 1715-1726.

Nakano, A., and Luini, A. (2010). Passage through the Golgi. Curr. Opin. Cell Biol. *22*, 471-478.

Nebenführ, A., Frohlick, J.A., and Staehelin, L.A. (2000). Redistribution of Golgi stacks and other

organelles during mitosis and cytokinesis in plant cells. Plant Physiol. *124*, 135-151.

Nebenführ, A., Gallagher, L.A., Dunahay, T.G., Frohlick, J.A., Mazurkiewicz, A.M., Meehl, J.B., and Staehelin, L.A. (1999). Stop-and-go movements of plant Golgi stacks are mediated by the acto-myosin system. Plant Physiol. *121*, 1127-1141.

Okamoto, M., Kurokawa, K., Matsuura-Tokita, K., Saito, C., Hirata, R., and Nakano, A. (2012). High-curvature domains of the ER are important for the organization of ER exit sites in *Saccharomyces cerevisiae*. J. Cell Sci. *125*, 3412-3420.

Orci, L., Amherdt, M., Ravazzola, M., Perrelet, A., and Rothman, J.E. (2000). Exclusion of Golgi Residents from Transport Vesicles Budding from Golgi Cisternae in Intact Cells. J. Cell Biol. *150*, 1263-1270.

Orci, L., Ravazzola, M., Meda, P., Holcomb, C., Moore, H.P., Hicke, L., and Schekman, R. (1991). Mammalian Sec23p homologue is restricted to the endoplasmic reticulum transitional cytoplasm. Proc. Natl. Acad. Sci. USA *88*, 8611-8615.

Osterrieder, A. (2012). Tales of tethers and tentacles: golgins in plants. J. Microsc. *247*, 68-77.

Paccaud, J.P., Reith, W., Carpentier, J.L., Ravazzola, M., Amherdt, M., Schekman, R., and Orci, L. (1996). Cloning and functional characterization of mammalian homologues of the COPII component Sec23. Mol. Cell. Biol. *7*, 1535-1546.

Parsons, H.T., Drakakaki, G., and Heazlewood, J.L. (2013). Proteomic dissection of the *Arabidopsis* Golgi and *trans*-Golgi network. Front. Plant. Sci. *3*, 298.

Patterson, G.H., Hirschberg, K., Polishchuk, R.S., Gerlich, D., Phair, R.D., and Lippincott-Schwartz, J. (2008). Transport through the Golgi Apparatus by Rapid Partitioning within a Two-Phase Membrane System. Cell *133*, 1055-1067.

Pelletier, L., Stern, C.A., Pypaert, M., Sheff, D., Ngô, H.M., Roper, N., He, C.Y., Hu, K., Toomre, D., Coppens, I., Roos, D.S., Joiner, K.A., and Warren, G. (2002). Golgi biogenesis in *Toxoplasma gondii*. Nature *418*, 548-552.

Persico, A., Cervigni, R.I., Barretta, M.L., and Colanzi, A. (2009). Mitotic inheritance of the Golgi complex. FEBS Lett. *583*, 3857-3862.

Pesacreta, T.C., and Lucas, W.J. (1985). Presence of a partially-coated reticulum in angiosperms. Protoplasma *125*, 173-184.

Polishchuk, R.S., Polishchuk, E.V., and Mironov, A.A. (1999). Coalescence of Golgi fragments in microtubule-deprived living cells. Eur. J. Cell Biol. *78*, 170-185.

Popoff, V., Adolf, F., Brügger, B., and Wieland, F. (2011). COPI Budding within the Golgi Stack. Cold Spring Harbor Perspectives in Biology *3*, a005231.

Preuss, D., Mulholland, J., Franzusoff, A., Segev, N., and Botstein, D. (1992). Characterization of the Saccharomyces Golgi complex through the cell cycle by immunoelectron microscopy. Mol. Cell. Biol. *3*, 789-803.

Puri, S., and Linstedt, A.D. (2003). Capacity of the Golgi apparatus for biogenesis from the endoplasmic reticulum. Mol. Cell. Biol. *14*, 5011-5018.

Puthenveedu, M.A., Bachert, C., Puri, S., Lanni, F., and Linstedt, A.D. (2006). GM130 and GRASP65-dependent lateral cisternal fusion allows uniform Golgi-enzyme distribution. Nat. Cell Biol. *8*, 238-248.

Rabouille, C., Hui, N., Hunte, F., Kieckbusch, R., Berger, E.G., Warren, G., and Nilsson, T. (1995). Mapping the distribution of Golgi enzymes involved in the construction of complex oligosaccharides. J. Cell Sci. *108*, 1617-1627.

Renna, L., Hanton, S.L., Stefano, G., Bortolotti, L., Misra, V., and Brandizzi, F. (2005). Identification and characterization of AtCASP, a plant transmembrane Golgi matrix protein. Plant Mol. Biol. *58*, 109-122.

Richter, S., Geldner, N., Schrader, J., Wolters, H., Stierhof, Y.D., Rios, G., Koncz, C., Robinson, D.G., and Jürgens, G. (2007). Functional diversification of closely related ARF-GEFs in protein secretion and recycling. Nature *448*, 488-492.

Rios, R.M., and Bornens, M. (2003). The Golgi apparatus at the cell centre. Curr. Opin. Cell Biol. *15*, 60-66.

Ritzenthaler, C., Nebenführ, A., Movafeghi, A., Stussi-Garaud, C., Behnia, L., Pimpl, P., Staehelin, L.A., and Robinson, D.G. (2002). Reevaluation of the effects of brefeldin A on plant cells using tobacco Bright Yellow 2 cells expressing Golgi-targeted green fluorescent protein and COPI antisera. Plant Cell *14*, 237-261.

Rizzo, R., Parashuraman, S., Mirabelli, P., Puri, C., Lucocq, J., and Luini, A. (2013). The dynamics of engineered resident proteins in the mammalian Golgi complex relies on cisternal maturation. J.

Cell Biol. *201*, 1027-1036.

Robinson, D.G., Scheuring, D., Naramoto, S., and Friml, J. (2011). ARF1 localizes to the Golgi and the *trans*-Golgi network. Plant Cell *23*, 846.

Robinson, M.S., and Kreis, T.E. (1992). Recruitment of coat proteins onto Golgi membranes in intact and permeabilized cells: effects of brefeldin A and G protein activators. Cell *69*, 129-138.

Rossanese, O.W., Soderholm, J., Bevis, B.J., Sears, I.B., O'Connor, J., Williamson, E.K., and Glick, B.S. (1999). Golgi structure correlates with transitional endoplasmic reticulum organization in *Pichia pastoris* and *Saccharomyces cerevisiae*. J. Cell Biol. *145*, 69-81.

Roth, J., Taatjes, D.J., Lucocq, J.M., Weinstein, J., and Paulson, J.C. (1985). Demonstration of an extensive *trans*-tubular network continuous with the Golgi apparatus stack that may function in glycosylation. Cell *43*, 287-295.

Saint-Jore, C.M., Evins, J., Batoko, H., Brandizzi, F., Moore, I., and Hawes, C. (2002). Redistribution of membrane proteins between the Golgi apparatus and endoplasmic reticulum in plants is reversible and not dependent on cytoskeletal networks. Plant J. *29*, 661-678.

Sato, K., and Nakano, A. (2007). Mechanisms of COPII vesicle formation and protein sorting. FEBS Lett. *581*, 2076-2082.

Sato, K., Nishikawa, S., and Nakano, A. (1995). Membrane protein retrieval from the Golgi apparatus to the endoplasmic reticulum (ER): characterization of the *RER1* gene product as a component involved in ER localization of Sec12p. Mol. Cell. Biol. *6*, 1459-1477.

Sato, K., Sato, M., and Nakano, A. (2001). Rer1p, a Retrieval Receptor for Endoplasmic Reticulum Membrane Proteins, Is Dynamically Localized to the Golgi Apparatus by Coatomer. J. Cell Biol. *152*, 935-944.

Sato, K., Sato, M., and Nakano, A. (2003). Rer1p, a retrieval receptor for ER membrane proteins, recognizes transmembrane domains in multiple modes. Mol. Cell. Biol. *14*, 3605-3616.

Sato, K., Ueda, T., and Nakano, A. (1999). The *Arabidopsis thaliana RER1* gene family: its potential role in the endoplasmic reticulum localization of membrane proteins. Plant Mol. Biol. *41*, 815-824.

Scheel, J., Pepperkok, R., Lowe, M., Griffiths, G., and Kreis, T.E. (1997). Dissociation of coatomer from membranes is required for brefeldin A-induced transfer of Golgi enzymes to the endoplasmic reticulum. J. Cell Biol. *137*, 319-333.

Schekman, R. (1992). Genetic and biochemical analysis of vesicular traffic in yeast. Curr. Opin. Cell Biol. *4*, 587-592.

Scheuring, D., Viotti, C., Krüger, F., Künzl, F., Sturm, S., Bubeck, J., Hillmer, S., Frigerio, L., Robinson, D.G., Pimpl, P., and Schumacher, K. (2011). Multivesicular Bodies Mature from the *Trans*-Golgi Network/Early Endosome in *Arabidopsis*. Plant Cell *23*, 3463-3481.

Schoberer, J., Runions, J., Steinkellner, H., Strasser, R., Hawes, C., and Osterrieder, A. (2010). Sequential depletion and acquisition of proteins during Golgi stack disassembly and reformation. Traffic *11*, 1429-1444.

Schoberer, J., and Strasser, R. (2011). Sub-compartmental organization of Golgi-resident N-glycan

processing enzymes in plants. Mol. Plant *4*, 220.

Schweizer, A., Fransen, J.A., Matter, K., Kreis, T.E., Ginsel, L., and Hauri, H.P. (1990). Identification of an intermediate compartment involved in protein transport from endoplasmic reticulum to Golgi apparatus. Eur. J. Cell Biol. *53*, 185-196.

Seemann, J., Jokitalo, E., Pypaert, M., and Warren, G. (2000). Matrix proteins can generate the higher order architecture of the Golgi apparatus. Nature *407*, 1022-1026.

Seguí-Simarro, J.M., and Staehelin, L.A. (2006). Cell cycle-dependent changes in Golgi stacks, vacuoles, clathrin-coated vesicles and multivesicular bodies in meristematic cells of *Arabidopsis thaliana*: a quantitative and spatial analysis. Planta *223*, 223-236.

Semenza, J.C., Hardwick, K.G., Dean, N., and Pelham, H.R. (1990). *ERD2*, a yeast gene required for the receptor-mediated retrieval of luminal ER proteins from the secretory pathway. Cell *61*, 1349-1357.

Shaywitz, D.A., Espenshade, P.J., Gimeno, R.E., and Kaiser, C.A. (1997). COPII Subunit Interactions in the Assembly of the Vesicle Coat. J. Biol. Chem. *272*, 25413-25416.

Shorter, J., and Warren, G. (1999). A Role for the Vesicle Tethering Protein, P115, in the Post-Mitotic Stacking of Reassembling Golgi Cisternae in a Cell-Free System. J. Cell Biol. *146*, 57-70.

Shorter, J., Watson, R., Giannakou, M.-E., Clarke, M., Warren, G., and Barr, F.A. (1999). GRASP55, a second mammalian GRASP protein involved in the stacking of Golgi cisternae in a cell-free system. EMBO J. *18*, 4949-4960.

Siniossoglou, S., Wimmer, C., Rieger, M., Doye, V., Tekotte, H., Weise, C., Emig, S., Segref, A., and Hurt, E.C. (1996). A novel complex of nucleoporins, which includes Sec13p and a Sec13p homolog, is essential for normal nuclear pores. Cell *84*, 265-275.

Sjöstrand, F.S., and Hanzon, V. (1954). Ultrastructure of golgi apparatus of exocrinecells of mouse pancreas. Exp. Cell Res. *7*, 415-429.

Slusarewicz, P., Nilsson, T., Hui, N., Watson, R., and Warren, G. (1994). Isolation of a matrix that binds medial Golgi enzymes. J. Cell Biol. *124*, 405-413.

Sparkes, I. (2011). Recent Advances in Understanding Plant Myosin Function: Life in the Fast Lane. Mol. Plant *4*, 805-812.

Staehelin, L.A., Giddings, T.H., Jr., Kiss, J.Z., and Sack, F.D. (1990). Macromolecular differentiation of Golgi stacks in root tips of *Arabidopsis* and *Nicotiana* seedlings as visualized in high pressure frozen and freeze-substituted samples. Protoplasma *157*, 75-91.

Staehelin, L.A., and Kang, B.-H. (2008). Nanoscale Architecture of Endoplasmic Reticulum Export Sites and of Golgi Membranes as Determined by Electron Tomography. Plant Physiol. *147*, 1454-1468.

Stefano, G., Renna, L., Chatre, L., Hanton, S.L., Moreau, P., Hawes, C., and Brandizzi, F. (2006). In tobacco leaf epidermal cells, the integrity of protein export from the endoplasmic reticulum and of ER export sites depends on active COPI machinery. Plant J. *46*, 95-110.

Storrie, B., Micaroni, M., Morgan, Garry P., Jones, N., Kamykowski, Jeffrey A., Wilkins, N., Pan,

T.H., and Marsh, B.J. (2012). Electron Tomography Reveals Rab6 Is Essential to the Trafficking of *trans*-Golgi Clathrin and COPI-Coated Vesicles and the Maintenance of Golgi Cisternal Number. Traffic *13*, 727-744.

Suda, Y., Kurokawa, K., Hirata, R., and Nakano, A. (2013). Rab GAP cascade regulates dynamics of Ypt6 in the Golgi traffic. Proc. Natl. Acad. Sci. USA *110*, 18976-18981.

Sztul, E., and Lupashin, V. (2009). Role of vesicle tethering factors in the ER–Golgi membrane traffic. FEBS Lett. *583*, 3770-3783.

Taatjes, D.J., and Roth, J. (1986). The trans-tubular network of the hepatocyte Golgi apparatus is part of the secretory pathway. Eur. J. Cell Biol. *42*, 344-350.

Takagi, J., Renna, L., Takahashi, H., Koumoto, Y., Tamura, K., Stefano, G., Fukao, Y., Kondo, M., Nishimura, M., Shimada, T., Brandizzi, F., and Hara-Nishimura, I. (2013). MAIGO5 Functions in Protein Export from Golgi-Associated Endoplasmic Reticulum Exit Sites in Arabidopsis. Plant Cell *25*, 4658-4675.

Takeuchi, M., Ueda, T., Sato, K., Abe, H., Nagata, T., and Nakano, A. (2000). A dominant negative mutant of Sar1 GTPase inhibits protein transport from the endoplasmic reticulum to the Golgi apparatus in tobacco and *Arabidopsis* cultured cells. Plant J. *23*, 517-525.

Takeuchi, M., Ueda, T., Yahara, N., and Nakano, A. (2002). Arf1 GTPase plays roles in the protein traffic between the endoplasmic reticulum and the Golgi apparatus in tobacco and *Arabidopsis* cultured cells. Plant J. *31*, 499-515.

Tang, B.L., Wong, S.H., Qi, X.L., Low, S.H., and Hong, W. (1993). Molecular cloning, characterization, subcellular localization and dynamics of p23, the mammalian KDEL receptor. J. Cell Biol. *120*, 325-338.

Teh, O., and Moore, I. (2007). An ARF-GEF acting at the Golgi and in selective endocytosis in polarized plant cells. Nature *448*, 493-496.

Toyooka, K., Goto, Y., Asatsuma, S., Koizumi, M., Mitsui, T., and Matsuoka, K. (2009). A mobile secretory vesicle cluster involved in mass transport from the Golgi to the plant cell exterior. Plant Cell *21*, 1212-1229.

Uemura, T., and Nakano, A. (2013). Plant TGNs: dynamics and physiological functions. Histochem. Cell Biol. *140*, 341-345.

Uemura, T., Suda, Y., Ueda, T., Nakano, A. Dynamic Behavior of the *trans*-Golgi Network in Root Tissues of Arabidopsis Revealed by Super-Resolution Live Imaging. Plant Cell Physiol. in press.

Uemura, T., Ueda, T., Ohniwa, R.L., Nakano, A., Takeyasu, K., and Sato, M.H. (2004). Systematic analysis of SNARE molecules in *Arabidopsis*: dissection of the post-Golgi network in plant cells. Cell Struct. Funct. *29*, 49-65.

Viotti, C., Bubeck, J., Stierhof, Y.D., Krebs, M., Langhans, M., van den Berg, W., van Dongen, W., Richter, S., Geldner, N., Takano, J., Jurgens, G., de Vries, S.C., Robinson, D.G., and Schumacher, K. (2010). Endocytic and secretory traffic in *Arabidopsis* merge in the trans-Golgi network/early endosome, an independent and highly dynamic organelle. Plant Cell *22*, 1344-1357.

Wei, J.-H., and Seemann, J. (2010). Unraveling the Golgi Ribbon. Traffic *11*, 1391-1400.

Witte, K., Schuh, A.L., Hegermann, J., Sarkeshik, A., Mayers, J.R., Schwarze, K., Yates III, J.R., Eimer, S., and Audhya, A. (2011). TFG-1 function in protein secretion and oncogenesis. Nat. Cell Biol. *13*, 550-558.

Xiang, Y., and Wang, Y. (2010). GRASP55 and GRASP65 play complementary and essential roles in Golgi cisternal stacking. J. Cell Biol. *188*, 237-251.

Yang, Y.D., Elamawi, R., Bubeck, J., Pepperkok, R., Ritzenthaler, C., and Robinson, D.G. (2005). Dynamics of COPII vesicles and the Golgi apparatus in cultured *Nicotiana tabacum* BY-2 cells provides evidence for transient association of Golgi stacks with endoplasmic reticulum exit sites. Plant Cell *17*, 1513-1531.

Yorimitsu, T., and Sato, K. (2012). Insights into structural and regulatory roles of Sec16 in COPII vesicle formation at ER exit sites. Mol. Cell. Biol. *23*, 2930-2942.

Zaal, K.J.M., Smith, C.L., Polishchuk, R.S., Altan, N., Cole, N.B., Ellenberg, J., Hirschberg, K., Presley, J.F., Roberts, T.H., Siggia, E., Phair, R.D., and Lippincott-Schwartz, J. (1999). Golgi membranes are absorbed into and reemerge from the ER during mitosis. Cell *99*, 589-601.

The major part of the chapter 2 has been published in Molecular Biology of the Cell (the American Society for Cell Biology) as an article entitled "*cis*-Golgi proteins accumulate near the ER exit sites and act as the scaffold for Golgi regeneration after brefeldin A treatment in tobacco BY-2 cells" by Y. Ito, T. Uemura, K. Shoda, M. Fujimoto, T. Ueda, and A. Nakano (2012, volume 23, Issue 16, pages 3203-3214).

Some of the figures and text have been published in International Review of Cell and Molecular Biology (Elsevier) as an article entitled "Formation and maintenance of the plant Golgi apparatus" by Y. Ito, T. Uemura, and A. Nakano (in press).